Title
Control, Estimation, and Communication Design Applied to ActiveVehicle Safety Systems

Author
Xu, Qing

Publication Date
2005-10-01

Peer reviewed

Control, Estimation, and Communication Design Applied to Active Vehicle Safety Systems

by

Qing Xu

B.S. (Beijing University) 1997
M.S. (University of California at Berkeley) 2000

A dissertation submitted in partial satisfaction of the
requirements for the degree of
Doctor of Philosophy

in

Engineering-Mechanical Engineering

in the

GRADUATE DIVISION
of the
UNIVERSITY of CALIFORNIA at BERKELEY

Committee in charge:

Professor Raja Sengupta, Co-Chair
Professor J. Karl Hedrick, Co-Chair
Professor Andrew Pakard
Professor Anant Sahai

Fall 2005

Control, Estimation, and Communication Design Applied to Active Vehicle Safety Systems

by

Qing Xu

Abstract

Control, Estimation, and Communication Design Applied to Active Vehicle Safety Systems

by

Qing Xu

Doctor of Philosophy in Engineering-Mechanical Engineering

University of California at Berkeley

Professor Raja Sengupta, Co-Chair

Professor J.K. Hedrick, Co-Chair

This thesis studies the joint design of control, estimation, and communication systems, focusing on their application to active vehicle safety systems. The active safety systems on-board a vehicle, such as collision avoidance systems, help the driver detect and defuse oncoming potential crash situations. They have received significant attention recently. Wireless communication and estimation are critical components of an active safety system enabling the vehicle to be aware of surrounding vehicles and the roadway. The information provided by the communication and estimation systems can be used by vehicle control systems such as Cooperative Adaptive Cruise Control (CACC) or driver assistance/warning systems.

This thesis makes advances in three areas — a benefit analysis of vehicle-vehicle communication-aided CACC system in highway traffic, the design of Medium Access Control (MAC) protocols for vehicle safety messaging over Dedicated Short Range Communication (DSRC), and the real-time estimation of a Markov process over a noisy digital communication channel.

We compare the influence of adaptive cruise control (ACC) and CACC systems on highway traffic behaviors. The main difference between the CACC systems and the ACC systems is that CACC systems have vehicles interact by exchanging information through communication. Communication is shown to decrease braking effort, increase average velocity, reduce congestion, and smooth shock waves. The positive results motivate us to design efficient communication and estimation systems for vehicle active safety system.

We next study the design of MAC protocols for vehicles to send safety messages to each other. The target is to send vehicle safety messages with high reliability and low delay. We propose and analyze several random access MAC protocols. The protocols are compatible with the national DSRC multi-channel architecture. Both analytical and simulation results show our approach is feasible for vehicle safety messages in DSRC. Our best protocol outperforms the popular standard IEEE 802.11 MAC protocol.

Finally, we study the real-time estimation of a Markov process over a memoryless noisy digital communication channel. The problem could model a vehicle estimating

in real time the position, relative velocity, and direction of neighboring vehicles using the information obtained by wireless communication. We derive structural results on the optimal encoder and decoder are derived. A recursive algorithm is given to jointly find a locally optimal encoder and decoder for the binary symmetric channel. For a memoryless Gaussian vector source and a binary symmetric channel, we find the optimal policy and derive the minimum mean squared error as a function of the variance of the source and the channel noise.

To my parents

Contents

List of Figures

List of Tables

Acknowledgements

I would like to thank my advisor Professor Raja Sengupta for his encouragement and advice, his confidence in my abilities, and his effort to keep my financial stability. I learned a lot from his dedication to work, his strong insight and intuition in research, his fast understanding ability, and his always inspiring presentation skill. I particularly thank him and his wife Carolyn for their family-like support and comfort during the most difficult period of my personal life.

I thank Professor J. Karl Hedrick for reading this thesis. I also thank him for his direction in the research work leading to my Master of Science thesis in Mechanical Engineering and the two years of financial support.

I thank Professor Anant Sahai for the helpful comments on this dissertation. I also thank him for the direction and advice on the work leading to my Master of Science thesis in EECS, which is finished at the same time as this dissertation. I thank him for teaching me how to do high quality research, and for his patience and understanding of my time constraint during my final year in the Pd.D. program.

I thank Professor Andrew Packard for the valuable comments. His enthusiasm toward students and dedication in teaching impressed me greatly.

Many thanks go to all my fellow students and colleagues in U.C. Berkeley and PATH for making them ideal places for studying and doing research: Marco Zennaro, Jeff Ko, Shahram Rezaei, Yeounsik Kang, Peter Seiler, Marc Torrent-Moreno, Aniruddha Pant, Duke Lee, Jim Misener, Han-Shue Tan, Swe-Kuang Tan, and Joel

VanderWerf. I learn from all of them tremendously in various ways. Special thanks go to Tony Mak for being such a wonderful coworker as well as friend. I thank Sivakumar Rathinam for all the help on works in and out of school, particularly for reading through part of the dissertation in deep night to help me meet the filing deadline.

I thank my colleagues Dr. Aleks Göllü, Dr. Meng-Shiung Kiang, and Eduardo Aliaga in PINC-solutions for their understanding and support when I wrote this dissertation and worked in the company at the same time. I thank Mr. Daniel Jiang of Daimler-Chrysler RTNA for his help during my summer internship under his supervision.

I thank all the friends I know in and outside of Berkeley for making my long time of study and living here so enlightening. Without specific order, they are: Bo Li, Hanfeng Li, Xiaogang Zhang, Xiaoyan Zhang, Haochuan Zhang, Hao Lin and Zhenyu, Li Yi, Fanqing Guo and Birong Su, Fang Lai, Jiang Zhu, Glenn Tuan, Feiyue Wang, Kun Zhou and Xiaoqing Ge, Xiangjun Wu, Shu Peng, Shuangxi and Jimmy Xu, Jihua Huang, Xin Zhu, and Heng Wang.

I thank Ning Zhang for the happy time we spent together.

Last but by no means least, I dedicate this dissertation to my parents. Without the love and support from them I could not have accomplished anything. I thank Mimi for being with me in the hardest time.

Chapter 1

Introduction

This thesis studies the design of control, estimation, and communication systems, focusing on their application to active vehicle safety systems. Control and estimation over communication networks is attracting increasing attention. For example see the recent special issues of the IEEE Transactions on Automatic Control [8] and Control Systems Magazine [7] on networked control system. This class of problems is also given considerable weight in [49] in its evaluation of future directions in control, dynamics, and systems. They see control over communication networks as the natural next phase of the information revolution. It would transform current communication networks, now mainly concerned with the transmission of information, to have more interaction with the physical world. As stated in [49], "Current control system technology is based on a simple communication architecture: all signals travel over synchronous dedicated links, with known (or worst-case bounded) delay and no

packet loss." Such an assumption is clearly not true when the communication links are shared by many nodes, i.e., control over networks, or when the communication link is wireless. New theories as well as practices need to be developed for the control system to be implemented in the future information-rich world.

In this thesis we focus on the application of integrated control, estimation, and communication systems to active vehicle safety systems. The active safety systems on-board the vehicle, such as the collision avoidance systems, help the driver detect and defuse oncoming potential crash situations. They have received significant attention recently [2]. One critical requirement of active safety system is the vehicle must be aware of the surrounding vehicles and roadway [86]. Conventionally this neighborhood awareness is achieved with multiple on-board sensors. Wireless communication can be used in such systems to replace many of the sensors and reduce the accuracy requirement of others, therefore decreasing cost and enhancing reliability and functionality [2]. An estimation system is then needed to establish a neighborhood map using the information received from vehicle-vehicle (V-V) or roadside-vehicle (R-V) communications. With the neighborhood map, one could improve vehicle safety and traffic congestion with either automated control systems such as Cooperative Adaptive Cruise Control (CACC) [71] [78] [81] and automated highway systems (AHS) [35], or driver assistance/warning system such as intersection decision systems (IDS) [86].

In support of the many efforts to improve vehicle safety and resolve traffic congestion with V-V and R-V communications, the Federal Communications Commission

(FCC) recently allocated a Dedicated Short Range Communications (DSRC) spectrum at 5.9GHz. DSRC envisages a short to medium range communications service supporting both public safety and private commercial applications using R-V and V-V communications. DSRC has a mandate to be used to enhance public safety, while supporting other transportation interests. It is intended to provide very high data transfer rates in circumstances where minimizing latency in the communication link and isolating relatively small communication zones are important. There is a North America DSRC standard program working jointly under the American Society of Testing and Materials (ASTM) and the Institute of Electrical and Electronics Engineers (IEEE) to develop a set of standards for full interoperatability throughout North America [2]. The communication systems proposed in this thesis are compatible with the DSRC architecture.

There are three sets of questions to answer in the joint control, estimation, and communication design applied to active vehicle safety applications:

1. What is the effect of communication on vehicle safety, travel efficiency, and passenger comfort? Is the effect positive? What is the cost for this benefit? Is the benefit significant enough to motivate us to implement such a system?

2. How can we design a wireless communication protocol to satisfy the reliability and latency requirements of vehicle safety communication? Is it feasible to meet such requirements? How should the design change with the varying vehicle traffic and communication data flow? What are the effects of the design

parameters on performance?

3. When vehicle state is transmitted over a noisy digital communication channel, and is estimated in real time on the receiving vehicle, what should be the design to minimize the estimation error? In particular, how should the state be digitized, and how should it be reconstructed based on the symbol received from the noisy channel?

Our answers to the above three questions form the three main chapters of the thesis. Below we give an overview of the thesis.

1.1 Thesis Overview

In Chapter 2, we comparatively assess the influence of adaptive cruise control (ACC) and cooperative adaptive cruise control (CACC) systems on highway traffic behaviors. The main difference between the CACC systems and the ACC systems is that CACC systems have vehicles interact cooperatively by exchanging information between them through communication. The goal is to study the design and implementation of vehicle-vehicle/roadside-vehicle communication. In addition, the impact of market penetration of ACC/CACC vehicles and controller aggression are also evaluated. Two simulation works are presented. The microscopic work simulates a single ACC/CACC vehicle using MATLAB/SIMULINK. A cut-in scenario and a braking scenario are tested. Vehicle-vehicle communication saves control effort in the former

scenario, while shows little effect in the latter. In the macroscopic work we simulate ACC/CACC controlled highway merging with SHIFT. Communication is shown to decrease braking effort, increase average velocity, reduce waiting-to-merge queue length, and smooth traffic shock wave caused by merging. The higher the market penetration of controlled vehicles the better the system performs. The aggressiveness of the controller has mixed influence, providing a tradeoff between efficiency and safety. The positive results motivate us to design efficient communication and estimation systems for vehicle active safety systems.

In Chapter 3, we study the design of Medium Access Control protocols for a vehicle to send safety messages to other vehicles. The target is to send vehicle safety messages with high reliability and low delay. The communication is one-to-many, local, and geo-significant. The vehicular communication network is ad-hoc, highly mobile, and with large numbers of contending nodes. The messages are very short, have a brief useful lifetime, but must be received with high probability. For this environment, we explore the efficacy of rapid repetition of broadcast message within its brief useful lifetime. We propose several random access protocols for medium access control. The protocols are compatible with the Dedicated Short Range Communications (DSRC) multi-channel architecture. Analytical bounds on the performance of the proposed protocols are derived. Simulations are conducted to assess the reception reliability and channel usage of the protocols. The sensitivity of the protocol performance is evaluated under various offered traffic and vehicular traffic flows. The results show

our approach is feasible for vehicle safety messages in DSRC.

Chapter 4 is about the real-time estimation of a Markov process over a memoryless noisy digital communication channel. The goal of system design is to minimize the mean squared estimation error. The problem could model a vehicle estimating in real time the position, relative velocity, and direction of neighboring vehicles with information obtained from wireless communication. We first show the optimal encoder and decoder can be memoryless in terms of the source symbols. We then prove the optimal encoder separates the real space with hyperplanes. In the case of the binary symmetric channel and scalar source, the optimal encoder can be a threshold. A recursive algorithm is given to jointly find a locally optimal encoder and decoder for the binary symmetric channel. For a memoryless Gaussian vector source and a binary symmetric channel, we show the optimal policy is to encode the principal component. We derive the minimum mean squared error as a function of the variance of source and the channel noise.

Chapter 5 concludes the thesis and proposes future work.

1.2 Thesis Contributions

The following are the main contribution made in this thesis.

1.2.1 Benefits of CACC System on Vehicle Traffic

We analyze the benefit of CACC system on vehicle traffic in Chapter 2. We show communication decreases braking effort, increases average velocity, reduces waiting queue length, and smoothes traffic shock wave caused by merging. Higher market penetration of controlled vehicles enhances the system performance. The aggressiveness of controller has mixed influence, providing a tradeoff between efficiency and safety.

1.2.2 Protocol Design for Vehicle Safety Messaging over DSRC

In Chapter 3 we propose several random access MAC protocols to send vehicle safety messages with high reliability and low delay in DSRC control channel. We derive analytical bounds on the performance of the proposed protocols. Simulations are conducted to assess the reception reliability and channel usage of the protocols. We evaluate the sensitivity of the protocol performance under various offered traffic and vehicular traffic flows. The results show our approach is feasible for vehicle safety messages in DSRC.

1.2.3 Real-time Estimation of a Markov Process over Noisy Digital Communication Channel

In Chapter 4 we study the real-time estimation of a Markov process over a memoryless noisy digital communication channel. We show the optimal encoder and decoder can be memoryless in terms of the source symbols. The optimal encoder is proved to be one separating the real space with hyperplanes. A recursive algorithm is given to jointly find a locally optimal encoder and decoder for the binary symmetric channel. For a memoryless Gaussian vector source and a binary symmetric channel, we show the optimal policy is to encode the principal component. We derive the minimum mean squared error as a function of the variance of the source and the channel noise.

Chapter 2

Comparative Analysis of ACC and CACC Systems

Adaptive Cruise Control (ACC) systems are the first driver control assistance systems entering the market that have the potential to influence traffic flow characteristics [71]. In conventional cruise control, the vehicle is commanded to maintain a preset velocity, regardless of the traffic environment. In adaptive cruise control systems, the vehicle tries to maintain a desired spacing and velocity with respect to the vehicle in front using the forward looking sensors (typically millimeter-wave radar or infrared laser). In this system, there is no communication between the vehicles or between a vehicle and roadside stations. Cooperative Adaptive Cruise Control system uses both the information from the forward looking sensors (as in ACC) and the information from neighboring vehicles through both vehicle-vehicle (V-V) and

roadside-vehicle (R-V) communications. Since the vehicles communicate with each other, they can perform control maneuvers cooperatively. Currently, vehicles with ACC systems are already available in the market, whereas CACC equipped vehicles are still in the research phase attracting high degree of interest.

We study the impact of V-V and R-V communications on the behavior of highway vehicles on both microscopic and macroscopic level. On the microscopic level we study a single vehicle in a cut-in scenario and a braking scenario. On the macroscopic we study vehicle traffics on two highways that merge. Essentially, we compare the ACC and the CACC system. In addition, we also study the effect of the design parameters such as market penetration and controller aggressiveness. The results of the effects of communication and other design parameters are illustrated through simulations. These results serve as the guideline for future analytical and experimental work.

The rest part of the chapter is organized as follows. Section 2.1 summarizes relevant previous work in publication. Section 2.2 describes the simulation scenario. Section 2.3 is the system modeling and implementation. Section 2.4 reports and discusses the simulation results. Section 2.5 summarizes the chapter and proposes future work.

2.1 Previous Work

There are many papers that analyze the effects of vehicles with ACC systems to the traffic behavior (congestion, delay, safety, emissions, fuel consumption). All the papers that deal with the macroscopic behavior have been based on analytical models and simulations. Experimental results are scarce since there are not yet enough ACC equipped vehicles to perform tests. Experimental results in [38] [83] address the microscopic behavior of the traffic flow. More extensive literature review of ACC systems up to their publication dates can be found in [71] and [88].

Much of the interest of the ACC systems concentrates on its impact on traffic flow capacity [71] [88] [21] [58] [18] [48]. Mixed responses have been found on the usefulness of these systems. For example, Zwaneveld and van Arem [88] concluded that vehicles equipped with ACC systems have little impact on congestion reduction whereas performs better on traffic flow stability. Chang and Lai [18] showed expected traffic flow effects at market penetrations of 30, 50, 80 and 100% ACC. They showed a non-linear increase with traffic flow capacity, leading to a maximum of 2750 vehicles/lane/hour with all ACC vehicles. At the same time, some work indicates that the application of ACC increases flow capacity only marginally or even decreases the capacity under some circumstances. For example, Cremer et. al. in [21] compares the effects of one macroscopic and four microscopic ACC models on traffic flow. Their results show little change in traffic flow at ACC market penetrations of 40% and 70%. The results of [48] show the ACC with a time-gap setting of 1.2 second would leave

traffic flow capacity essentially unchanged from the baseline manual driving conditions, 1.0 second time gap could cause noticeable but small increases in flow capacity, and 1.4 second time gap decreases capacity, all at 100% market penetration. It was necessary to reduce the time gap to 0.8 second to increase the capacity in the 10% range at market penetrations of 50% or higher. It seems that the divergence of the highway system modeling, the ACC controller design, and the simulation and experimental tools prohibits us to draw easy conclusions on the effect of ACC system on the highway traffic flow capacity.

The performance of ACC system on smoothing and stabilizing the highway traffic, thus reducing shock waves is another focus of interest, and the results in this aspect are more encouraging. Many previous papers indicate that ACC vehicles stabilize traffic flow by filtering the impact of rapidly accelerating lead vehicles, thus reducing the shock waves in the traffic [71] [17] [70] [84] [24]. Analytical results regarding some specific concepts of stability of ACC system were also obtained, e.g. string stability [17] and traffic flow stability [24]. Other performance variables that have been studied are trip time, trip delay, [42] [84] traffic speed and time gaps [70]. Besides the macroscopic behavior, the performance of individual vehicle under ACC is also studied. [42] [34] [38] It seems the ACC system has more obvious benefit on driving comfort and safety than on traffic flow.

Contrary to the literature available on ACC systems, the literature for CACC is rare. This is because the concept of using communication with the adaptive cruise

control systems is new. Shladover, et. al. [71] compared the performance of human driver, ACC, and CACC system. In their CACC system design, the preceding vehicle continuously transmits the acceleration and braking capacity information to the follower via point-to-point vehicle-vehicle communication. Integrating this information with the radar measurement, the CACC system drives the vehicles with much smaller inter-vehicle distance than both ACC and human-driven cases, without sacrificing safety. Therefore the capacity of highway is greatly enhanced. Part of our work is based on the simulation they built, but our communication system design in CACC is different from theirs.

Hedrick, et al [34] built a thorough vehicle model for a BMW test vehicle. They experimentally validated all the components in the model, and implemented the model with SIMULINK and C language. An ACC controller was designed using sliding surface technique. Gain scheduling was applied to the resulting controller for different combinations of range and range rate. The controller was integrated in the SIMULINK vehicle model and tested in various scenarios. Their simulation was on the level of individual vehicle, therefore the macroscopic behavior of the traffic flow could not be observed. Part of our simulation is based on their work.

2.2 Simulation Scenarios

The following two simulation studies are conducted:

- One Vehicle CACC Simulation (OVC): Studies the response of one vehicle equipped with a CACC system to the changing traffic environment.
- Highway Merging Control simulation (HMC): Studies the effect of merging vehicles equipped with CACC systems from two highways.

2.2.1 One-vehicle CACC simulation (OVC)

Two scenarios, *Braking* and *Cut-in*, are simulated in OVC.

In *Braking* scenario, two vehicles are driving in the same lane with the follower being automatically controlled. We compare the behavior of the following vehicle when its control system is CACC with the case when the control system is ACC. In the simulation, the preceding vehicle brakes and the follower applies an appropriate braking input in order to maintain the desired spacing and velocity. In the ACC scheme, the follower measures the range and range rate with radar and sensors. The range rate is differentiated to obtain acceleration, and the braking of the preceding vehicle is detected from the sign of acceleration. In the CACC system, whenever the preceding vehicle brakes, it transmits a "brake light" message to the CACC following vehicle via V-V communication. The CACC vehicle, upon receiving the message, brakes strongly enough for safety without causing any discomfort to the passenger.

Both vehicles are assumed to have V-V communication capability when the follower is a CACC vehicle.

In *Cut-in* scenario, initially an ACC/CACC vehicle is following its preceding vehicle. Then a third vehicle in the adjacent lane cuts in between the two vehicles, and becomes the new preceding vehicle of the ACC/CACC vehicle. Without communication, the ACC vehicle detects the cut-in vehicle when the latter passes the lane border. The ACC controller then commands the vehicle to brake, sometime abruptly, to make space in front for the cut-in vehicle. With CACC system using V-V communication, the cut-in vehicle transmits the equivalent of a "turning light" message to the CACC vehicle at the instant it starts the cut in maneuver from the centerline of the adjacent lane. The CACC vehicle then has approximately half of lane change time to slow down and make space for the cut-in vehicle. In CACC scheme we assume the cut-in vehicle and the CACC vehicle to have V-V communication capability, while the "old" preceding vehicle does not have to communicate.

2.2.2 Highway Merging CACC Simulation (HMC)

In HMC, vehicles merge into the main lane from a merge-in lane, and the two lanes join at a merge-in point (MP), as illustrated in Figure 2.1. In the figure cars B and C are the main lane vehicles, and car A is in the merge-in lane.

Some or all of the main lane vehicles are ACC/CACC controlled while others are driven by humans. The market penetration of the ACC/CACC vehicles in the

main lane is controllable. Therefore we can study the interaction between the human-driven vehicles and the controlled vehicles, as well as the effect of different market penetration of the controlled vehicles.

Figure 2.1: Highway Layout of HMC

The procedure of merge-in in CACC scheme is as follows.

1. *Head merging vehicle is generated*

   At the instant the first vehicle in the merge-in lane enters the main lane, the second vehicle in the lane becomes the new "head merging vehicle". For convenience, assume car A in Figure 2.1 is the new head merging vehicle. In CACC system, the moment it becomes the head merging car, car A broadcasts a message to all the main lane vehicles within its communication range. The communication could be realized by either V-V communication with A being the broadcaster, or R-V communication with the aid of a roadside station at MP. The message contains the position of the merge-in point and the time needed by vehicle A to enter the main lane. The time the vehicle requires to reach the main lane consists of two parts: the time required to reach the merge-in point and the waiting time at the merge-in point for a safe gap. If A is not at the

merge-in point when it becomes the head, it keeps driving at the original speed in the merging lane. If A is already at the merge-in point when it becomes the head (e.g. when there is a queue formed in the merging lane), we assume a metering light at the MP commanding A to wait for a certain amount of time before it attempts to merge. The length of the time the head merging vehicle waits is set to be the reciprocal of the input flow rate of the merging lane. For example, for merge-in lane flow rate of 1200 vehicles/hour/lane, the average waiting time is about 3 seconds.

2. *Head merging vehicle drives to or waits at merge-in point*

   After receiving the warning message from the head merging vehicle, each main lane vehicle determines the relevance of the message to itself. The relevance is determined as follows. If a main lane vehicle C (see Figure 2.1) finds that at the anticipated time when vehicle A arrives in the main lane, A will cut in between C and its current preceding vehicle B, C regards the message as relevant. In response to the relevant message, C brakes promptly but smoothly to increase the gap between itself and vehicle B. If a car finds a message irrelevant, it simply discards it. The information needed in making the decision includes: the position of merge-in point and the predicted time A will merge in (obtained from the communicated message, which is in turn obtained from GPS and/or digital map), the position of C and its velocity (obtained from e.g. GPS and speedometer), and position and velocity of the preceding vehicle B (obtained

from radar measurements).

3. *Head merging vehicle waits for acceptable gap in main lane*

   When it arrives at the MP, the head merging vehicle stops and observes the gap between the passing main lane vehicles. It waits to merge until an acceptable gap appears, according to the gap acceptance model to be described in 2.3.4. If the main lane traffic is too busy such that the head merging vehicle has to wait for excessively long time, a queue of waiting cars forms in the merge-in lane. Notice that the waiting period in this step is different from the one in Step 2. The waiting in Step 2 is either commanded by the metering light or required for the head merging vehicle to drive to the MP, therefore it is unavoidable and is about the same for all merging vehicles. However the waiting in Step 3 is for the head merging vehicle to find a safe gap, and the length of the waiting is random depending on the main lane traffic. An efficient merging system should make this waiting time as short as possible for every merging vehicle.

4. *Head merging vehicle merges in*

   The head merging vehicle merges in the gap it feels safe. At this instant, the main lane vehicle right behind it sees the merging vehicle, and responds by necessary braking. The head merging vehicle's initial velocity in the main lane is designed to be that of the main lane vehicle right in front of it. Now the second vehicle in the merging lane, if any, becomes the new head merging vehicle, and

we are back in step one and the above procedure is repeated.

In the ACC scheme there is no communication. Therefore we have only the last two steps in the above procedure. We repeat them here for clarity.

1. *Head merging vehicle waits for acceptable gap in main lane*

2. *Head merging vehicle merges in*

Clearly, there is no cooperation between the merging vehicles and the main lane vehicles.

2.3 System Modeling and Design

This section describes the models implemented in the simulation and the controller design. The OVC models are implemented with MATLAB/SIMULINK. The HMC simulation is built using SHIFT, a language developed by California PATH to simulate dynamic network of hybrid automata. [55] For both simulations, we give detailed explanation of three critical components, i.e. vehicle model in 2.3.1, controller design in 2.3.2, and communication system in 2.3.3. For OVC, these three components essentially cover the whole system, however there are other components in HMC which are independent of the above three models. These HMC components are described in 2.3.4.

2.3.1 Vehicle Model

Vehicle model in OVC

The OVC uses the vehicle model of a BMW test vehicle built by Hedrick et.al. [34]. The model includes the following components, each is further composed of many sub-models:

- longitudinal vehicle dynamics
- Wheel dynamics
- Unlocked engine dynamics

- Torque converter
- Lockup logic
- Gear shifting, and
- Throttle/brake actuator models

Each component is experimentally validated with the vehicle driven in test track or urban streets. The parameters are either estimated from experiment results or provided by the manufacturer. The well-studied vehicle model enables us to observe the performance of the controller under the influence of the nonlinear dynamics of the mechanical components of a vehicle. The details of modeling and validation of each component of the vehicle model are summarized in [34].

The OVC models are implemented in simulation using SIMULINK package of Matlab. SIMULINK uses a graphical interface to build models in block diagram form. Figure 2.2 shows the highest level of the SIMULINK vehicle model. The upper portion of this picture contains the vehicle model subsystems and the lower portion contains the controller subsystems.

We now give a brief overview of the system by following the flow of the model from left to right. In the upper left of Figure 2.2 are the brake and driveline subblocks. The two actuators inputs, brake and throttle load, enter these blocks. Specifically, the brake subsystem takes in the brake actuator input load and outputs the net brake torque. This net brake torque enters the wheel dynamics block, which implements

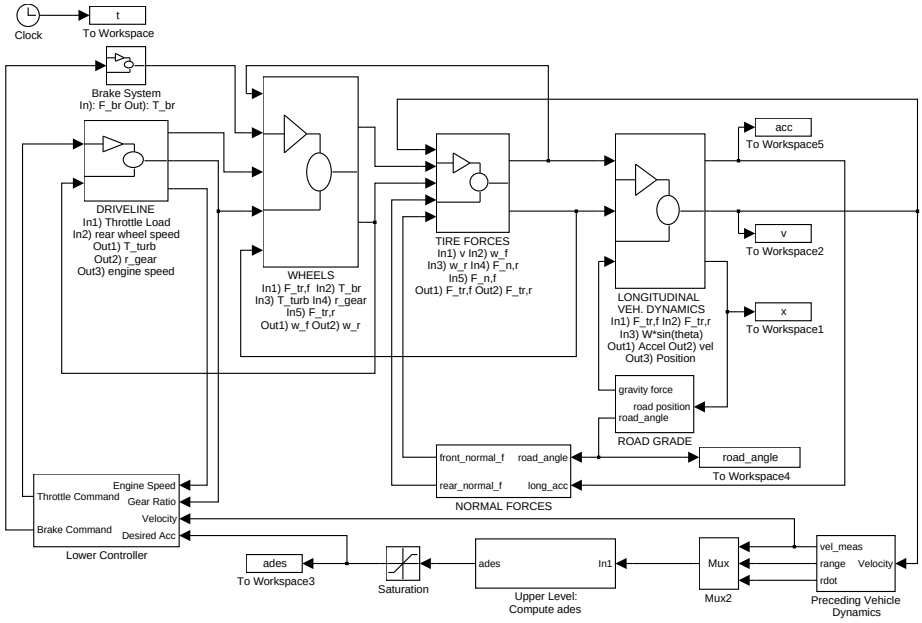

Figure 2.2: SIMULINK diagram of vehicle model and ACC/CACC controller

the wheel dynamics equations for each wheel. The driveline block implements the engine map, torque converter equations, lockup logic, and gear map. The inputs to this block are throttle load and rear wheel angular velocity and the outputs are engine speed, gear ratio and torque converter output torque. The previously mentioned wheel dynamics block uses the brake torque (from the brake subsystem) and the turbine torque and gear ratio (both from the driveline block) as inputs. It also inputs the front and rear tractive forces (which are generated by the tire forces block, yet to be described). This block then outputs the front and rear wheel angular velocities which are used by the tire forces block. The tire forces block also uses the vehicle velocity and normal forces on each tire to generate the tractive forces using governing equations

of wheel dynamics. These normal forces are generated by the normal forces block, which implements the vehicle pitch due to acceleration and road grade integrated in the longitudinal vehicle dynamic equations. Finally, the longitudinal vehicle dynamic equations are implemented in the longitudinal dynamics block. This block uses the tractive forces and gravitational force acting in the longitudinal direction to generate the vehicle velocity and position.

The controller is then implemented in the lower half of the SIMULINK diagram. This controller can be removed and/or replaced if other testing is desired. This part can be described by following the flow from right to left. The first block on the lower right simulates the dynamics of the preceding vehicle. This block integrates a given preceding vehicle velocity profile. The controller inputs the range and range rate generated by the preceding vehicle block. If the controller is ACC then these are all the inputs, while CACC controller also inputs the signal communicated by the preceding vehicle. The controller has two levels. The upper level computes a desired vehicle acceleration using a free flow controller and an ACC or CACC controller (all to be described later). The lower level then tracks this desired acceleration using the throttle and brake actuators. The lower level also includes switching logic to prevent the application of the throttle and brakes at the same time, thus when accelerating the brakes are not applied while when decelerating the throttle is not running.

Vehicle model in HMC

In HMC, due to the large number of simulated components and the complication of the scenario, we use the simple longitudinal vehicle model in equation (2.1) to save computation load.

$$\begin{aligned} \ddot{x}(t) &= a(t) \\ \tau\dot{a}(t) + a(t) &= u(t) \end{aligned} \tag{2.1}$$

The model composed of a double integrator and a first-order lag, where $x(t)$ and $a(t)$ are respectively the position and acceleration, and $u(t)$ is the commanded acceleration from the controller. The flow of information among the simulation components is the following:

- Sensors output range and range-rate to the controller.
- Controller outputs acceleration command to the first-order lag.
- Lag outputs actual acceleration to vehicle dynamics.
- Dynamics integrates and outputs velocity.
- Velocities of all vehicles are integrated to update their positions, which can then be read again by sensors.

2.3.2 Controller Design

ACC Controller

The ACC controller is designed with the sliding surface technique in order to regulate the range error and range rate error.

The sliding surface is defined in equation (2.2).

$$S = (v_p - v) + \Lambda \cdot (r - r_{des}) \tag{2.2}$$

In (2.2) v_p and v are respectively the velocity of the preceding vehicle and the ACC/CACC vehicle, therefore $v_p - v$ is the range rate, or equivalently the relative velocity. r and r_{des} are the range and desired range, therefore the latter term in (2.2) is the range error to eliminate. The gain Λ is a design parameter which determines the speed of the convergence of range error to zero, once we are on sliding surface.

Instead of the commonly used time-gap model for the desired range, we use the desired range defined in equation (2.3), which is a curve fitting result of human driver behavior provided by the manufacturer of the OVC test vehicle. [34]

$$r_{des}(t) = t_h * v^{k_0} + \text{offset} = 6.33 * v^{0.48} + 2 \tag{2.3}$$

We observe that the increasing rate of this desired range is smaller than the time-gap model when the velocity is high.

We derive the desired acceleration to drive the range error and range rate to the

sliding surface, thus both to converge to zero with time. For this we need to have

$$\dot{S} = -K \cdot S \tag{2.4}$$

where K is also a design parameter which determines the decay speed of S.

Substituting (2.2) and (2.3) in (2.4) we obtain the ACC controller as in equation (2.5):

$$a_{des} = \frac{1}{1 + k_o t_h v^{k_o - 1}} \cdot [(\Lambda + K) \cdot \dot{r} + \Lambda \cdot K \cdot (r - r_{des})] \tag{2.5}$$

In the equation $r(t)$ and $\dot{r}(t)$ are the range and range rate, and $r_{des}(t)$ is the desired range. The desired acceleration a_{des} is the control command, and $\Lambda + K$ and $\Lambda \cdot K$ are the controller gains. We observe the influences of Λ and K to the controller are symmetric. Gain scheduling is used to deal with different relation of the range and range rate. The rough rule is that for shorter range (closer to the predecessor), and more negative range rate (slower than preceding vehicle), the controller reacts more aggressively. The details are in [34] and omitted here. The absolute value of the acceleration commanded by the controller is a measure of control effort. For the same level of performance on range error and range rate responses, better controller design demands less control effort. The acceleration of the ACC/CACC controllers is bounded to be between -3m/s/s and 2m/s/s for safety and comfort purpose, but such limits do not apply to the human drivers (details in 2.3.4).

CACC Controller

When CACC scheme is applied, the desired range is changed properly and the same controller structure as in equation (2.5) is used to track this modified desired range. Both in the cut-in scenario of the OVC and the HMC, whenever a CACC vehicle receives a "relevant" message warning it of a vehicle cutting in front in t_{cut_in} time, it "modifies" the desired range in the way shown in Figure 2.3. The modified desired range increases linearly in the time before cut-in/merging vehicle's arrival such that the CACC vehicle decelerates as aggressively as necessary without having to brake excessively hard. At the anticipated arrival time of the merging vehicle, the desired range increases to twice as large as the original value.

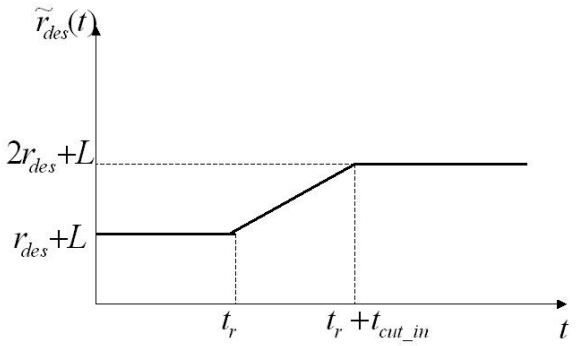

Figure 2.3: Modifying the Desired Range in the CACC Controller

The linear increase of the desired range with time can be represented in equation (2.6).

$$\tilde{r}_{des} = \left[1 + \frac{(t - t_r)}{t_{cut\_in}}\right] * r_{des} + \frac{(t - t_r)}{t_{cut\_in}} * L \tag{2.6}$$

In the equation, r_{des} is the desired range defined in (2.3), $\tilde{r}_{des}$ is the modified desired range for the CACC controller, t_r is the instant of the reception of the warning message, t_{cut_in} is the estimated time left for the arrival of the cut-in vehicle, and L is the vehicle length.

In the braking scenario of OVC we interrupt the command of the ACC controller (2.2) and apply the smaller (larger in absolute value) of the ACC control command generated by (2.5) and the (negative) acceleration of the preceding vehicle, which is received from V-V communication.

Free-driving Controller

When a vehicle has no vehicle ahead of it or has at least 100 m of clearance to the preceding vehicle, the controller (of the automatic vehicle) is in the free driving mode. In this mode, the controller attempts to maintain a desired velocity, which was assigned when the vehicle entered the simulation. The distribution of desired velocity is taken from a normal distribution with a mean of 28.9 m/s (65 mph) and a standard deviation of 4.4 m/s (10 mph). Each type of controller uses an error-based control law:

$$u(t) = -k_f(v - v_{des}) \tag{2.7}$$

Where v and v_{des} are respectively the actual and desired velocity. In addition, acceleration is limited to $\pm 2m/s/s$.

The initial velocity of a newly generated vehicle, as it enters the simulation, is distributed in the same way as the desired velocity in free-driving state.

2.3.3 Communication Model

Two particular concepts of V-V/R-V communication are applied in our work. However seemingly simple, they help overcome many challenging problems in V-V/R-V safety communications.

Location-based Broadcast

The first one is location-based broadcast (LBB) [79] [78], in which the sender broadcasts a message to all of the receivers in the communication range, and the physical location of the sender is written in the broadcast message. Each receiver determines the relevance of the message and the proper response by itself. Useful information for the sender in processing the message includes the relative physical position of itself to the sender (e.g. in front, behind, left lane, distance, etc.), the nature of the message (e.g. braking, lane changing, accident, congestion, etc.), and other information in the message (velocity, acceleration, etc.). By applying LBB we avoid the difficulty of network addressing and physical-location/communication-address mapping. The realization of LBB requires the interaction of wireless communication with

other relevant techniques such as sensor fusion, GPS/INS, and digital map. It should be noticed that LBB is not suitable for all types of vehicle safety applications, and sometimes unicast is unavoidable.

Event-driven Communication

The other important concept underlying our implementation is event-driven communication. In this kind of communication, the transmission of a message is driven by particular events, e.g. cut-in, merging, hard braking of preceding vehicle, etc. Event-driven communication is in contrast to time-driven communication, in which vehicles transmit certain information (e.g. position, velocity, acceleration, road condition, etc.) to targeted receivers in every constant period of time (e.g. 100msec) [2] [71]. When large number of senders are competing for the channel, as is the case in V-V communication, event-driven communication reduces the load of channel and gives high priority to emergency message, thus simplifies the communication protocol design. Event-driven communication conveys less information than time-driven communication therefore is not sufficient for some applications. Our study helps find out which application can be supported by event-driven communication, and which application requires more complicated communication scheme.

2.3.4 Other Models in HMC

There are more models in HMC than in OVC since the former simulates much more complicated system. They are described one-by-one below.

Highway Model

The highway is one lane and has one entrance and one exit at two ends, with only passenger cars on it. Vehicles enter from left end at 0 m, and exit simulation at 700 m at the right end of the simulated highway segment. The merge-in point is at 500 m from the left end. In both the main lane and the merging lane vehicles are generated by an exponential distribution source with a given flow rate, which determines the time gap between two consecutive vehicles. The initial velocity is set as described in 2.3.2. The lateral motion of vehicles and geometry of merge-in ramp are not modelled, therefore in simulation the merging vehicles wait at 500 m after being generated, forming a queue sometimes, and pop in the main lane instantaneously when condition is satisfactory.

Sensors

Since by the time we conducted this work no generic model and parameters for sensor noise were available, we assumed all sensors to be perfect in the simulation. The simulations will be repeated in the future with more realistic sensor model.

Braking Capabilities

In our simulation, hard braking is unlikely. However, to meet safety standards, our controllers must be able to handle such situations. We use a distribution of light vehicle braking capabilities from the NAHSC Task C3(1) Interim Report [9], assuming dry pavement. Engine braking is not modelled separately in HMC (unlike in OVC). Brake dynamics are not explicitly modelled, although the first-order lag applies to deceleration as well as to acceleration.

Human Driver Model

We use the COSMODRIVE model of Song-Delorme [66] because it has more room for tuning, and incorporates recent research on perception [36]. Human drivers do not respond to the V-V/R-V communication messages.

Merging Model

We assume that merging is under human control in all cases, since automated control of merging is unlikely to be available in the near future. The human driver at the head of the merge queue waits until the gap between passing vehicles is of an acceptable length. When such a gap appears, the driver merges into it at the velocity of traffic. Our model for gap acceptance of human drivers is borrowed from the Ph.D. dissertation of K. Ahmed [11]. This model has been calibrated with driving data, and including it in our simulation produces realistic-looking traffic patterns. In this

model, the driver of the merging vehicle is more likely to merge in when seeing a good gap, but the decision making model is probabilistic. A good gap cannot guarantee a merging, which also depends on other factors such as relative speed, perception delay, number of failed previous attempts, etc. In CACC, the relevant main lane vehicles try to make a more acceptable gap for the merging vehicle when the latter arrives, but it is (the model of) human driver, not any automated controller, who makes the decision of merging.

2.4 Simulation Results and Discussion

In this section we present and discuss the simulation results. The results for OVC and HMC are presented separately. The simulation system should be validated with experiment or measurement data of real world. The validation of the OVC system was performed experimentally and reported in [34]. The validation of the HMC model will be presented shortly below.

2.4.1 One Vehicle CACC Simulation

In OVC we compare the influence of ACC and CACC on the behavior of a single vehicle. We observe the performance of the vehicle in tracking the desired range and range rate, and the control effort with which to attain this tracking. In highway environments, it is more probable for a vehicle to brake hard than to accelerate suddenly. Therefore, the focus of the control effort is much more on the braking behavior than on the (positive) accelerating behavior. The braking effort in this thesis refers to the absolute value of the negative acceleration. Since in the implementation of the vehicle model, the brake and throttle are never applied at the same time, the negative acceleration of the vehicle is always due to the application of the brake. An optimal system should well track the desired range and range rate with as little a control effort (especially in the braking stage) as possible.

The range and velocity for the *cut-in* scenario are shown in Figure 2.4. The velocity of the preceding vehicle is fixed to be 12.5 m/s in the simulation. At the

beginning of simulation the follower (i.e. the CACC or ACC vehicle) is 150 meters behind the preceding vehicle and driving at 25 m/s. The follower brakes to track the preceding velocity. The cut-in happens at 10 second, making the range to drop instantaneously. The range after this instant becomes the range to the new preceding vehicle. For simplicity we set the cut-in vehicle's longitudinal velocity to be the same as the old receding vehicle. There is little difference on the range, though the velocity of CACC vehicle responds earlier than that of the ACC vehicle.

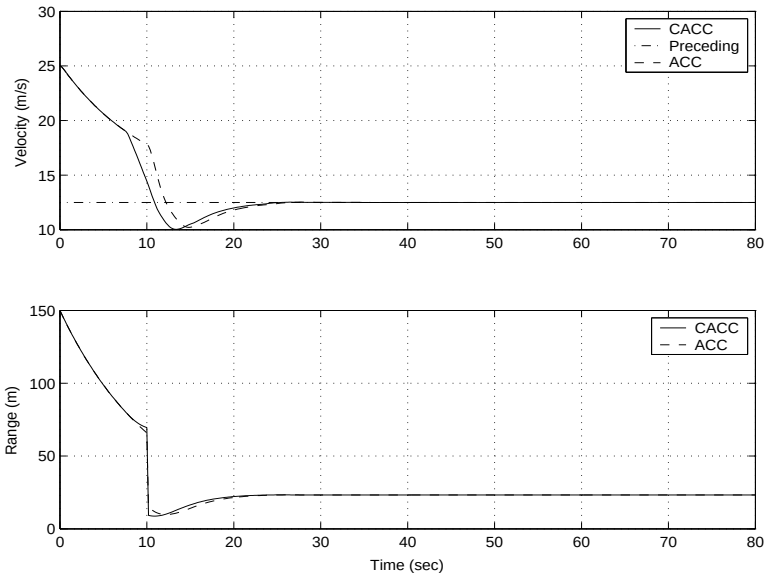

Figure 2.4: OVC: Range and velocity for ACC and CACC vehicles in cut-in scenario

Figure 2.5 shows the corresponding acceleration of the ACC vehicle and CACC vehicle in the *cut-in* scenario. The cut-in happens at 10 seconds for both ACC and CACC cases. The ACC vehicle detects the cut-in vehicle shortly after 10 seconds, and then has to apply a hard brake of -2.5 m/s/s to slow down. After this hard brake, the velocity of the ACC vehicle decreases to a safe value. The acceleration thus goes back

to the normal value, and finally converges to zero as the ACC goal is achieved. On the other hand, in the bottom subplot, because of the V-V communication, the CACC vehicle responds 2.5 seconds before the vehicle in the adjacent lane cuts in, which is half of the lane change time of the cut-in vehicle. Because the CACC vehicle has a longer response time, it brakes much more softly than the ACC vehicle. The braking effort is smaller than 0.5 m/s/s, and the sharp notch shortly after 10 second in the top subplot disappears. Combining the observations of Figures 2.4 and 2.5, we see that the V-V communication saves large amount of control effort without sacrificing controller performance, which means more safety and comfort for the passenger.

In the *braking* scenario of OVC we conduct the simulation using preceding velocity profiles collected by driving the test vehicle on street. The purpose is to simulate the brakings of a typical vehicle in real traffic. Simulations with different profiles are run. In all of them we see little benefits of CACC system over ACC system. Figure 2.6 is the range and range rate of the ACC/CACC controlled vehicle in one of the braking scenarios. We can see CACC vehicle has a little faster time response than ACC vehicle, but the difference is not significant enough. The control effort comparison also shows the same result, which we omit here. The reason for this similarity in the performance may be due to the idealized delay-free and noiseless forward-looking sensor model we implemented. In the simulation the response time gained by addition of communication is not long enough for the vehicle to produce much difference in performance. The gain in response time is further trivialized after

the command signal is filtered by the much slower vehicle dynamics to obtain the response in vehicle motion. With the perfect sensor model in simulation, the event-driven communication does not help much in a scenario like braking warning.

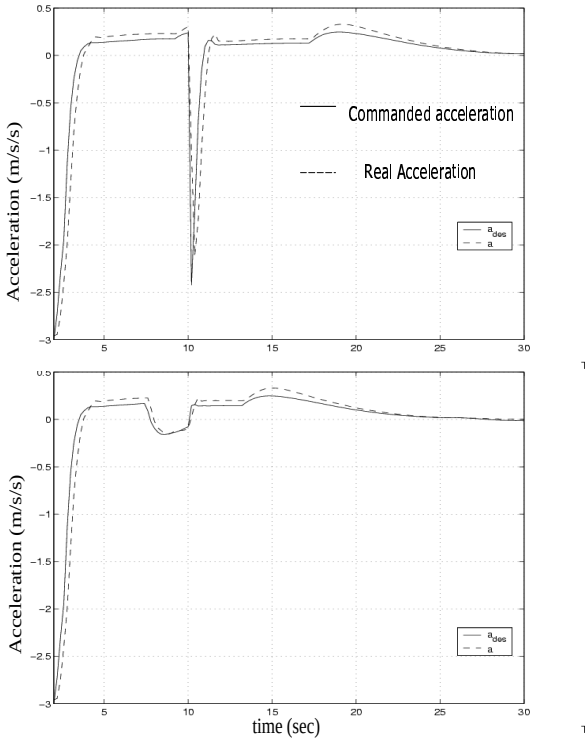

Figure 2.5: OVC: Acceleration of CACC and ACC vehicle in Cut-in Scenario. Upper:CACC. Bottom:ACC

2.4.2 Highway Merging CACC Simulation

This subsection presents the following results: validation of the system which shows the reliability of all the simulation results, and the performance of the validated system with the effect of various design parameters. The performance variables are the following.

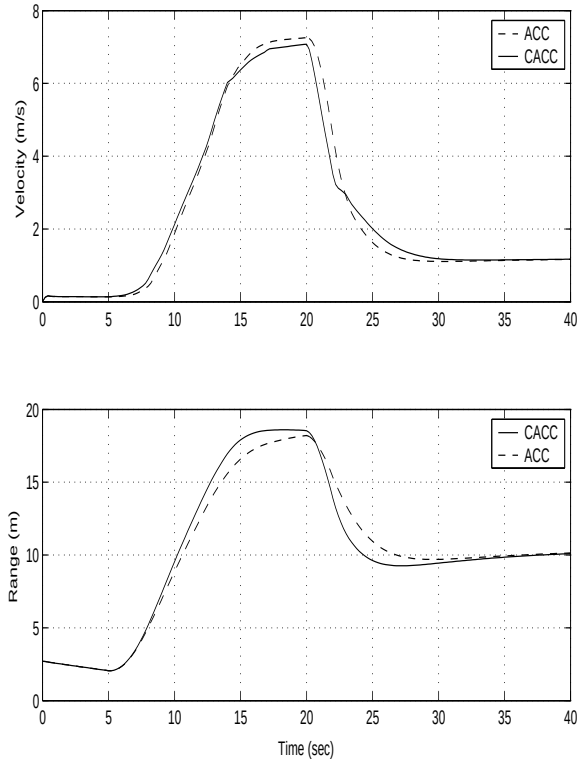

Figure 2.6: OVC: Range and velocity for ACC and CACC vehicles in braking scenario

1. *Average Velocity of Main Lane Vehicles*

   The average velocity indicates the average trip time a vehicle spends on the simulated segment of highway, therefore a high average velocity for main lane vehicles means an efficient transportation system.

2. *Braking Effort of Main Lane Vehicles*

   The maximum braking effort over the duration of the trip (the absolute value of the minimum negative acceleration) is used as the indication of the cost for the corresponding efficiency performance. The maximum braking effort tells us how hard a vehicle has to brake for the disturbance of the traffic. Too large braking effort is dangerous, causes passenger discomfort, and sometimes not achievable. Since the only major disturbance for all main lane vehicles is merging, the maximum braking for most vehicles is directly or indirectly due to the merging vehicles.

3. *Queue length of Waiting-to Merge Vehicles*

   The above two variables indicate the performance of the main lane vehicles. The main lane traffic should be disturbed as less as possible by the merging, but system design should not sacrifice the merging lane either. Since we do not model the dynamics of merging vehicles or the geometry of the ramp, one of the best variables we can use to indicate the merging lane efficiency is the length of the queue of waiting vehicles. For the same input flow rate of main lane and

merging lane, a good control system design shortens the queue.

We study the impact of the following three categories of independent variables on the performance variables described above:

1. *ACC or CACC*

   It is equivalent to the indicator variable of system being with or without vehicle-vehicle/roadside-vehicle communication.

2. *Market Penetration of ACC/CACC Vehicles*

   A system with half of vehicles controlled by ACC certainly performs differently to a system with all vehicles being ACC. We observe this difference via simulation. Notice in this thesis we never mix ACC with CACC vehicles. In the mixed cases, the vehicles are composed of either ACC vehicles mixed with human drivers, or CACC vehicles mixed with human drivers. Whenever we say the mixed case of $X\%$ of ACC vehicles, by default there are $(100 - X)\%$ human-driven vehicles. The same is true for CACC vehicles.

3. *Aggression of Controller*

   As stated above the CACC controller uses the same control structures as the ACC controller, only that the CACC controller tracks a modified desired range when receiving a warning message from a "relevant" vehicle. Therefore obviously the aggression of the controller (2.5) plays a critical role in determining

the time-response characteristics and the control effort in both systems. We adjust the controller gains $\Lambda + K$ and $\Lambda \cdot K$ in equation (2.5) and compare the performance of the system with strong gains to that of the system with weak gains.

System Validation

As presented above, all of the models we applied in the over-all simulation system are taken from published work, each being well analyzed and validated individually or directly from measurement, e.g. the human driver model, the gap acceptance model, and the braking capability distribution. However never before were they integrated to form one system to simulate all aspects of the highway behavior. Therefore before conducting any simulation, we need to first validate the overall system.

We run the simulation in the "all-human" scenario, i.e. all automated control components (ACC or CACC) are turned off. The flow rate of the merging lane is set to 0. The system is thus no more than a simulation of a one-lane straight highway segment without any entrances or exits except for at the ends. We compare the simulated results with the measurement data of real highway taken from the freeway Performance Measurement System (PeMS) [3]. [1] The PeMS system collects the real-time measurement data of major highways in California with loop detectors and stores it in database. We compare the flow-density (Q-K) relations of the two sets of data

[1] PeMS is a collaborated project of the Department of Transportation of California, University of California at Berkeley, and California PATH.

in Figure 2.7. The measurement data we use here is arbitrarily taken from one lane of highway I-80E at sensor 313111, which is located in city of Sacramento, on the day March 15, 2003. Similar results are observed when other PeMS measurement data are used. Based on the conclusion of [33], we perform two-portion linear fitting on the data, with the left portion representing the un-congested flow-density relation while the right portion representing the relation in the queues formed on highway (compare with Figure 4 of [33]). Since there is not an freeway exit in our simulation besides the end point at 700 meters, we cannot observe the "queue discharged" Q-K behavior in [33]. The results show that the simulation data is quite close to the measurement data. They both obey the two-portion linear model, and the maximizing density values are quite close. The peak flow values differ by about 8%. The result shows that the overall simulation system is a reliable tool to study the behavior of the highway traffic.

The error could come from any component of our model, and from our ignorance of lane-changing — we use the measured data of one lane of the 4-lane I-80E highway instead of the data of a real one-lane highway.

Having validated the system, we now study the performance of the HMC. In all the following sections, the initial conditions are the same. The input flow rate for the main lane is 2000 vehicles/lane/hour and the flow for the merge lane is 600 vehicle/lane/hour, and the initial velocity of the main lane vehicles are assigned as described in section 2.3.2. We simulate the system for long enough time for 30 minutes

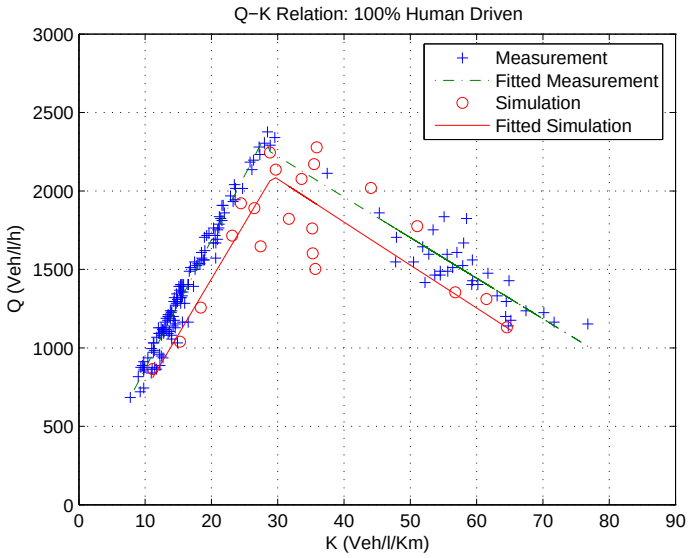

Figure 2.7: System Validation for HMC: Comparison of Simulation Data with Measurement Data from PeMS

trip time of vehicles, thus typically more than 1,000 vehicles appear in the main lane.

Average Velocity for Main Lane Vehicles

In Figure 2.8, we compare the average velocity performance for four cases: CACC system with strong controller, CACC system with weak controller, ACC system with strong controller, and ACC system with weak controller. We expect to observe the role played by V-V/R-V communication as well as by controller aggressiveness in this set of results. [2]

The system simulated in Figure 2.8 has 100% market penetration of controlled vehicles (i.e. 100% CACC vehicles if the system is CACC and 100% ACC vehicles if the

[2]As described in 2.3.2 ACC and CACC controllers have the same structure and the difference lies in the desired range. Here, CACC system with strong controller and ACC system with strong controller basically means that the control gains are the same. The same is true for the weak controller also.

system is ACC). The figure shows the cumulative probability distribution function of the average velocity, therefore the y-value is the portion of vehicles with average velocity lower than abscissa. We observe clearly that in term of average velocity, strong controller performs better than weak controller (given that both are ACC or both are CACC), and for the same controller aggressiveness CACC system outperforms ACC system. For instance, the percentage of vehicles with average velocity smaller than 15 m/s is respectively about 10%, 25%, 40%, and 58% for CACC with strong controller, ACC with strong controller, CACC with weak controller, and ACC with weak controller.

CACC system performs better than ACC system due to the benefit of communication. With V-V/R-V communication the main lane vehicles know about the merging in advance, therefore the relevant vehicle brakes smoothly in longer response time. Its followers also have a smoothed brake period and their average velocity do not suffer so much from the merging disturbance as in the system where vehicles do not prepare for the merging. Strong controllers respond more promptly to the disturbance than weaker controllers. Therefore the more aggressively controlled vehicles are disturbed for shorter time, and disturbance propagate to less of its following vehicle. The system-wide behavior of average velocity does not suffer so much as when weaker controller is applied.

Figure 2.9 is the empirical cumulative distribution function of the average velocity for different market penetration of CACC. It is evident that the curves for higher

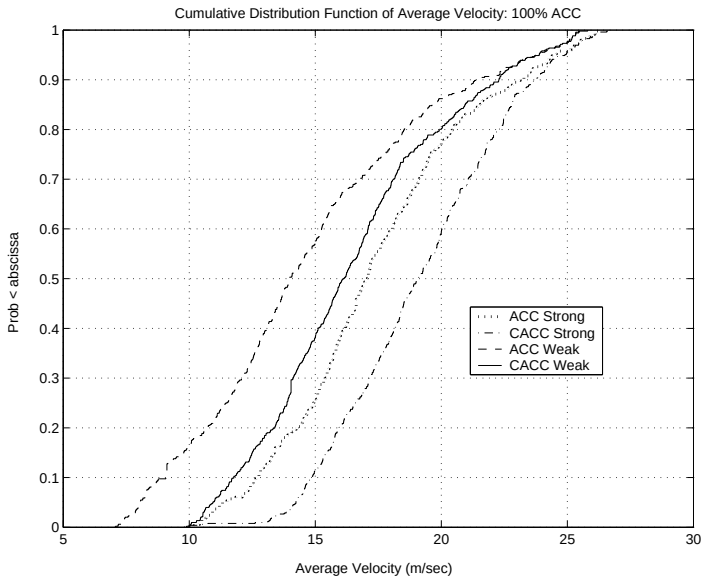

Figure 2.8: HMC: CDF of Average Velocity (Market Penetration = 100%)

percentage of CACC vehicles lie below the curves for lower percentage. This means that lower percentage case has more vehicles running with average velocity lower than a given value. For example, when 20% of all vehicles are CACC, there are about 60% vehicles having average velocity lower than 10 m/s, while almost no vehicle drives slower than 10 m/s if all of the vehicles are CACC (100% curve). The highest velocity in all cases shown is close to about 28m/s. This is because a vehicle generally has highest velocity possible when it enters the simulation, where we set the initial velocity to around 28.9 m/s (See section 2.3.2). For some lucky vehicles the average velocity is about the same as the initial velocity, but most vehicles have to slow down once they are in the highway segment because of the merging disturbance. Similar effects of market penetration is observed in the ACC system. These results tell us

that system with higher market penetration of controlled vehicle benefits all vehicles on highway by saving trip time. The result agrees with intuition since with higher percentage of controlled vehicle, the beneficial impact brought by ACC or CACC is larger.

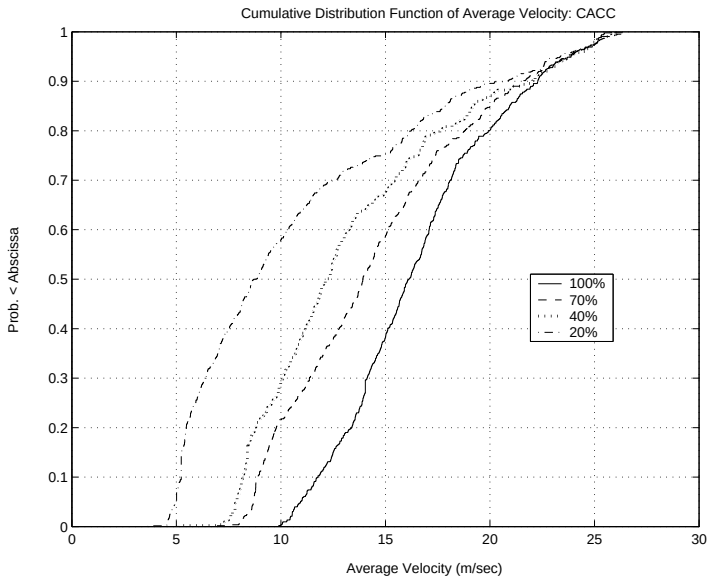

Figure 2.9: HMC: CDF of Average Velocity of CACC vehicles

Maximum Braking Effort of Main Lane Vehicles

Figure 2.10 compares the same four cases as in Figures 2.8, but focuses on the maximum braking effort, i.e. the minimum negative acceleration exerted by a vehicle in the duration of simulation. Shown here are the CDF's of the maximum braking effort. The main observation is that for given controller, integration of V-V/R-V communication saves braking effort, while for a given system (either with or with-

out communication), weak controller utilizes less braking effort than strong controller (except for some small braking effort values). For example, the percentage of vehicles executing maximum braking effort larger than 1.5 m/s/s (minimum negative acceleration smaller than -1.5 m/s/s) is approximately 8%, 20%, 30%, and 50% for CACC with weak controller, ACC with weak controller, CACC with strong controller, and ACC with strong controller.

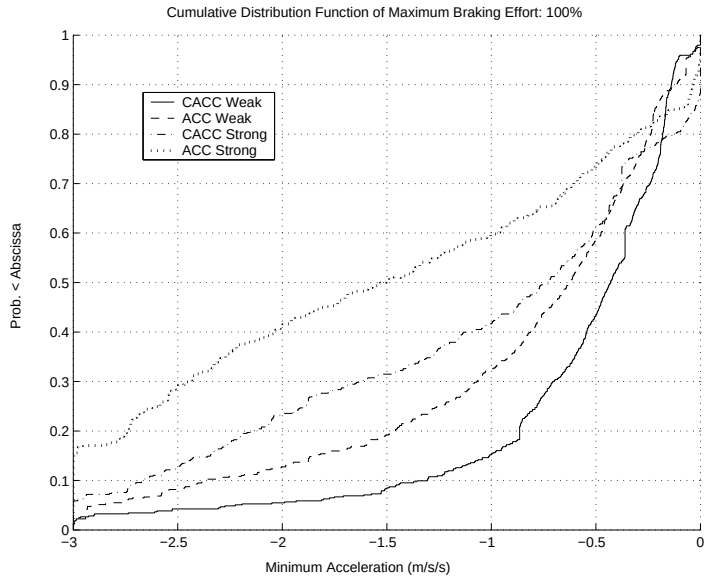

Figure 2.10: HMC: CDF of Maximum Braking Effort (Market Penetration = 100%)

Figure 2.11 shows the empirical CDF of maximum braking effort for different market penetration of CACC vehicles. It could be regarded as the cost of the efficiency performance shown in Figures 2.9. It is clear that if better controlled vehicles enter the traffic, the less the braking effort is. This is because, as shown in the figure, the curves for higher percentage cases are below the curves for lower percentage cases. For

example, in 20% CACC vehicle case, more than 85% of all vehicles have maximum braking effort larger than 1 m/s/s (minimum negative acceleration smaller than -1 m/s/s), while only about 40% vehicles experience maximum braking effort larger than this value when 100% of vehicles are CACC. Similar influence of market penetration is observed for ACC system. Combining these results with those shown in Figure 2.9, we conclude that higher market penetration of ACC/CACC vehicle always brings advantage over lower market penetration in both the "gain" and the "cost".

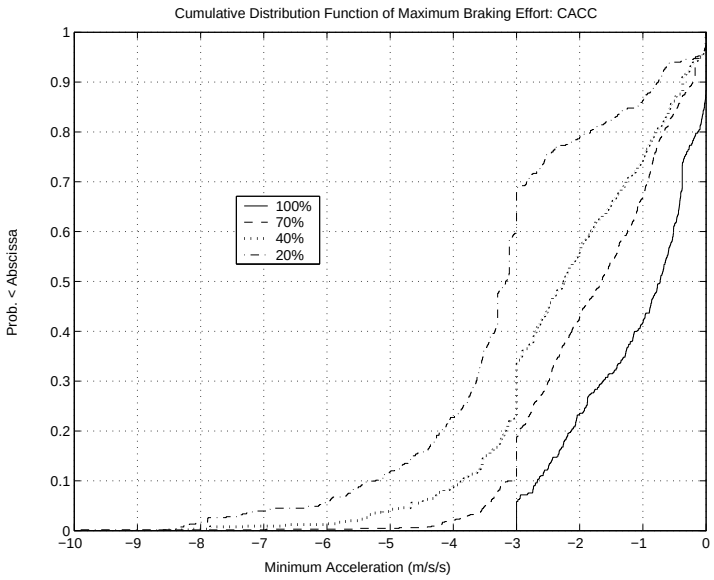

Figure 2.11: HMC: CDF of Maximum Braking Effort of CACC vehicles

Figure 2.12 shows the average maximum braking effort vs. percentage of controlled vehicle for various cases. The former value is obtained by averaging the maximum braking effort of all main lane vehicles appeared in the simulation. Evidently, for both ACC and CACC systems, the higher the market penetration, the smaller the average

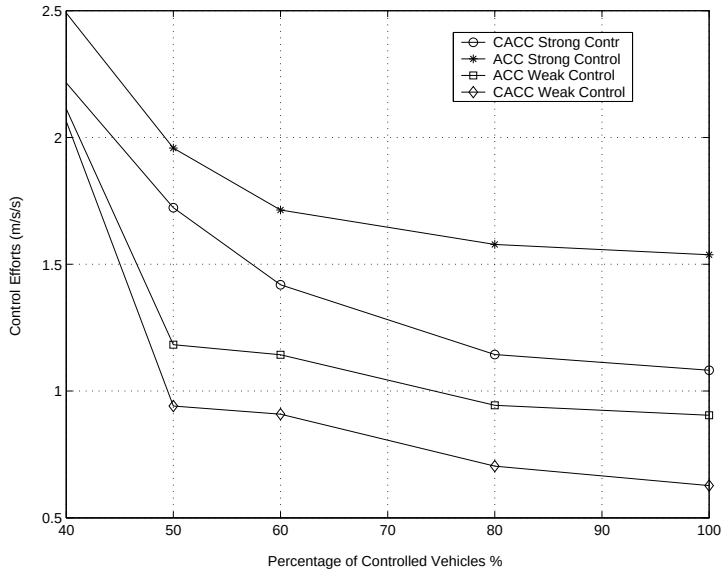

Figure 2.12: HMC: Average Maximum Braking Effort

braking effort. With the same percentage of controlled vehicle, CACC system spends less braking effort than ACC system. Also for the same market penetration, either in a CACC system or ACC system, a weak controller saves control effort over a strong controller.

Communication makes the CACC vehicle aware of the merging in advance, therefore the irrelevant vehicles can ignore the merging vehicle and the relevant vehicle can brake smoothly in longer response time. The chance of abrupt braking is decreased, and the all the following vehicles brake less than in the scenario without communication. The result shown here agrees with the microscopic results shown in section 2.4.1. Combining the results shown in Figures 2.8, 2.10, and 2.12, we can see that communication makes the highway traffic more efficient with lower cost.

For a given disturbance a stronger controller responds more aggressively, sometime over-responds. Therefore although it makes the system respond faster to the disturbance, as shown in Figure 2.8, the benefit is gained with cost on control effort. Hence we have a tradeoff between efficiency and passenger comfort/safety. [3]

One cannot draw conclusion about the relation of cases of CACC with weak controller and of ACC with strong controller cases, although the former performs better in the particular tests shown here.

Trajectories of Main Lane Vehicles and Shock Wave

Figure 2.13 is the trajectories of vehicles in the main lane between 900 second and 1000 second for ACC and CACC HMC simulations. It shows the position of vehicles relative to the starting point at a given instant. Each curve corresponds to the trajectory of one vehicle. The merge-in point is at 500 meters. The horizontal line at 500 meter represents queued merging vehicles. Merging vehicles can be identified by a curve which lies entirely above this line. In both of these two cases we have 100% controlled vehicles on highway. In the period between 910 seconds to 970 seconds, we can see clearly a shock wave propagates in the opposite direction of the traffic in the ACC system. In the shockwave, each vehicle travelling between approximately 150 meters and 350 meters has to apply a brake to slow down due to the merging vehicle. All the vehicles lie in the wave are clustered together with

[3]Notice the average velocity cannot increase unboundedly with stronger and stronger controller due to acceleration saturation and vehicle dynamics.

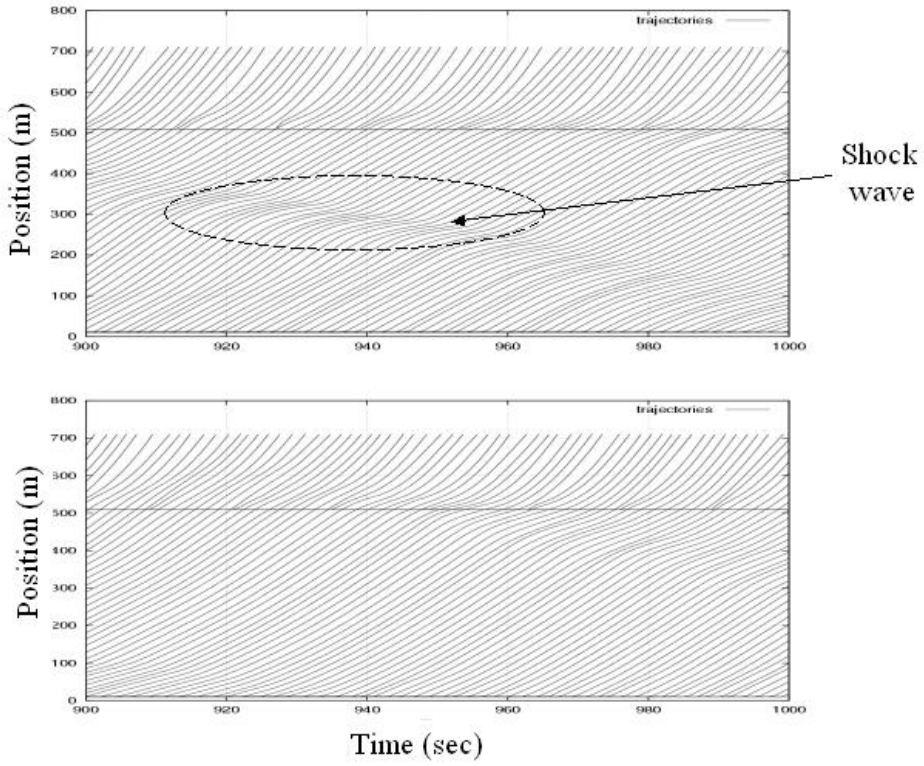

Figure 2.13: HMC: Trajectories of Vehicles, Top: ACC, Bottom: CACC

much smaller range relatively the the scenario before the merge. About 10 seconds later, the system recovers and vehicles speed up to usual velocity, and the shock wave propagates upstream until the system recovers at around 970 second. However this shock wave is smoothed in the bottom figure. Notice that the initial conditions for simulations are the same for the two cases. This type of phenomena is common in our simulation results. It confirms the advantage of CACC system over ACC system in terms of average velocity and braking effort. The reason lies in the following two facts:

- In the CACC system, the relevant main lane vehicle receives the warning message. Hence, it can brake smoothly to increase the gap to the preceding vehicle.
- When the merging vehicle enters the main lane, the gap is already large enough for safety, and the main lane vehicles behind it do not need to brake hard compared to the braking efforts required in a ACC system.

Queue Length in Merging Lane

Figure 2.14 shows the length of the queue of the waiting vehicles in the merge-in lane from 600 to 1000 second. Results for four cases are plotted here. The top curve is for 50% ACC main lane vehicles. In the middle, two curves standing for 100% ACC and 50% CACC are quite close to each other. The bottom curve is for 100% CACC. The queue length keeps increasing because we intentionally inject a large flow rate of the entering vehicles to stress the scenario simulated. Figure 2.15 shows the time-

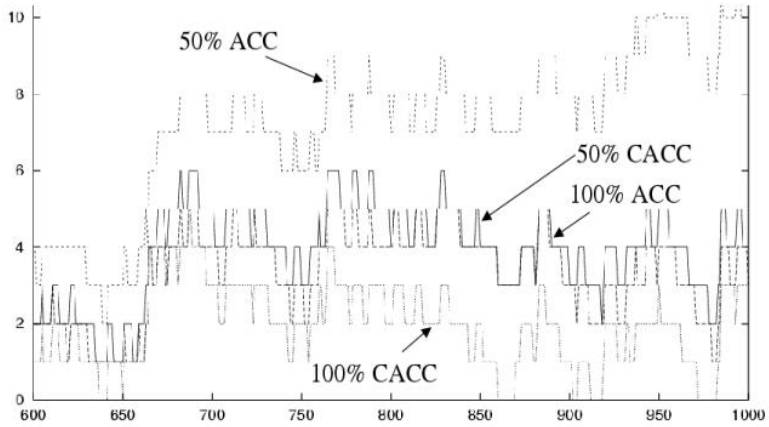

Figure 2.14: HMC: Queue Length of Waiting-to-merge Vehicles

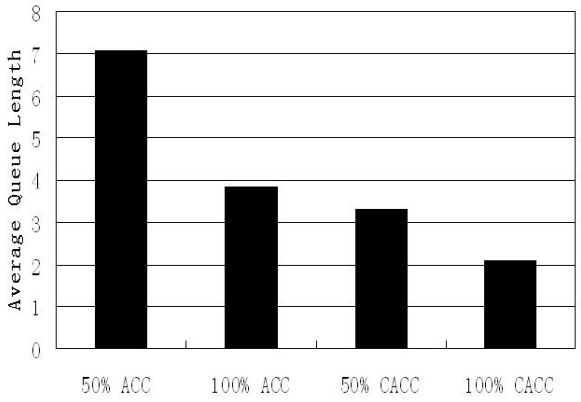

Figure 2.15: HMC: Average Queue Length of Waiting-to-merge Vehicles

averaged queue length for the same four cases. Clearly, system with larger percentage of ACC (CACC) vehicles has shorter waiting queue. For the same percentage, the queue in CACC highway is up to 4 vehicles shorter than in ACC highway. Due to the communication, the relevant main lane vehicles have longer time to make a good gap in front. By the time the merging vehicle arrives at MP, it is more likely to see an acceptable gap and merge in than reject the gap and wait. Therefore in average

the merging cars wait for shorter time in CACC highway. Communication enhances the efficiency of the system.

2.5 Summary

We built mathematical models of vehicles under adaptive cruise control and cooperative adaptive cruise control. We implemented the models in two simulations to comparatively study the performance of the two control schemes on both microscopic and macroscopic level. A few conclusions drawn from the simulation results are listed below.

- Vehicle-vehicle/Roadside-vehicle communication brings benefit to the highway traffic in increasing average velocity, decreasing braking effort, smoothing shock wave, and shortening the queue length of merging vehicles. Given all other conditions same, A CACC system almost always outperforms an autonomous ACC system in efficiency with less cost.

- Higher market penetration is beneficial for both ACC and CACC systems in terms of average vehicle velocity, braking effort, and merging queue length.

- With other conditions same, an aggressive controller design increases the average velocity, therefore enhances the efficiency. However a weaker controller saves braking effort.

The many encouraging results justify the motivation of implementing V-V/R-V communication into vehicles control applications. The important work now is to design protocols as well as hardware to realize such communication with high Quality

of Service (i.e. low probability of failure, short time delay) and low cost (i.e. low channel occupancy, low cost or no need for infrastructure construction, low increase in the vehicle price, etc.). Subsequent chapters of the thesis will explore these issues.

Better modeling of the sensors used in the simulation should be conducted and the simulation should be repeated. In particular, one should further study the effect of communication system on scenarios like the braking scenario in OVC.

Chapter 3

Vehicle-to-vehicle Messages in Dedicated Short Range Communication (DSRC)

Dedicated Short-Range Communications (DSRC) is 75 MHz of spectrum at 5.9 GHz allocated by the Federal Communications Commission (FCC) to "increase traveller safety, reduce fuel consumption and pollution, and continue to advance the nation's economy [19]." This promising development is designed to support vehicle-to-vehicle and vehicle-to-infrastructure communication using a variant of the IEEE 802.11a technology [2]. DSRC will support safety-critical communications, such as collision warnings, as well as other valuable Intelligent Transportation System applications, such as Electronic Toll Collection (ETC), real-time traffic advisories, digital map up-

date, etc. The versatility of DSRC greatly enhances the likelihood of its deployment by various industries and adoption by consumers.

The 2004 FCC ruling [20] specifies DSRC will have six service channels and one control channel. The control channel is to be regularly monitored by all vehicles. The FCC has recognized safety messages and "safety of life" messages. Safety of life is to have the highest priority, whether originated by vehicles or roadside transmitters. The non-safety data transfers have the lowest priority. Given these requirements, we adopt the reasonable assumption that safety communications take place in the control channel[1]. Further, a licensed roadside unit could use the control channel to inform approaching vehicles of its services (often non-safety applications) and conduct the actual application in one of the service channels. For example, a roadside unit could announce a local digital map update in the control channel and transfer this data to interested vehicles in a service channel.

This chapter explores the feasibility of sending safety messages from vehicle to vehicle in the DSRC control channel. We begin by specifying appropriate latency, reception probability, and efficiency metrics for inter-vehicle safety communications. With these quality of service metrics identified, appropriate Layer 2 MAC protocols are then proposed and evaluated.

We evaluate our protocol with both simulation and analysis methods. In the evaluations nodes only send safety messages in the control channel. We do not study any

[1]However, the techniques described in this chapter could be applied to service channel monitored by all vehicles.

non-safety messaging specifically. We use the fraction of time occupied by the safety messages as a performance metric to (indirectly) show the impact safety messages have on non-safety messages (details in 3.2.2). We believe that generally the more time is left to non-safety service announcements in the control channel, the easier it is to design non-safety communication. In the rest of the chapter, all messages refer to safety messages, and the channel refer to the control channel by default.

In both simulation and analysis we use the simple collision model for the interference between packets, i.e., whenever two packets within the interference range of one common receiver transmit at the same time, both packets collide and will be dropped. Collision model is a widely-used simple model in MAC protocol analysis, e.g. in [15], and [31], [69]. It is the model implemented in network simulator NS-2 [5], based on which we develop a DSRC simulator. We do not consider cumulative interference.

Safety messages are time sensitive. When vehicles send safety messages to each other while travelling at high speed, can they be received with small delay and high probability? Can DSRC handle time and loss sensitive vehicle-vehicle communication? Can it do so without infrastructure, i.e., in *ad hoc* setting? Will there be enough room on the control channel for the other non-safety communications required by DSRC, e.g., service announcements? By the end of the chapter we have an answer to these questions.

The rest of the chapter is structured as follows. Section 3.1 reviews the relevant literature and technologies. Section 3.2 is the problem formulation, Section 3.3

Table 3.1: Typical DSRC Data Traffic Requirements

Applications	**Packet Size(bytes) /Bandwidth**	**Allowable Latency (ms)**	**Network Traffic Type**	**Message Range(m)**	**Priority**
Intersection Collision Warning/ Avoidance	∼100	∼100	Event	300	Safety of Life
Cooperative Collision Warning	∼100/ ∼10Kbps	∼100	Periodic	50 - 300	Safety of Life
Work Zone Warning	∼100/ ∼1Kbps	∼1000	Periodic	300	Safety
Transit Vehicle Signal Priority	∼100	∼1000	Event	300 - 1000	Safety
Toll Collection	∼100	∼50	Event	15	Non -Safety
Service Announce- ments	∼100/ 2Kbps	∼500	Periodic	0 - 90	Non -Safety
Movie Download (2 hours of MPEG 1): 10 min. download time	>20 Mbps	N/A	N/A	0 - 90	Non -Safety

discusses the protocol design, Section 3.4 presents the mathematical analysis of the protocols, and Section 3.5 shows the simulation results. Section 3.6 summarizes the chapter.

3.1 Literature Review and Related Technologies

In ad hoc vehicular networks, TDMA, FDMA, or CDMA are difficult due the need to dynamically allocate slots, codes, or channels without centralized control. We base our designs on random access [69]. ALOHA [10] and CSMA [69] are the earliest studied random access protocols. MACA [41], MACAW [14], FAMA and its variants [31] all use the RTS/CTS scheme. Our communication is broadcast (see Section 3.2) therefore we cannot use RTS/CTS.

In the literature there are more complex protocols that support QoS. But none of them are suitable for vehicle safety messaging. HIPERLAN/1 [12], "Black Burst" [65], and the Enhanced Distributed Coordination Function (EDCF) of IEEE 802.11e [76] are all designed to reduce access delay of time-sensitive communications. The HIPERLAN/1 and Black Burst approaches have no scheme to combat hidden terminals. In EDCF, when the number of contending packets of equal priority is large the probability of collision is high. This is the case for vehicle safety communications (Section 3.2).

Reference [56] reviews the existing variants of the 802.11 DCF to support QoS. Its authors conclude that the design of a mechanism to provide predictable QoS in an 802.11 network is still an open problem. We use a different definition of QoS (Section 3.2). Reference [87] gives an overview of DSRC applications and assesses the characteristics of the IEEE 802.11 MAC and PHY layers in this context. It is anticipated that the current 802.11 specifications will need to be suitably altered to meet the QoS requirements of DSRC applications.

Cellular networks achieve time sensitive communication to vehicles moving at high speeds. However, this is accomplished with the aid of base stations. Cellular base stations are significantly more expensive than their supposed DSRC equivalent, i.e., 802.11 access points. Moreover, cellular handles only infrastructure to mobile communication.

3.2 Problem Formulation

To evaluate the feasibility of sending vehicle-vehicle safety messages, the first task is to identify key operational characteristics of the system under study, specifically the transmission of safety communications in an automotive DSRC system. The second task is specifying appropriate Quality of Service (QoS) metrics that suitably assess the feasibility of vehicular safety applications over DSRC. As discussed below, these metrics characterize the latency and probability of reception of individual packets, as well as the aggregate channel efficiency.

3.2.1 The DSRC Safety Environment

We begin with an assessment of the offered safety traffic. When the offered traffic is large, reliability, latency, and channel efficiency deteriorate. In wired networks offered traffic is measured by the total bits/second produced by all the senders. However, in wireless networks, a more appropriate measure of offered traffic is bit-meters/second [32], i.e., a network able to transmit a bit 100 meters, may not be able to transmit the same bit 200 meters. Therefore the offered traffic depends on the safety message rate (messages/sec), size (bytes/message), message range (meters), and the density of vehicles producing these messages.

A vehicle at high freeway speeds (90 mph) moves 2 meters within its lane in 50 msec. This is usually not a significant movement at high speed. Thus messages repeating faster than once every 50 msec are unlikely to provide significantly new

Table 3.2: Offered Traffic Parameter Ranges

Message Generation Interval (msec)	50, 100, 200	
Packet Payload Size (Bytes)	100, 250, 400	
Data Rate (Mbps)	6, 9, 12, 18, 24, 36, 48, 54	
Average Vehicle Distance (m)	10 (jammed)	30 (smooth)
Message Range (m)	10-100	30-300
Lane Number	4, 8	

information. On the other hand an update slower than once every 500 msec is probably too slow. Driver reaction time to stimuli like brake lights can be of the order of 0.7 seconds and higher. Thus if updates come in slower than every 500 msec, the driver may realize something is wrong before the safety system. This would make the driver think the safety system not effective, and is undesirable for deployment. Message sizes have been chosen to permit sender or receiver location as per the SAE J1746 standard, GPS, NTCIP hazard codes, and standard protocol headers to be included. Safety messages are usually short. Communication is more difficult at high vehicle densities. The 10 meters per vehicle represents the jammed highway. The 30 meters per vehicle represents the highway at capacity. Likewise, the 4 to 8 lane range spans the usual to large roads.

Safety application designers would prefer large message ranges to smaller ones. On the other hand large message ranges make network design more difficult. The 300-meter message range corresponds to the comfortable stopping distance of a high speed car. When the road is jammed, neighboring cars will be much closer. Therefore it should not be necessary to send safety messages over the same distance. We assume

a top range of 100 meters for jammed roadways, or approximately 10 inter-vehicle distances.

Table 3.2 summarizes above discussions and gives ranges of the parameters determining the offered traffic. Our evaluation is based on these ranges.

3.2.2 Quality of Service Metrics for DSRC Safety Messages

Reliable communication in networks has typically meant retransmitting a message till it is acknowledged by the recipient(s). This is appropriate for file transfers since even one missing byte may render the entire file unusable. Thus reliable transmission protocols like TCP acknowledge each byte and retransmit any packet not appropriately received. For DSRC, although reliability is necessary, the short useful lifetime of safety messages discourages against an acknowledgement/retransmission paradigm. Instead of designing for perfect reliability, we argue that a more useful goal is to deliver a safety message within its (short) lifetime with very high probability. If a safety application is generating updates every 100 msec and a particular message has still not been received 100 msec after it was created, a new message, obsoleting the old one, will already have been created. There appears to be little value in attempting to re-deliver an outdated message when a new message could be sent instead. Therefore we have focused on the design of a local-area communication service delivering messages within their lifetime with high probability. The lifetime is the delay requirement.

If the active safety systems on the vehicle assist the driver rather than substitute for her, we think probabilities of reception failure of 1/1000 to 1/100 per message is adequate. In any case, most safety messages should be consumed by an estimator. For example, the warnings from the slowly moving or stopped vehicle should be consumed by an estimator of the position of the damaged vehicle relative to the receiver, conditioned on all received messages and possibly sensor information as well. Since an estimator leverages correlations in the time series of messages, it is usually robust to the loss of messages, unless the losses occur in bursts.

We think of the delay and reception probability as the QoS requirement of the message. To capture both of them, we define the Probability of Reception Failure (PRF) as the probability a randomly chosen receiver within the message range fails to receive a safety message within a given time delay. Formally, let $\mathcal{N}$be the set of all nodes in the network, $T(m)$ be the indicator function of the transmission of a safety message from a node $m \in \mathcal{N}$, $R_m(n)$ be the indicator function of the successful reception of a safety message from a node $m \in \mathcal{N}$ by a node $n \in \mathcal{N}$, $D_{m \to n}$ be the delay between the generation of a safety message at node m and the reception of the message by node n, and $S(m, L)$ be the set $\{n \in \mathcal{N} : ||\overline{nm}|| = L\}$. Then we have the following definition.

Definition 3.1. The probability of failure $PRF(L, \tau)$ of a vehicular network composed of nodes in set $\mathcal{N}$, for a given transmitter-receiver distance L, and a given delay τ, is the following

$$PRF(L,\tau) \triangleq \sum_{m\in\mathcal{N}} \sum_{n\in S(m,L)} P\left((R_m(n)=0)\cup(D_{m\to n}>\tau)|T(m)=1\right) P\left(T(m)=1\right)$$

In Appendix B we will see the interference experienced by a receiver is larger when it is further from the transmitter. The worst case therefore is when the transmitter-receiver distance is the message range. Also we require the delay to be the lifetime of the safety message. Therefore all the PRF results we present in this chapter are $PRF(Message\_Range, Message\_Life\_Time)$. Our evaluation focuses on senders that generate periodic or Poisson distributed messages.

We assume that the safety messages are to be sent on the control channel. However, the control channel also has to communicate other non-safety messages for the remaining channels to be useful. Therefore the fraction of the control channel time occupied by safety messages (the channel efficiency) is important as well. This is measured by channel busy time (CBT). We consider the nodes within the interference range of each other. For a given time period T in the control channel, part of it is occupied by successful or unsuccessful safety messages, and the rest are either idle or used by the non-safety service announcements. Let T_{safety} be the total length of the time periods within T that is occupied safety messages. Then we have the following definition:

Definition 3.2. The channel busy time of a network is defined by:

$$CBT \triangleq \frac{T_{safety}}{T}$$

Notice that CBT is the channel busy time *for safety messages only*. The rest 1-CBT fraction of T may still be busy, but for non-safety messages which we do not model here. We use CBT to study the influence of safety messages to non-safety messages. In our simulation we take the whole simulation time as T, and average the CBT at various regions in the network to obtain the results.

Ideally, both PRF and CBT should be low.

Most safety messages produced by a vehicle are useful to many vehicles. For example, the stopped vehicle warning is useful to all approaching vehicles. Therefore we have focused on a broadcast service.

We have proposed a communication service able to execute at least the vehicle-vehicle communication without any roadside or base station infrastructure, i.e, an ad-hoc service. This would be good for deployment.

Since 802.11a radios are designed to transmit over distances of 200 to 300 meters, i.e., the upper end of the message range in Table 3.2. Hence we propose a single hop, local area communications service.

In summary, we propose a service to broadcast messages while meeting QoS requirements in vehicular ad-hoc local-area networks.

3.3 Protocol Design

3.3.1 General Considerations

In a wireless ad-hoc network there are two obstacles to the reliable reception of messages. If two transmitters within the interference range of a same receiver transmit concurrently, their transmissions collide at the receiver. The receiver does not receive either message. To combat this problem one designs a Medium Access Control (MAC) protocol, i.e., a set of rules by which a radio decides when to transmit its messages and when to keep silent. Secondly, even if there is no collision, the wireless channel may attenuate the transmitted power so much that it is swamped by thermal noise. This is combated by selecting the transmission energy to be high enough to reach all receivers within the message range with high probability, when there are no collisions.

Transmission energy is determined by transmission power, modulation, and error coding. DSRC radios are to be based on the 802.11a radio. In our evaluation we set the transmission energy control parameters to model the 802.11a radio transmitting over a 20 MHz channel at 5.4 GHz and focus on the MAC design problem, i.e., is there a MAC able to deliver safety messages with sufficiently high reliability and small delays? The stochastic modelling of the wireless vehicle-to-vehicle communication channel is an open problem. We use the deterministic Friis Free-space model for short distances and the Two-ray model for longer distances [44], i.e, if the distance between the transmitter and receiver antennas is d, then the power of the signal

decreases as d^2 when the distance is short and d^4 when the distance is large.

In unicast communication reliability is enhanced by policies based on receiver feedback, e.g. RTS/CTS, TCP, or WTP. These require the sender to learn the identity of its receiver(s). When there are many receivers or the network is highly mobile, meaning the set of receivers can change a lot, learning identities may itself require significant communication. Therefore we have chosen to evaluate ways to enhance reliability without receiver feedback.

Our strategies repeat each message without acknowledgement in combination with CSMA and its variants. Our repetition schemes are designed for overlay on CSMA. The following is the specifications of our various designs.

3.3.2 Protocol Specifications

Figure 3.1 is an illustration of the idea of repetitive transmission. It shows two transmitters within interference range of one receiver each generating a message at the same time. Every repetition of the message is a new packet. At each transmitter the protocol evenly divides the message lifetime into $n = \lfloor \frac{\tau}{t_{trans}} \rfloor$ slots, where $\lfloor x \rfloor$ is the maximum integer not greater than x, τ is the lifetime, and t_{trans} is the time needed to transmit one packet. We randomly pick any k ($1 \leq k \leq n$) slots to repetitively transmit the message. If any one or more of the packets corresponding to the message are received without collision at a given receiver, the message is received within its useful lifetime. On the other hand, the message fails if all of its transmitted packets

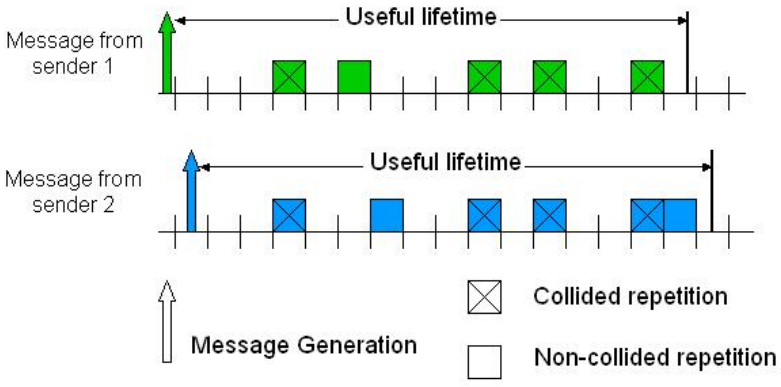

Figure 3.1: The Concept of Repetitive Transmission

are lost due to collisions.

Our protocols use two schemes to reduce PRF, repetition and carrier sensing. Carrier sensing is in the 802.11 MAC. In all the cases but two, our protocol is an overlay on the standard MAC like ALOHA [10] or Carrier Sensing [69]. We call this overlay the MAC extension layer.

Our MAC extension layer would lie between the Logical Link Control layer (IEEE 802.2) and the standard MAC layer. Its role is to generate and remove repetitions. The state machine of the MAC extension layer is shown in Figure 3.2. Upon receiving a message from the LLC, the MAC Extension transits from IDLE to REPETITION GENERATION state. In this state, the system schedules multiple repetitions of this message in the selected time slots within the message lifetime. Each repetition is an event with a slot number. All these events ordered by slot numbers form a queue called the Packet Event Queue. Once the queue is formed, the system transits back to the IDLE state. Whenever a packet event expires, the MAC extension transits

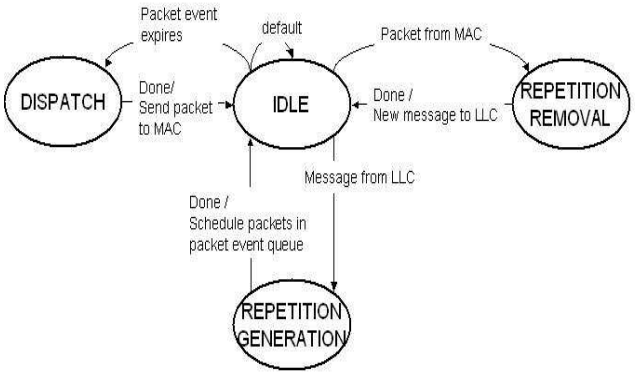

Figure 3.2: MAC Extension Layer State Machine

to the DISPATCH state and sends the packet down to the MAC. The system then transits back to IDLE. Whenever the MAC Extension receives a packet from the MAC, the system transits from the IDLE to the REPETITION REMOVAL state. If the message ID in this packet has not been seen before, it is from a new message, and the new message is passed up to the LLC. If the message ID in this packet has been seen before, the packet is eliminated.

The following are different protocols designed and evaluated by us. They share the same MAC extension layer. As described above, the protocols slot the time locally for each radio. All the protocols we design can be classified into two classes, synchronous and asynchronous. Synchronous protocols slot time to a global clock like in slotted ALOHA [10], i.e. a local slot in each radio starts at the beginning of one global slot of the same size. Asynchronous protocols do not globally slot the time.

1. Asynchronous Fixed Repetition (AFR)

   AFR is configured by setting the number of repetitions k. The protocol randomly selects k distinct slots among the total n slots in the lifetime. The protocol is called "fixed" because the packet is always repeated a fixed number of times, i.e., k. The radio does not listen to the channel (i.e. perform carrier sensing) before it sends a packet with AFR.

2. Asynchronous p-persistent Repetition (APR)

   The p-persistent repetition protocol determines whether to transmit a packet in each of the n slots in the lifetime with probability $\frac{k}{n}$, where k is again a configuration parameter of the protocol. The average number of transmissions of a message is k. However, for each realization the exact number of repetitions varies. Like AFR, the radio does not listen to the channel before it sends a packet.

3. Synchronous Fixed Repetition (SFR)

   This protocol is the same as AFR except that all the slots in all the nodes are synchronized to a global clock.

4. Synchronous p-persistent Repetition (SPR)

   The SPR protocol is the same as the APR protocol except for the synchronization of transmissions by all nodes into common slots.

5. Asynchronous Fixed Repetition with Carrier Sensing (AFR-CS)

   AFR-CS has its own MAC shown in Figure 3.3. AFR-CS generates the repetitions in the same way as in the AFR protocol. Whenever a packet is passed down from the MAC Extension, MAC transits from the IDLE to the CARRIER SENSING state. In the CARRIER SENSING state, the system checks the channel status using carrier sensing [69]. If the channel is busy, the system drops the packet and transits back to the MAC IDLE state. If the channel is idle, the system transits to the MAC TX state, and passes the packet down to the physical layer (PHY). It then transits back to the MAC IDLE state. In MAC IDLE, if PHY sends a packet up, the system transits to the MAC RX state and checks the integrity of the packet. If the packet is corrupted, it is dropped and the system transits back to the MAC IDLE state. Otherwise, the packet is passed up to the MAC Extension layer, and the system transits back to the MAC IDLE state.

6. Asynchronous p-persistent Repetition with Carrier Sensing (APR-CS)

   This is similar to AFR-CS except that the slots for message repetitions are selected in the p-persistent manner.

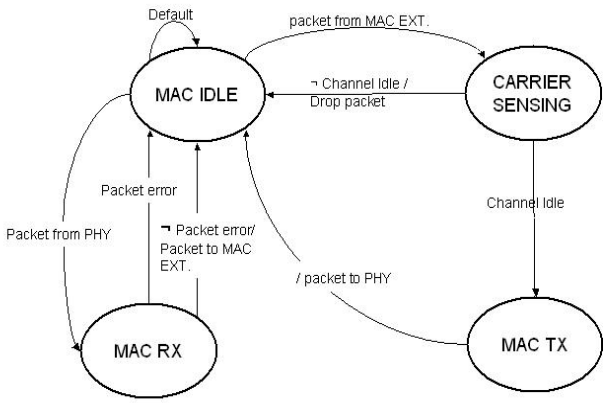

Figure 3.3: MAC Layer State Machine of the AFR-CS protocol

3.4 Mathematical Analysis

For the SPR and APR protocols we have developed mathematical expressions for the probability of reception failure (PRF). These expressions can be processed using Matlab.

We assume the message generation process is Poisson. Poisson process is models the superposition of large number of independent periodic processes with same interval and random starting time. [28] Hence it is a good model for the overall communication traffic generated by the many safety applications in one vehicle. We further assume the message generation processes of different vehicles are independent. Then the overall message generation process of all vehicles within interference range of any receiver is also Poisson. [28] However the network traffic is composed of the repetitions of the messages. This is not Poisson. For example, in Figure 3.1, the process of the arrows is Poisson, but that of the rectangles is not. Hence our analysis is different from others in literature such as [15] and [69].

Table 3.3 lists the notation used in the mathematical analysis.

The main results are Theorem 3.9 for SPR and Theorem 3.10 for APR. These give tight upper and lower bounds on PRF. The number of interferers is critical to the PRF. Appendix B describes how we calculate the number of interferers for a given transmitter/receiver pair.

Table 3.3: Notations in Protocol Analysis

n	Maximum possible number of repetitions in lifetime, total slots number
k	Average number of repetitions for a message
p_j	The jth repetition packet for a message
S	Event that at least one of the repetitions succeeds within the lifetime
S_j	Event that the p_j is successful at a randomly chosen receiver
t_j	The instant that the jth repetition starts
τ	Lifetime of a message
T_j	Event that there is at least one interfering message generated in $(t_j - \tau, t_j]$
λ	The rate of message generation at each individual node
m	Total number of interfering nodes around a receiver

Probability of Reception Failure: SPR protocol

We prove the main result, Theorem 3.9, utilizing a series of lemmas. The lemmas and main theorem are listed below. The proof of the main theorem is presented in this chapter, while proofs of lemmas are in the appendix.

Lemma 3.3 and Lemma 3.4 lower bound the PRF.

Lemma 3.3. ***PRF for One Single Repetition in the SPR Protocol***

For all $1 \leq j \leq k \leq n$*, the PRF of* p_j *at any randomly chosen receiver is given by*

$$P(\neg S_j) = 1 - e^{-m\lambda\tau\frac{k}{n}}, \tag{3.1}$$

Proof. See Appendix A.1 □

Lemma 3.4. ***Lower Bound on the PRF for Multiple Repetitions in the SPR Protocol***

Suppose p_1,p_2,...,p_r are any r repetitions transmitted for one message, then the probability of failure of all of them is greater than the product of the probability of failure of each one of them. Formally,

$$P(\neg S_1 \wedge \ldots \wedge \neg S_r) > \prod_{j=1}^{r} P(\neg S_j) = (1 - e^{-m\lambda\tau\frac{k}{n}})^r, \forall 1 \leq r \leq k \leq n \tag{3.2}$$

Proof. See Appendix A.2 □

Lemmas 3.5 through 3.8 provide the upper bound on the probability of reception failure. This turns out to be quite close to the lower bound. The bounds are pretty tight.

Lemma 3.5. *The PRF of a single repetition p_j for the SPR protocol, conditioned on the event T_j, i.e. there is at least one other message generated in $(t_j - \tau, t_j]$, is as follows.*

$$P(\neg S_j | T_j) = 1 - e^{-m\lambda\tau\frac{k}{n}} + e^{-m\lambda\tau}$$

Proof. See Appendix A.3 □

From lemmas 3.3 and 3.5 we can obtain the following.

Corollary 3.6. *1.*

$$P(\neg S_j) < P(\neg S_j | T_j)$$

.

2. When the total transmission rate is high, i.e. $m\lambda \gg 1$,

$$P(\neg S_j) \approx P(\neg S_j | T_j)$$

.

Lemma 3.7. *For all* $1 \leq r \leq k \leq n$,

$$P(\neg S_r | \neg S_1 \wedge \ldots \wedge \neg S_{r-1}) < P(\neg S_r | T_r) \tag{3.3}$$

where T_r *is the event that there is at least one message generated in* $(t_r - \tau, t_r]$.

Proof. See Appendix A.4 □

Lemma 3.8. ***Upper-Bound on the PRF for Multiple Repetitions in the SPR Protocol***

For all $1 \leq r \leq k \leq n$,

$$P(\neg S_1 \wedge \ldots \wedge \neg S_r) < \prod_{j=1}^{r} P(\neg S_j | T_j) = (1 - e^{-m\lambda\tau\frac{k}{n}} + e^{-m\lambda\tau})^r \tag{3.4}$$

Proof. The inequality follows from the chain rule, Lemma 3.5, and Lemma 3.7. □

Combining the bounds provided by Lemmas 3.4 and 3.8, we prove the main theorem as follows.

Theorem 3.9. ***Bounds on the PRF of the SPR Protocol***

The PRF of the SPR protocol satisfies the following inequality.

$$\left(1 - \frac{k}{n} e^{-m\lambda\tau\frac{k}{n}}\right)^n < P(\neg S) < \left(1 - \frac{k}{n} e^{-m\lambda\tau\frac{k}{n}} + \frac{k}{n} e^{-m\lambda\tau}\right)^n \tag{3.5}$$

Proof. Let the random variable K denote the total number of packets transmitted for a randomly chosen message. From lemmas 3.4 and 3.8, the PRF for the message conditioned on $K = r$ satisfies the following inequality.

$$\begin{aligned} & (1 - e^{-m\lambda\tau\frac{k}{n}})^r \\ < \; & P(\neg S | K = r) \qquad (3.6) \\ = \; & P(\neg S_1 \wedge \ldots \wedge \neg S_r) \\ < \; & (1 - e^{-m\lambda\tau\frac{k}{n}} + e^{-m\lambda\tau})^r \qquad (3.7) \end{aligned}$$

Now let p and q be defined as in equations (3.8) and (3.9) below.

$$p = (1 - e^{-m\lambda\tau\frac{k}{n}} + e^{-m\lambda\tau}) \qquad (3.8)$$

$$q = (1 - e^{-m\lambda\tau\frac{k}{n}}) \qquad (3.9)$$

Then equation (3.7) becomes

$$q^r < P(\neg S | K = r) < p^r$$

We show below the proof of the left-hand side of the inequality (3.5) for simplicity of presentation. The proof of right-hand side follows the exact steps except for the changing of direction of inequality and replacing q with p.

$$
\begin{aligned}
P(\neg S) &= \sum_{r=0}^{n} P(\neg S|K=r)P(K=r) \\
&> \sum_{r=0}^{n} q^r P(K=r) \\
&= \sum_{r=0}^{n} q^r \begin{pmatrix} n \\ r \end{pmatrix} \left(\frac{k}{n}\right)^r \left(1-\frac{k}{n}\right)^{n-r} \\
&= \sum_{r=0}^{n} \begin{pmatrix} n \\ r \end{pmatrix} \left(q\frac{k}{n}\right)^r \left(1-\frac{k}{n}\right)^{n-r} \\
&= \left(1-\frac{k}{n}+q\frac{k}{n}\right)^n \\
&= \left(1-\frac{k}{n}e^{-m\lambda\tau\frac{k}{n}}\right)^n
\end{aligned}
$$

In the above $\begin{pmatrix} n \\ r \end{pmatrix} = \frac{n!}{r!(n-r)!}$. We applied the Binomial Theorem in the proof. The right hand side can be proved in exactly the same way.

□

Probability of Reception Failure: APR Protocol

The analysis for APR protocol is similar to that of the SPR protocol. In APR, if a repetition is transmitted at time t, any other repetitions transmitted in the interval $[t-t_{trans}, t+t_{trans})$ can collide with it. The transmitted repetition is vulnerable in two slots in contrast to one in the SPR protocol. Remember t_{trans} is the time duration of a repetition. Therefore for the repetition to be successful we require no other

repetitions are transmitted in the two-slot interval. We have similar series of lemmas as listed in Subsection 3.4. Using the lemmas we obtain the following theorem.

Theorem 3.10. ***Bounds on the PRF for the APR Protocol***

The probability of reception failure at the receiver of one message for APR protocol satisfies the following inequality.

$$\left(1-\frac{k}{n}e^{-m\lambda\tau\left[2\frac{k}{n}-\frac{k^2}{n^2}\right]}\right)^n < P(\neg S) < \left(1-\frac{k}{n}e^{-m\lambda\tau\left[2\frac{k}{n}-\frac{k^2}{n^2}\right]}+\frac{k}{n}e^{-m\lambda\tau}\right)^n \tag{3.10}$$

For both SPR and APR in the parameter range we are interested in (Table 3.2), the upper and lower bounds are quite tight. In the rest of this chapter we present analytical results with the right hand sides of both (3.5) and (3.10), but the corresponding results for the left hand sides are not distinguishable when plotted.

The number of interferers m in equations (3.5) and (3.10) is calculated by:

$$m = \frac{\mathbf{2\cdot\ Interference\ Range}}{\mathbf{Meters\ per\ Vehicle}}\cdot\ \mathbf{Lane\ number} \tag{3.11}$$

The procedure to calculate the interference range, given the transmitter-receiver distance, the message range, and the date rate, is given in Appendix B.

3.5 Simulation Results

In this section we present and discuss numerical results of the performance of the protocols. The results are obtained from wither simulation or analysis. First the implementations of the simulations are presented in 3.5.1. In subsection 3.5.2 we validate the simulation with analytical results. We compare the performance of all the candidate protocols in 3.5.3. Among them AFR-CS protocol is found to best meet the communication requirements of vehicle safety applications. We discuss our finding in optimal transmission data rate in 3.5.4. Finally we report and discuss in 3.5.6 the sensitivity of the performance of AFR-CS protocol on design parameters.

3.5.1 Simulation Implementations

We have developed a DSRC simulator to conduct the simulations. The simulator is based on two others, namely SHIFT [55] and NS-2 [5].

We use SHIFT to simulate highway vehicle traffic. SHIFT is a computer language developed in California PATH for simulating dynamic networks of hybrid automata, in particular the vehicle traffic system. It is open-source and can be downloaded from Internet. We implemented microscopic models for merging, lane changing, gap acceptance, vehicle following, etc. The detailed description of the vehicle traffic simulation is in [71]. We use COSMODRIVE [66] cognitive model for human driver modelling which includes Hoffmann model of range-rate perception [37]. Figure 3.4 is a screenshot of the vehicle traffic simulated by SHIFT.

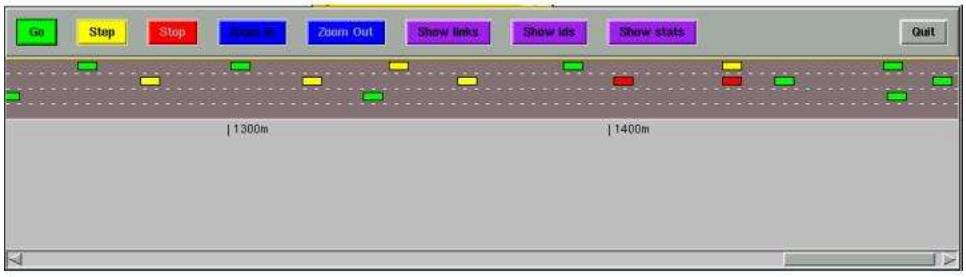

Figure 3.4: A Typical Traffic Screen-shot of SHIFT

We use NS-2 (abbreviation of Network Simulator) to simulate wireless communication network. NS-2 is a discrete event simulator for networking research. It is also a free open source software downloadable from Internet [5], with most popular protocols implemented in various OSI layers. We implement our protocol on top of 802.11 MAC, with the latter in broadcast mode. We change the physical layer settings such that the simulated communication takes place in 5.9 GHz DSRC channel rather than the original 2.4 GHz 802.11b channel. We implement the model of Atheros' 802.11a radio [47]. The reception SINR thresholds for all data rate supported in IEEE 802.11a physical layer standard are listed in Table 3.4, which are useful in our discussions on optimal transmission data rate in section 3.5.4. We use the wireless extension of NS-2 developed by Monarch project [4]. Friis free-space channel model is used for short TX/RX distance and Two-ray model is used for long distance. Parameters in Table 3.6 are used in implementations besides those already listed in Tables 3.5 and 3.2. Whenever applicable they are set according to IEEE 802.11a standard on physical and MAC layers [6].

Table 3.4: SINR Thresholds for 802.11-supported Data Rate in Simulated Radio Model

Data Rate (Mbps)	Reception SINR Threshold (dB)
6	6
9	8
12	9
18	11
24	14
36	18
48	23
54	25

Table 3.5: Nominal Setting Parameters

Message Generation Interval (msec)	100
Useful Life Time (msec)	100
Packet Payload Size (Bytes)	100
Desired Communication Range (m)	80
Average Distance Between Vehicles (m)	30
Lane Number	4

In the DSRC simulator we first simulate the vehicle traffic with SHIFT, then feed the generated trace file as the "node movement file" in the wireless communication simulation of NS-2. In the future it is possible to extend our combined simulation by implementing vehicle safety applications and feedback to it the output of V-V communication simulation. The simulation system then will become a closed-loop system, with the vehicle traffic component and wireless communication component influencing each other and vehicle safety application being the bridge between them.

Thus the DSRC simulator is the standard NS-2 release plus

- SHIFT
- The radio model for 802.11a at 5.4 GHz
- The repetition protocols
- A different data structure that changes the run-time of NS-2 from quadratic to linear in the number of nodes. Figure 3.5 shows the run-time comparisons. This enhancement has enabled us to simulate networks with up to a thousand vehicles.

3.5.2 Validation of Simulation

Figure 3.6 shows the analytical and simulated PRF of the APR and SPR protocols in the nominal setting summarized in Table 3.5. The analytical plots are from

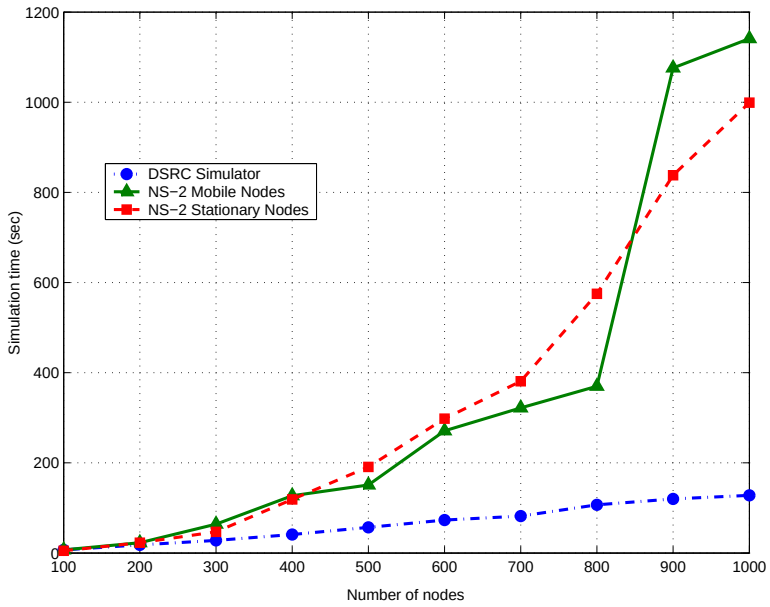

Figure 3.5: Improvement on the Scalability of the DSRC Simulator over NS-2

Table 3.6: Other Simulation Parameters

MAC header	24 Bytes
FCS	4 Bytes
PLCP header + tail	46 Bytes
Preamble Duration	16 μs
Antenna Gain	4 dB
Channel Frequency	5.9 GHz
Channel Width	20 MHz
Thermal Noise Level	-96 dBm

inequalities (3.5) and (3.10). The analytical and simulation results match well. Intuition suggests when a message is repeated more than once the chances of it being received may rise. On the other hand repetition increases the aggregate number of collisions, implying repetition beyond a certain level should be counter-productive. Figure 3.6 confirms it. In both analysis and simulation, there is an optimal number of repetitions. This optimal number is different for different message ranges, message generation rates, vehicular traffic densities, message sizes, etc.

The reason that the simulation results in Figure 3.6 are consistently better than the analytical ones is the following. Since the message generation process is Poisson rather than periodic, the lifetime of two or more consecutive messages from the same node can overlap. The repeated packets of a prior message can thus select the same time slot to transmit as the packets of a later message. In the mathematical analysis we treat previous messages the same as messages from the other nodes, i.e. the node's packets from a prior message can collide with its packets from a later message. In simulation we let the packets from the latest message overwrite any colliding packets from earlier messages. This is more realistic. Therefore we see an enhanced performance in simulation.

3.5.3 Comparison of the Repetition Protocols

Figure 3.7 shows the performance of the protocols as a function of the number of repetitions. The curves are based on output from the DSRC simulator. CSMA pa-

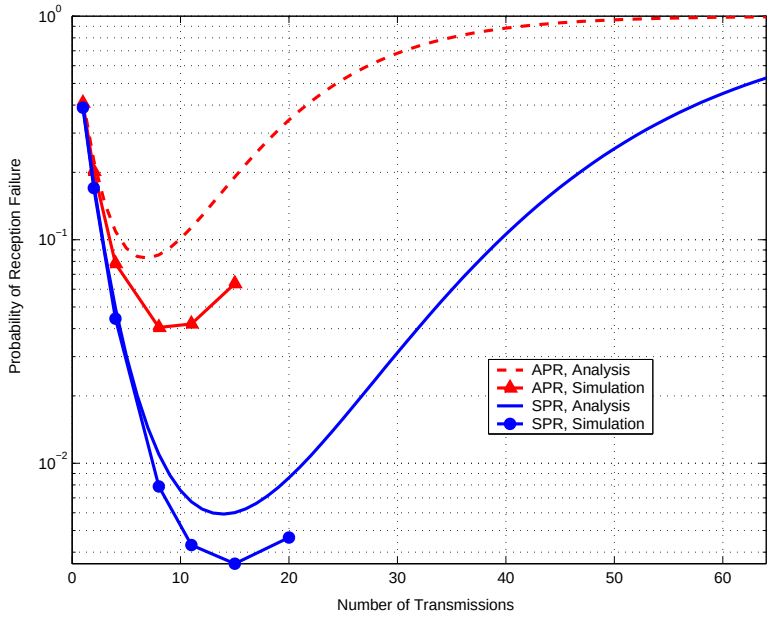

Figure 3.6: Validation of Simulation Results with Analytical Model

rameters (e.g., DIFS) have been kept fixed at their 802.11 values. As will be discussed shortly, there is an optimal data rate for a protocol under a given setting. In this figure we show the simulation results of all the protocols at their respective optimal rate. The best protocols are AFR-CS and SFR. But SFR would require a clock synchronization infrastructure. Therefore AFR-CS seems to be the best solution. Note also the PRF improvement over 802.11a is one order of magnitude. This shows that repetition helps combat interference by giving a transmitter more chances to transmit, and making interfering nodes transmit at different time. The better performance of AFR-CS protocol over that of 802.11 indicates that repetition reduces the hidden terminal effects without using RTS/CTS.

Clearly, for the same repetition methods (i.e. fixed repetition or p-persistent rep-

etition), synchronous protocol outperforms asynchronous protocol, since synchronous protocol eliminates the partial overlap between packets from different nodes. This observation agrees with the previous results on the slotted and non-slotted ALOHA [59]. Also it is obvious that for the same repetition method, a CSMA protocol is better than a non-CSMA protocol. This result is expected since in CSMA each node listens before transmission, therefore many potential collisions are avoided. The reception failures for CSMA protocols are mostly due to hidden terminals. Fixed repetition protocols outperform corresponding p-persistent protocols. The reason is that the fixed repetition protocols are better at maintaining the number of repetitions for each message, i.e. there is less fluctuation between the actual number of repetition of each message and the expected number of repetitions.

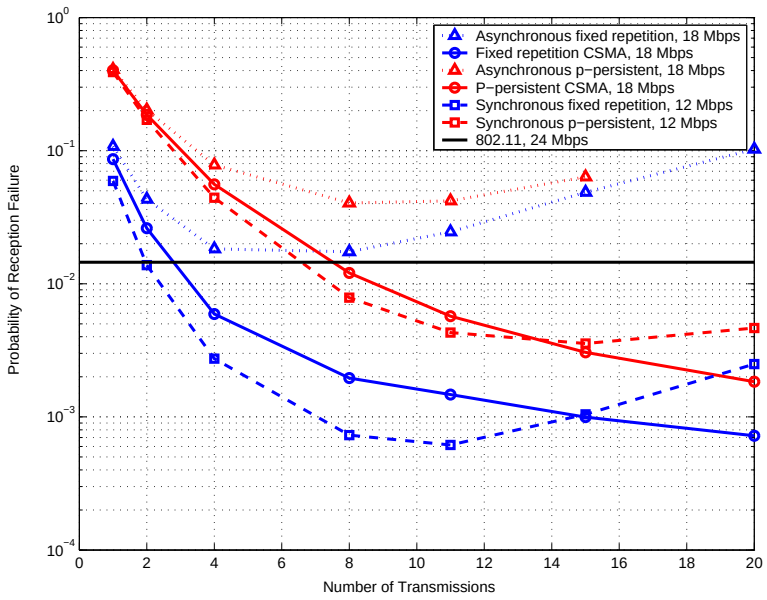

Figure 3.7: Probability of Reception Failure for Proposed Protocols under Nominal Setting

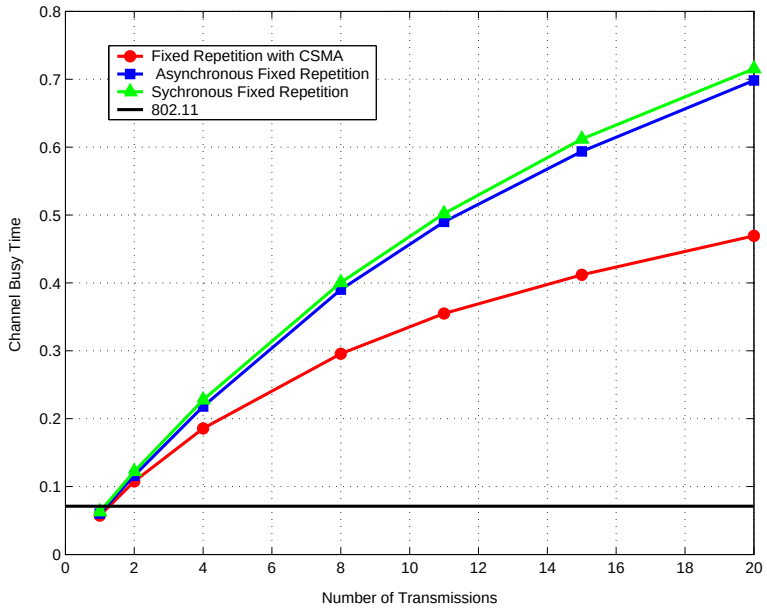

Figure 3.8: Channel Busy Time for Fixed Repetition Protocols

Figure 3.8 is the CBT versus repetition number for all the fixed repetition protocols. It shows that CBT increases with the repetition number. With the same number of repetitions the AFR-CS protocol has smaller CBT than other proposed protocols. Not surprisingly, the 802.11 has small CBT since it does not repeat. These plots are for the nominal parameters in Table 3.5. Therefore the rest of our evaluation uses AFR-CS. In Figure 3.7, the PRF of AFR-CS keeps decreasing with number of transmissions. However the PRF shown in the plot already levels off. In another test, we keep increasing the number of repetitions and observe that the probability of reception failure of AFR-CS protocol does increase as observed in other protocols, though at very large repetition numbers.

The Channel Busy Time is a measure of the fraction of channel capacity left over

for non-safety messages. As the repetition number goes up so should CBT. Thus there is an inverse relationship between PRF and CBT up to the optimal repetition number. Curves in Figure 3.9 show this tradeoff. As the quality of service to the safety applications is raised, that of other applications in control channel comes down. Therefore these curves are a good way of evaluating the performance of our protocols. In Figure 3.9 we further compare the best two protocols in Figure 3.7, SFR and AFR-CS. The figure indicates that up to 50% CBT in the nominal setting, the performances of AFR-CS and SFR are indeed quite close. Since SFR and AFR-CS outperform other protocols in both PRF and CBT, and AFR-CS is easier to deploy than SFR , the rest of our evaluation uses AFR-CS.

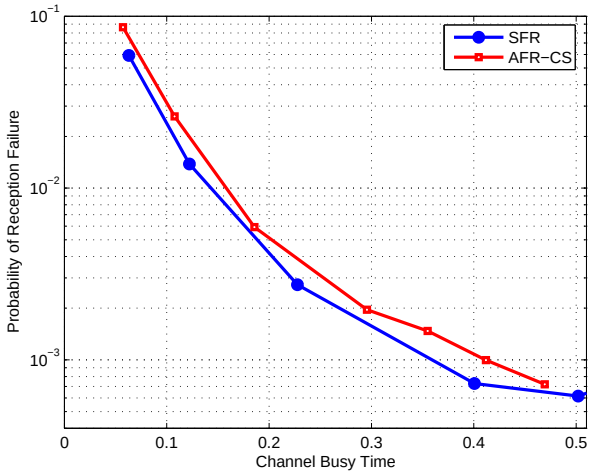

Figure 3.9: Comparison of AFR-CS and SFR Protocols in the Nominal Setting

Equations (3.5) and (3.10) show performance depends on the number of interferers. In an actual traffic simulation this number varies in complex patterns. Nevertheless,

since the vehicle traffic does not change much within the transmission of one message, we can regard it as a series of snapshots when evaluating the number of interferers. Hence, the single number evaluated by (3.11) is a good predictor of the performance. Figure 3.13 shows that for small transmission time the dynamics of the topology makes almost no difference to aggregate network performance. The curve for 30-meter headway, 60-meter message range, 8 lanes and the curve for 20-meter headway, 80-meter message range, and 4 lanes are clustered together because they have the same number of interferers calculated by (3.11), i.e., 113. The number of interferers for the nominal case is 75.

3.5.4 Optimal Data Rate

IEEE 802.11a standard applies Orthogonal Frequency Division Modulation (OFDM) technique at physical layer. The channel is partitioned into 54 sub-channels, and data is coded, modulated and transmitted at 48 of the 54 sub-carriers. A given transmission data rate corresponds to a combination of modulation scheme and coding rate in each sub-carrier. The supported data rates and corresponding combinations are listed in Table 3.7. From communication theory we know the reception SINR threshold increases with the data rate [57]. We use the reception SINR threshold specifications of Atheros' 802.11a radio shown in Table 3.4.

Intuition suggests that for each number of interferers and repetition number there may be an optimal data rate. If the transmission rate is raised, the transmission

Table 3.7: Rate Dependent Parameters in IEEE 802.11a

Data Rate (Mbps)	Modulation	Coding Rate
6	BPSK	1/2
9	BPSK	3/4
12	QPSK	1/2
18	QPSK	3/4
24	16-QAM	1/2
36	16-QAM	3/4
48	64-QAM	2/3
54	64-QAM	3/4

time reduces, tending to reduce the probability of collision. On the other hand the power required to cover the message range also rises, thereby raising the number of interferers. On either side of inequality (3.5), higher data rate increases the total number of slot n, which reduces PRF if all other parameters are fixed. On the other hand, higher data rate requires higher SINR, therefore higher transmission power to reach the same range, which increase the number of interferers m. Larger m increases PRF. Mixing these two effects suggests there may be an optimal data rate.

Figure 3.10 shows this trend by plotting the right hand side of inequality (3.5) in Matlab with various data rates supported by 802.11, and the SINR requirement for each data rate listed in Table 3.4. All other parameters are from the nominal setting in Table 3.5. Clearly, up to 12 Mbps, the PRF decreases with the data rate. But after this value the PRF increases, making 12 Mbps the optimal data rate for the SFR protocol in the nominal parameter setting. Figure 3.11 shows this trend for AFR-CS protocol with the nominal parameter combination in Table 3.5. This result

Table 3.8: Optimal Data Rate for Various Protocols in the Nominal Setting

Protocol	Optimal Data Rate (Mbps)
SFR	12
AFR	18
SPR	12
APR	18
APR-CS	18
AFR-CS	18
802.11	24

is obtained by simulation. Table 3.8 shows the optimal data rates for all the protocols in the nominal parameter setting obtained from simulations. Note both simulation and analysis tell us for the SFR in the nominal parameter setting the optimal data rate is 12 Mbps.

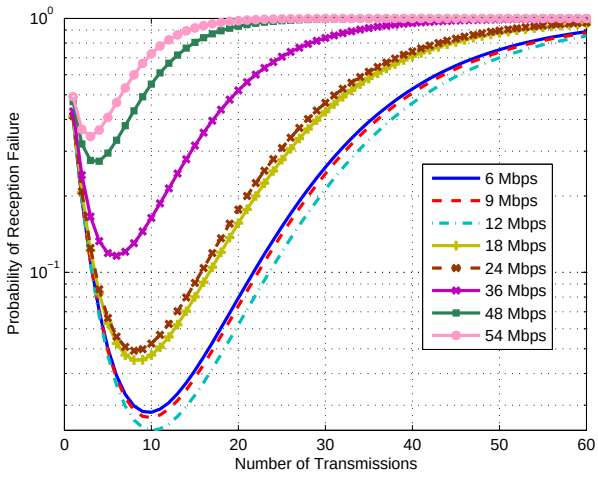

Figure 3.10: Probability of Reception Failure of SFR at Various Data Rate Under the Nominal Setting: Analytical

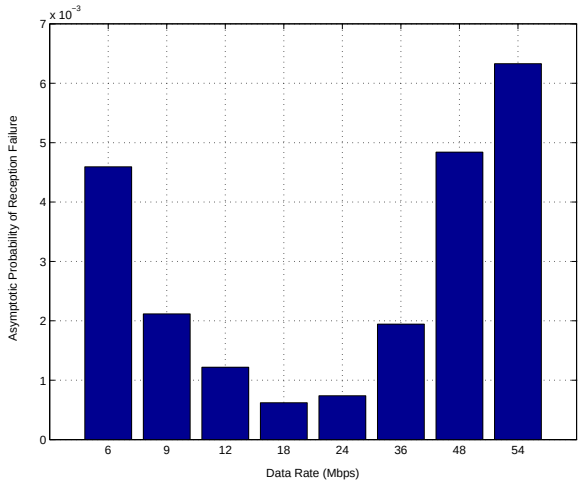

Figure 3.11: Probability of Reception Failure for Various Data Rate Under the Nominal Setting: Simulation

3.5.5 Bursts of Reception Failures

Figure 3.12 shows the probabilities of bursts of failures of different lengths for the nominal parameters in Table 3.5. The probabilities are small. This is due to the memoryless feature of the channel in simulation. The probability for a receiver seeing two or more consecutive failures is negligible. This is good for estimation.

3.5.6 Sensitivity of AFR-CS Protocol on Design Parameters

Figure 3.13 illustrates equation (3.11). Here we plot PRF vs. CBT, without explicitly showing repetition number. The performance of a protocol is bad if it has high PRF for given CBT, or if it requires high CBT to achieve a given PRF. There are three groups of curves, with worst-case interferer number being equal for curves in the same group and unequal across groups. Clearly, the more the interferers, the worse

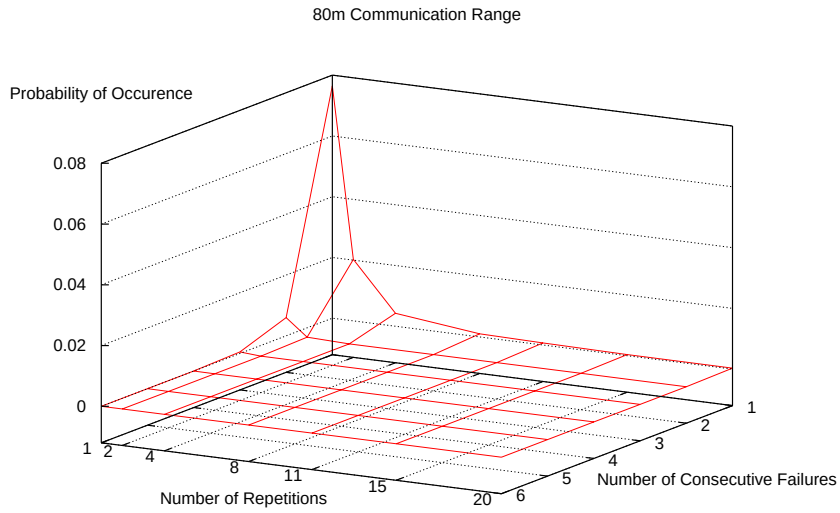

Figure 3.12: Probability of Message Failure Bursts: AFR-CS

the performance of the protocol. Curves representing superior performance are to the lower-left of the plot. Figure 3.13 shows that for small transmission time the dynamics of the topology makes almost no difference to aggregate network performance. The curve for 30-meter headway, 60-meter message range, 8 lanes and the curve for 20-meter headway, 80-meter message range, and 4 lanes are clustered together because they have the same number of interferers calculated by (3.11), i.e., 113. The number of interferers for the nominal case is 75.

Since cases with the same interferer number have equivalent impact on the performance of the protocol, they also have the same optimal data rate. We cannot distinguish them when observing the protocol performance. Thus although we cannot study all possible combinations of parameters, the results reported here actually rep-

resent much broader scope in vehicle communication environment than those shown in Table 3.2. For example, although only 4 lanes and 8 lanes are studied in the paper, some results for 10-lane cases can be obtained with different vehicle density or communication range.

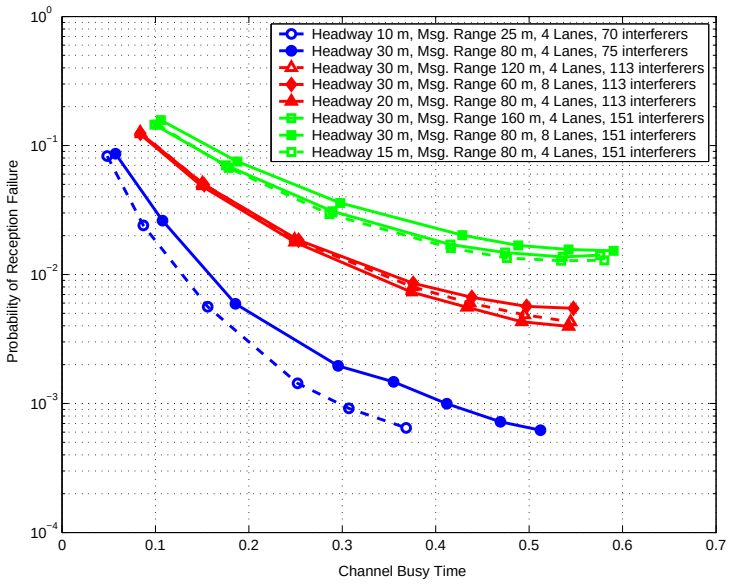

Figure 3.13: Performance of AFR-CS Protocol as a Function of Interferer Number

We further study the sensitivity of the performance of AFR-CS protocol on parameters listed in Table 3.2. Figures 3.14, 3.15 and 3.16 respectively show the sensitivity results for various communication ranges, message generation intervals, and packet sizes. As stated above, except for the varying parameters we study the sensitivity for, all other parameters take values in Table 3.5.

Not surprisingly, Figures 3.14 indicates that increase on communication range degrades the performance of the protocol. Larger communication range requires higher

transmission power from each vehicle, therefore in the same network topology, more vehicles are interfering with each other. For the same CBT, both PRF and CBT increase with communication range when the probability of failure is kept constant. If we require the probability of reception failure be lower than 0.01 and CBT be lower than 50%, with all other parameters taking values in Table 3.5 and data rate being 18 Mbps, the maximum allowed communication range lies between 120 m and 180 m.

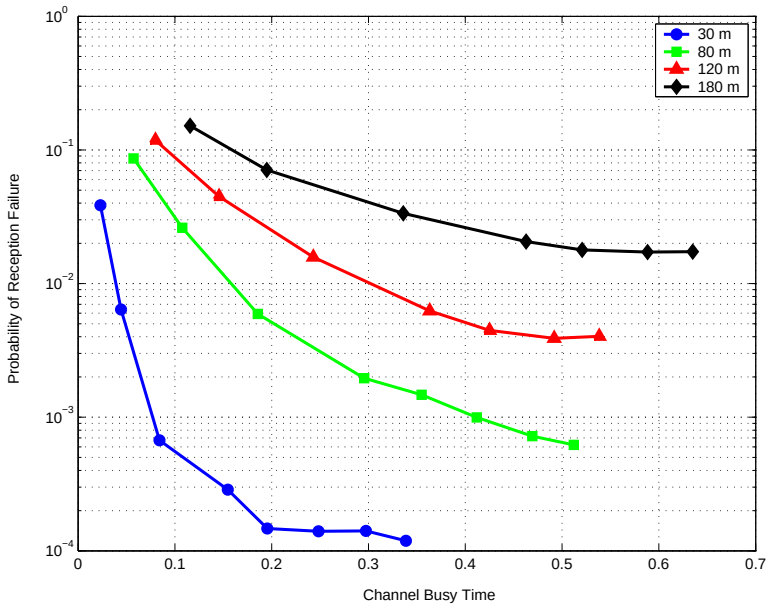

Figure 3.14: Probability of Reception Failure for Various Communication Ranges

Observing Figure 3.15 and 3.16, we can see smaller message interval and larger packet size degrade the protocol performance. These also agree with engineering intuition.

Figure 3.17 pulls these various results together to get a sense of the feasibility of supporting safety applications on the control channel. Feasibility depends on a

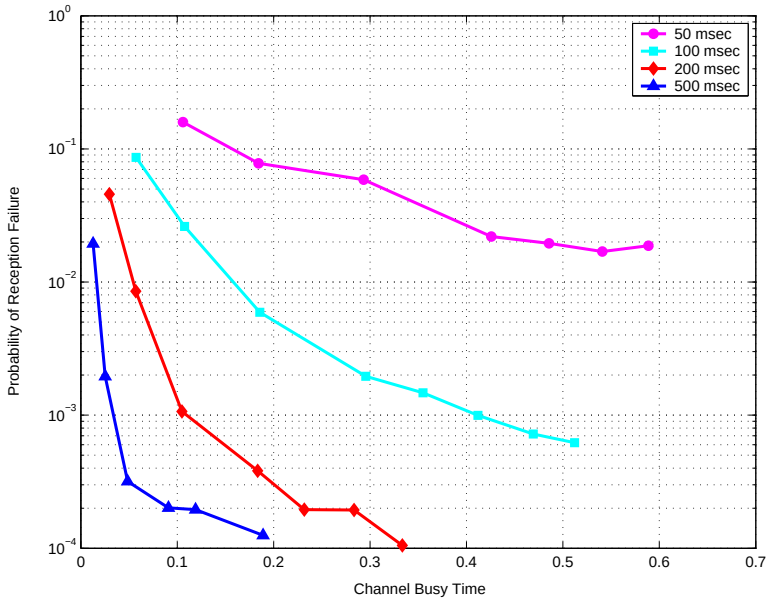

Figure 3.15: Probability of Reception Failure for Various Message Generation Intervals

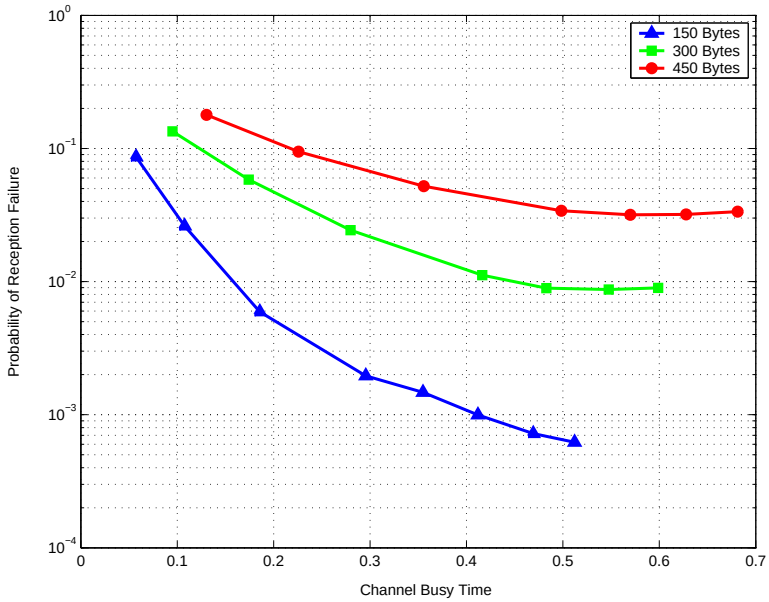

Figure 3.16: Probability of Reception Failure for Various Packet Sizes

PRF and CBT requirement. Given a PRF and CBT requirement and a combination of parameter values within the ranges in Table 3.2, our simulation data can show whether it meets the requirements. We do this by assuming the AFR-CS protocol and optimizing the protocol for repetition number, transmission rate, and selecting the modulation and code rate to minimize the power required to cover the message range. Figure 3.17 shows feasibility for a PRF less than 1/100 and a CBT less than 50%. For example, the 200 msec message rate, 250 byte message at 140 interferers is feasible. This corresponds to a 30 meter, 4 lane highway at capacity (2200 vehicles/hour/lane) with a message range of 150 meters. Likewise the 10 meter headway (jammed road), 4 lanes, and 50 meter message range is also feasible since it has the same interferer number. Figure 3.18 shows the feasibility regions when we require the PRF to be lower than 0.001, and the CBT still lower than 50%. The higher PRF requirement makes feasibility regions smaller than those in Figure 3.17. For example, in Figure 3.17, the 200 msec message rate, 250 byte message is feasible at 160 interferers, however the same message rate and message size combination is feasible only at less than 30 interferers.

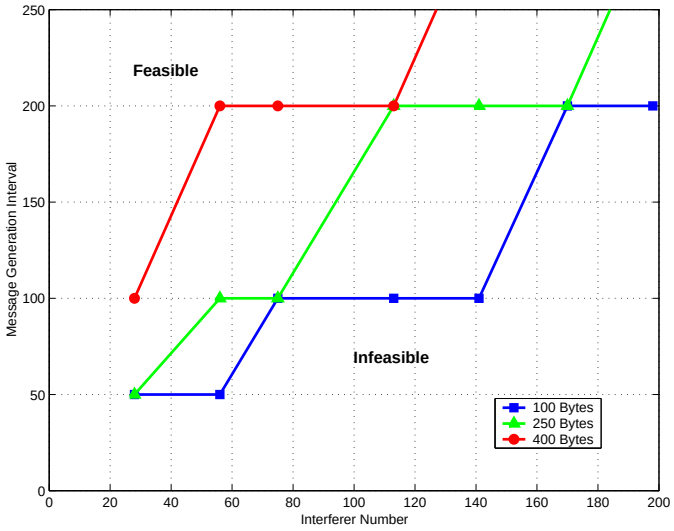

Figure 3.17: Feasibility Regions for $<$ 0.01 Probability of Reception Failure and $<$ 50% CBT

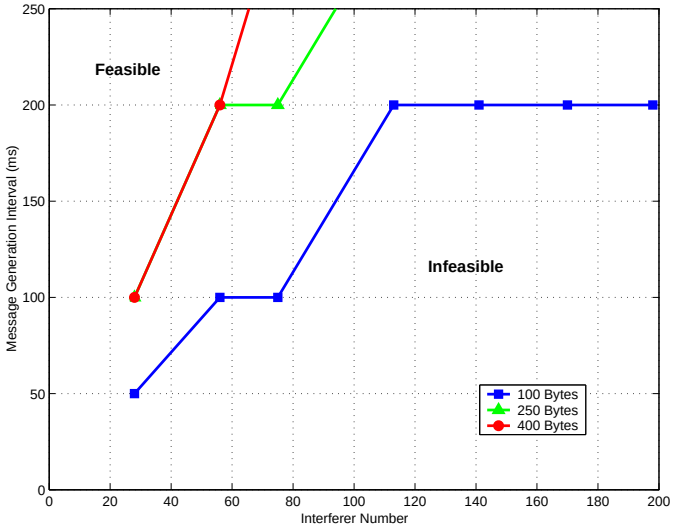

Figure 3.18: Feasibility Regions for $<$ 0.001 Probability of Reception Failure and $<$ 50% CBT

3.6 Summary

Our evaluation exercise shows DSRC safety messaging on the control channel is feasible for some typical cases. Messages generated every 200 msec is a good rate, since a driver reaction time of 0.7 seconds or higher in near-miss situations means, an on-board safety system relying on communicated messages may be able to recognize the situation faster, thereby providing timely assistance to the driver. Moreover, the interpretation of most safety information will require the sender to include its position in the message. Most likely, the position information will be derived from GPS. Most commercial off-the-shelf GPS does not update faster than 5 Hz. The 250 byte message size is also adequate. If a highway reaches its capacity flow between 50 to 55 mph, at these speeds almost all light-duty passenger vehicles are able to easily stop within 150 meters. Thus this is an adequate value for the message range. Safety system designers have a reasonable chance of designing safety systems within these offered traffic limits.

When the highway is at capacity with 30 meters headway,at these offered traffic levels the network delivers a PRF as low as 1/100. At the same time, when the highway is jammed, e.g. the headway is 15 meters, a message range of 80 meters, which covers 5 cars in both direction, also produces PRF lower than 1/100.

The probability of successive losses is much lower. Thus if the vehicle does not learn of the emergency in 200 msec it will learn in 400 msec. Moreover, our evaluation is conducted assuming all vehicles transmit all the time. If communication becomes a

general way of learning the vehicle neighborhood then this will be the case, i.e., each vehicle will regularly transmit its position, velocity, turn signal status, etc., for the benefit of others. Our analysis is in this case because it represents the largest offered traffic. Therefore, we think of our PRF's as a worst-case.

This evaluation exercise also provides some design insights. All message ranges may not be feasible at all vehicular traffic densities. This indicates the need for power adaptation. Our results on the optimal data rate at different vehicular traffic densities suggest the need for adaptive modulation control. This adaptation should be with respect to the flows of the vehicles. The repetition MAC is simple, easily added to the well-established IEEE 802.11a protocol, works without infrastructure, and should deliver adequate performance on most rural and many urban or inter-urban roads. In some urban areas with high density traffic, e.g. 8-10 lanes, the PRF's may be too high. When there are many non-safety applications in the control channel such as service announcements, the CBT due to the safety traffic may be too high. In these settings, it may be best to use roadside radios to coordinate vehicle transmissions for more efficient use of the control channel. Vehicles would then follow the ad-hoc protocol till they detect a controlling roadside radio. Thereafter they would communicate according to the roadside control protocol and switch back to ad-hoc operation on not hearing the roadside radio again. This is an idea currently under investigation.

Chapter 4

Real-time Estimation of a Markov Process Over a Noisy Digital Communication Channel

This chapter is about the design of encoders and decoders optimized to estimate the state of a stochastic dynamical system across a digital but noisy communication channel. Control and estimation over communication networks is attracting increasing attention. For example see the recent special issues of the IEEE Transactions on Automatic Control [8] and Control Systems Magazine [7] on networked control system. This class of problems is also given considerable weight in [49] in its evaluation of future directions in control, dynamics, and systems. They see control over communication networks as the natural next phase of the information revolution. It

would transform current communication networks, now mainly concerned with the transmission of information, to have more interaction with the physical world. We ourselves have built control and estimation systems over digital communication networks for cars and airplanes [25][64][80][29][46]. For an audio-visual description of one of our systems see [1].

Here we present results on real-time estimation of the state of a Markov process over a noisy communication channel. Figure 4.1 shows the system schematically. A discrete-time continuous-valued Markov source is passed through an encoder at each discrete time-step. The encoder produces the input to the communication channel. The communication channel is assumed to have a finite, discrete alphabet. Thus we consider digital communications. The input and output alphabets are the same. In general the channel may output a symbol different from the one that is input, i.e., the channel is noisy. The channel is also memoryless. The output of the channel is fed to the decoder. The decoder is permitted to have memory. Its job is to output an estimate of the state of the Markov process. There are no communication delays.

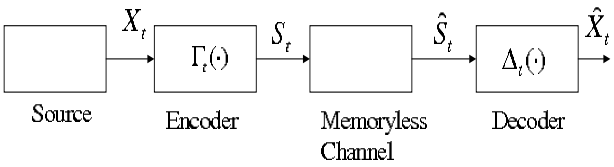

Figure 4.1: State Estimation over Memoryless Channel

Our aim is to choose the encoder and decoder at each time-step to minimize the mean squared difference between the state of the Markov process and its estimate

at the output of the decoder at the same time step. In other words, the encoder and decoder are to be designed for real-time minimum mean-square error estimation (MMSE). The Real-time has to do with the emphasis on choosing the encoder and decoder at time t to minimize the estimation error at time t. This distinguishes our formulation from the rate distortion, source and channel coding problems in information theory. Our objective function is the same as that in Kalman filtering [39]. However, the emphasis on the digital communication channel distinguishes this problem from Kalman's.

We review relevant previous works in section 4.1. The problem statement is in section 4.2. The rest of the chapter is composed of two parts. The first part presents the structural results. There are three theorems and an algorithm in this part. The encoder at time t is permitted to be any function of the states up to time t. In section 4.3, Theorem 4.1 shows the encoder may be restricted, without loss of optimality, to a function of the current state of the Markov process and the probability mass function of the memory of the decoder conditioned on the current state. This says the encoder can be causal and memoryless. Theorem 4.3 merely asserts that since ours is an MMSE problem, for any given encoder the optimal decoder is the conditional expectation of the state of the Markov process given all past channel outputs. Theorem 4.4 shows the encoder may be restricted, without loss of optimality, to a threshold type. In section 4.4 we present an iterative algorithm that converges to a locally optimal encoder and decoder for the binary symmetric channel. The algorithm

synthesizes these results from control and information theory to derive a computational scheme to get optimal encoders and decoders for minimum mean-square error estimation. The algorithm itself turns out to be related to others well established in quantization and rate distortion theory. [13][16][45] The second part of the chapter studies the special case of memoryless Gaussian vector source over binary symmetric channel. We show that the globally optimal encoding is to do a threshold encoding of the principal component. We also derive expressions for the minimum mean square error.

4.1 Previous Work

We situate our problem in a literature situated partly in control and partly in information theory. The problem of optimal estimation of a linear Gaussian Markov process, when the measurement is contaminated by an independent white Gaussian process, was studied by Kalman in [39] and [40]. However when the state is transmitted over a digital communication channel the state measurement, which is a real vector, has to be quantized into bits. Then the bits are transmitted over the noisy channel and are decoded on the other side. Thus the optimality of the orthogonal projection of the state onto the manifold generated by the observations no longer holds.

The problem of estimating state over a digital communication channel was first introduced in [75]. Nair and Evens extend this work in [51] [52] [53] and [50]. All these references consider a noise-less though bit-rate constrained channel, The system output at each time-step can be quantized into R bits, which are then transmitted over the channel without error. We consider both the bit rate limit and the channel noise, i.e., the bits received may not be the same as those transmitted.

In [67] Tatikonda derived the bit rates necessary for the controllability, observability, and stability of a dynamical system. Once again, the communication channel was assumed to be error free.

Walrand and Varaiya [72] studied the optimal coding-decoding problem. They consider a discrete alphabet source, and the Hamming distance as a measure of dis-

tortion. Our source is continuous valued. They also allow the encoder to have noiseless feedback from the channel which we do not assume.

Sahai studied the estimation problem of an unstable process over noisy channel in [61] and [60]. He considers the stability of the estimation. We on the other side study stable process, but concern more with the optimal performance in estimation.

Şimşek and Varaiya [23] extended the work of Sahai and studied the estimation over a binary symmetric channel. They derive conditions for stability. Once again, they assume channel feedback. We on the other hand find the optimal design to minimize the mean square estimation error without channel feedback.

Neuhoff and Gilbert [54] studied causal source codes, and show that the performance of memoryless coding is as good as any other causal coding at the minimum bit rate required to achieve a given distortion. We show similar results but in the presence of a noisy channel. They solve a pure source coding problem.

Quantization over a noisy channel problem was first introduced in [43]. They studied scalar quantization. Farvardin [26] extended the result to provide an iterative algorithm which converges to a locally optimal encoder for a given channel and distortion measure. Vector quantization is studied in [27]. The authors show the geometric structure of channel-optimized vector encoders and the implications on the complexity of encoding. We extend their results from the memoryless process to the Markov process. They provide an iterative algorithm to get a local optimum for any stationary source and discrete memoryless channel. We on the other hand present an

algorithm for a Markov source, and binary symmetric channel.

Teneketzis [68] studied the real-time estimation of a discrete-time Markov process. They present a structural results similar to our first theorem. They assume a discrete-valued Markov source. We generalize their result to a continuous valued Markov source. Their cost function is also slightly different. They optimize the sum of all errors from the beginning to the current time, and design all the encoders and decoders at one time to minimize this sum. We on the other hand optimize the encoder and decoder at the current instant to minimize the distortion at the current instant, assuming the prior encoders and decoders are already fixed.

Xu and Hespanha study optimal communication logics for networked control systems in [82]. They derive communication policies for the optimal control of an estimator-based networked control system architecture to reduce communication load. Unlike us, they do not consider quantization of the communication signals. The channel in their problem is also error free. In [85] the authors study the minimal rate requirements for state estimation in linear time-invariant systems. For different estimation distortion criterion, they find the minimum data rate required from the channel. The channel they consider again has a constraint on data rate, but is noiseless. We consider noisy channels.

4.2 Problem Statement

The system is shown in Figure 4.1. We describe each part of it below.

1. Source:

   $X_t \in \mathbb{R}^n$ is a Markov process.

2. Encoder: Define $X_1^t \triangleq \{X_1, X_2, \cdots, X_t\}$.

$$S_t = \Gamma_t(X_1^t) \tag{4.1}$$

   where $S_t \in \mathrm{L} = \{1, 2, \cdots, K\}$ and $K \in \mathbb{N}^+$.

3. Channel: Memoryless

$$\hat{S}_t = H_t(S_t, N_t) \tag{4.2}$$

   where $N_t \in \{1, 2, \cdots, \gamma\}$ and $\gamma \in \mathbb{N}^+$. N_t is independent for different t and independent of S_t. $\hat{S}_t \in \mathrm{L}$.

4. Receiver memory update:

   (a) At $t = 1$, $M_1 = l_1(\hat{S}_1)$.

   (b) At $t > 1$, $M_t = l_t(\hat{S}_t, M_{t-1})$.

   where $M_t \in \mathrm{W}_t = \{1, 2, \cdots, \kappa_t\}$ and $\kappa_t \in \mathbb{N}^+$. Denote the space of probability mass functions in W_t as $\mathbb{P}^{\mathrm{W}_t}$, and the probability mass function of M_t as P_{M_t}.

Define the probability mass function of M_t conditioned on $X_t = x_t$ as $P_{M_t(x_t)} \triangleq P(M_t \mid X_t = x_t)$.

5. Decoder:

$$\hat{X}_t = \Delta_t(\hat{S}_t, M_{t-1}) \tag{4.3}$$

6. Cost Function:

$$E\{\|X_t - \hat{X}_t\|^2\} \tag{4.4}$$

The Real-time Estimation Problem: At each time $t = \tau$, given $\Gamma_1^{\tau-1} \triangleq \{\Gamma_1, \Gamma_2, \cdots, \Gamma_{\tau-1}\}$, $\Delta_1^{\tau-1} \triangleq \{\Delta_1, \Delta_2, \cdots, \Delta_{\tau-1}\}$, and $l_1^{\tau} \triangleq \{l_1, l_2, \cdots, l_{\tau}\}$, find the encoder $\Gamma_\tau(\cdot)$, and decoder $\Delta_\tau(\cdot)$, such that $E\{\|X_\tau - \hat{X}_\tau\|^2\}$ is minimized.

4.3 The Structure of the Optimal Encoder and Decoder

In this section we prove three structural results about the real-time estimation problem. Firstly, by Theorem 4.1 we prove that for a given decoder, the optimal encoder for real-time estimation of the state of a Markov process is separable, i.e., it need not depend on the previous states. This is an extension of the result in [68] to a continuous-valued source. Our proof is also similar although our cost function is a bit different, as discussed in section 4.1. Lemma 4.2 is an intermediate result used to prove Theorem 4.1. Then Theorem 4.3 asserts the optimal decoder for any given encoder is the expected value of the state conditioned on the previously channel outputs. Finally we prove in Theorem 4.4 the optimal encoder is a hyper-plane encoder. It partitions the real space with hyper-planes, and maps the X_t values in each subspace to a distinct symbol. This result is based on Theorem 4.1. The proof technique is similar to [26].

4.3.1 The Optimal Encoder

This subsection is about the structure of the optimal encoder for the real-time Markov process estimation problem. The result is in Theorem 4.1.

Theorem 4.1. *For any t, one can replace Γ_t with some Γ_t^**

$$\Gamma_t^* : \mathbb{R}^n \times \mathbb{P}^{\mathrm{W}_t} \to \mathrm{L}$$

so that $s_t = \Gamma_t^*(x_t, P_{M_{t-1}(x_{t-1})})$ *without loss of optimality.*

Like [68], we prove the theorem with a two-stage lemma, i.e., Lemma 4.2. This approach first appeared in [74].

Below in Lemma 4.2 we consider a vector Markov process. The states in the first two time instants are $X_1 \in \mathbb{R}^n$ and $X_2 \in \mathbb{R}^n$. The encoder at stage 1 is $\Gamma_1 : \mathbb{R}^n \to \mathrm{L}$ with $S_1 = \Gamma_1(X_1)$. The encoder at stage 2 is $\Gamma_2 : \mathbb{R}^{n\times n} \to \mathrm{L}$ with $S_2 = \Gamma_1(X_1, X_2)$. $S_t \in \mathrm{L} = \{1, 2, \cdots, K\}$ for $t = 1, 2$. Then we have the following lemma.

Lemma 4.2. *Two-stage lemma:*

Consider a two-stage system where

$$\Gamma_2 : \mathbb{R}^{n\times n} \to \mathrm{L}$$

so that $S_2 = \Gamma_2(X_1, X_2)$*, then one can replace* Γ_2 *with* Γ_2^**,*

$$\Gamma_2 : \mathbb{R}^n \times \mathbb{P}^{\mathrm{W}_1} \to \mathrm{L}$$

so that $S_2 = \Gamma_2^*(X_2, P_{M_1}(x_1))$ *without loss of optimality.*

Proof. With a given design $d \triangleq (\Gamma_1, \Gamma_2, l_1, l_2, \Delta_1, \Delta_2)$, define $\hat{\rho}_2(X_2, M_1, S_2, N_2) \triangleq \|X_2 - \Delta_2(M_1, H_2(S_2, N_2))\|^2$. Define $P^d_{M_1(x_1)} \triangleq P^d(M_1 = m_1 \mid X_1 = x_1)$ to be the probability mass function of M_1 conditioned on $X_1 = x_1$, under design d. It depends on Γ_1 and l_1 but not Γ_2. We then have for any $X_1 = x_1$, $X_1 = x_2$

$$
\begin{aligned}
& E^d\{\|X_2 - \hat{X}_2\|^2 \mid X_1 = x_1, X_2 = x_2\} \\
= \;& E^d\{\|X_2 - \hat{X}_2\|^2 \mid X_1 = x_1, X_2 = x_2, P^d_{M_1(x_1)}\} \\
= \;& E^d\{\|X_2 - \Delta_2(M_1, H_2(S_2, N_2))\|^2 \mid X_1 = x_1, X_2 = x_2, P^d_{M_1(x_1)}\} \\
= \;& E^d\{\hat{\rho}_2(X_2, M_1, S_2, N_2) \mid X_1 = x_1, X_2 = x_2, P^d_{M_1(x_1)}\} \\
= \;& \sum_{m_1}\sum_{s_2}\sum_{n_2} P^d(M_1 = m_1, S_2 = s_2, N_2 = n_2 \mid X_1 = x_1, X_2 = x_2, P^d_{M_1(x_1)}) \cdot \hat{\rho}_2(x_2, m_2, s_2, n_2) \\
= \;& \sum_{s_2} P^d(S_2 = s_2 \mid X_1 = x_1, X_2 = x_2) \left[\sum_{n_2} P(N_2 = n_2) \cdot [\sum_{m_1} P^d_{M_1(x_1)}(m_1)\hat{\rho}(x_2, m_1, s_2, n_2)]\right]
\end{aligned}
$$

Now consider a new design $\hat{d}$ where $\Gamma_2^* : \mathbb{R}^n \times \mathbb{P}^{\mathrm{W}_1} \to \mathrm{L}$ is chosen as follows: For any given $x_2 \in \mathbb{R}^n$ and any given $P_{M_1} \in \mathbb{P}^{\mathrm{W}_1}$

$$
\begin{aligned}
& \Gamma_2^*(x_2, P_{M_1}(x_1)) \\
= \;& \arg\min_{s_2 \in \mathrm{L}} \left\{\sum_{n_2} P(N_2 = n_2) \cdot \left[\sum_{n_2} P(N_2 = n_2) \left[\sum_{m_1} P^d_{M_1(x_1)}(m_1)\hat{\rho}(x_2, m_1, s_2, n_2)\right]\right]\right\}
\end{aligned}
$$

Keep the decoders the same in the new design. Then, under the new design $\hat{d} = (\Gamma_1, \Gamma_2^*, l_1, l_2, \Delta_1, \Delta_2)$, for all x_1,

$$P^d_{M_1(x_1)} = P^{\hat{d}}_{M_1(x_1)}$$

and

$$
\begin{aligned}
& E^{\hat{d}}\{\|X_2 - \hat{X}_2\|^2 \mid X_2 = x_2, P^d_{M_1(x_1)}\} \\
= \;& E^{\hat{d}}\{\|X_2 - \hat{X}_2\|^2 \mid X_1 = x_1, X_2 = x_2, P^d_{M_1(x_1)}\} \\
\leq \;& E^{d}\{\|X_2 - \hat{X}_2\|^2 \mid X_1 = x_1, X_2 = x_2, P^d_{M_1(x_1)}\} \\
= \;& E^{d}\{\|X_2 - \hat{X}_2\|^2 \mid X_2 = x_2, P^d_{M_1(x_1)}\} \qquad (4.5)
\end{aligned}
$$

Therefore

$$E^{\hat{d}}\{\|X_2 - \hat{X}_2\|^2\} \leq E^{d}\{\|X_2 - \hat{X}_2\|^2\}$$

□

Using Lemma 4.2, we can prove Theorem 4.1. The basic idea is to aggregate the system state from time 1 to $t-1$ into one "super-state" at the first stage, and view the state at t as the second stage so that the two-stage lemma can be applied.

Proof of Theorem 4.1

Proof. The given t-stage system can be considered as a two-stage system by setting

$$\begin{aligned}
\bar{X_1} &\triangleq (X_1, X_2, \cdots, X_{t-1}) \\
\bar{X_2} &\triangleq X_t \\
\bar{N_1} &\triangleq (N_1, N_2, \cdots, N_{t-1}) \\
\bar{N_2} &\triangleq N_t \\
\bar{S_1} &\triangleq (S_1, S_2, \cdots, S_{t-1}) \\
\bar{S_2} &\triangleq S_t \\
\bar{\hat{S}_1} &\triangleq (\hat{S}_1, \hat{S}_2, \cdots, \hat{S}_{t-1}) \\
\bar{\hat{S}_2} &\triangleq \hat{S}_t \\
\bar{M_1} &\triangleq M_{t-1} = \phi(\bar{X_1}, \bar{N_1}) \\
\bar{M_2} &\triangleq M_t \\
\bar{\hat{X}_1} &\triangleq (\hat{X}_1, \hat{X}_2, \cdots, \hat{X}_{t-1}) \\
\bar{\hat{X}_2} &\triangleq \hat{X}_t \\
\hat{\Gamma}_2(\bar{X_1}, \bar{X_2}) &\triangleq \Gamma_t(X_1, X_2, \cdots, X_t) \\
\bar{l}_2(\bar{M_1}, \bar{\hat{S}_2}) &\triangleq l_t(M_{t-1}, \hat{S}_t)
\end{aligned}$$

Then by the two-stage lemma there is an encoder Γ_2^* that has the structure

$$\bar{s}_2 = \Gamma_2^*(\bar{x}_2, P_{\bar{M_1}}(x_1))$$

which does not increase the cost. This corresponds to

$$s_t = \Gamma_t^*(x_t, P_{M_{t-1}}(x_{t-1}))$$

□

4.3.2 The Optimal Decoder

The following theorem characterized the optimal decoder for any given encoder.

Theorem 4.3. *For any encoder Γ_t the optimal decoder Δ_t is*

$$\hat{X}_t = \Delta_t(\hat{S}_t, M_{t-1}) = E_{\Gamma_1^t, l_1^{t-1}}\{X_t \mid \hat{S}_t, M_{t-1}\}$$

Proof. This is a well-known result in estimation theory. It appears in, for example, Theorem 1 of [39]. The proof is omitted here. □

4.3.3 Optimality of the Hyper-plane Encoder

Theorem 4.1 opens a way to use quantization techniques for noisy channels. The following theorem is similar to the result in [26]. Unlike the quantization problem, in our problem the receiver memory needs to be considered.

Theorem 4.4. *For any given decoder, the optimal encoder for the real-time estimation problem is a hyperplane encoder. In particular, let the reconstruction points be $\{c_1, c_2, \cdots, c_{\hat{K}}\}$, where and $1 \leq i \leq \hat{K}$ and $c_i = \Delta(\hat{S}_t = i, M_{t-1})$ depends on the*

memory of the receiver. Define $A_i \triangleq \{x_t : \Gamma_t^*(x_t, P_{M_{t-1}}) = i\}$*, then* A_i *and* A_l *are separated by the hyper-plane*

$$\{x_t \in \mathbb{R}^n : 2\sum_{j=1}^{\hat{K}} \Big[P(\hat{S}_t = j \mid S_t = l) - P(\hat{S}_t = j \mid S_t = i)\Big] \cdot \langle x_t, c_j \rangle$$
$$= \sum_{j=1}^{\hat{K}} \Big[P(\hat{S}_t = j \mid S_t = l) - P(\hat{S}_t = j \mid S_t = i)\Big] \cdot \|c_j\|^2\}$$

$A_i \cap A_l = \emptyset, \forall 1 \leq i, l \leq K, i \neq l$*, and* $\cup_{i=1}^{K} A_i = \mathbb{R}^n$.

Proof. An optimal encoder should map all the vectors in a way such that all the x_t mapped to the i-th region, i.e. $S_t = i$, produce smaller mean squared error than if they are mapped to any other, say, l-th region. Denote the set of vectors mapped to the i-th region by an optimal encoder as A_i^* Then all the vectors in A_i^* should satisfy the following equation for any given l other than i.

$$\begin{aligned}
& E\{\|x_t - \hat{x}_t\|^2 \mid S_t = i\} - E\{\|x_t - \hat{x}_t\|^2 \mid S_t = l\} \\
= \;& x_t^2 - 2E\{\langle x_t, \hat{x}_t \rangle \mid S_t = i\} + E\{\hat{x}_t^2 \mid S_t = i\} - x_t^2 + 2E\{\langle x_t, \hat{x}_t \rangle \mid S_t = l\} - E\{\hat{x}_t^2 \mid S_t = l\} \\
= \;& 2\left(E\{\langle x_t, \hat{x}_t \rangle \mid S_t = l\} - E\{\langle x_t, \hat{x}_t \rangle \mid S_t = i\}\right) + \left(E\{\hat{x}_t^2 \mid S_t = i\} - E\{\hat{x}_t^2 \mid S_t = l\}\right) \\
= \;& \sum_{j=1}^{\hat{K}} \Big[P(\hat{S}_t = j \mid S_t = l) - P(\hat{S}_t = j \mid S_t = i)\Big] \langle x_t, c_j \rangle \\
& - \sum_{j=1}^{\hat{K}} \Big[P(\hat{S}_t = j \mid S_t = l) - P(\hat{S}_t = j \mid S_t = i)\Big] \cdot \|c_j\|^2 \\
\leq \;& 0
\end{aligned}$$

where $\langle a, b \rangle$ denotes the inner product of a and b.

For any given $1 \leq l \leq \hat{K}$, consider the following sets

$$A_{il} \triangleq \{x_t \in \mathbb{R}^n : 2\sum_{j=1}^{\hat{K}} \Big[P(\hat{S}_t = j \mid S_t = l) - P(\hat{S}_t = j \mid S_t = i)\Big] \cdot \langle x_t, c_j \rangle$$
$$\leq \sum_{j=1}^{\hat{K}} \Big[P(\hat{S}_t = j \mid S_t = l) - P(\hat{S}_t = j \mid S_t = i)\Big] \cdot \|c_j\|^2\}$$

For any l, the vectors in A_i^* are in the set A_{il}, hence

$$A_i^* = \bigcap_{l \neq i} A_{il} \tag{4.6}$$

The regions A_i^* and A_l^* are separated by the hyperplane

$$\{x_t \in \mathbb{R}^n : 2\sum_{j=1}^{\hat{K}} \Big[P(\hat{S}_t = j \mid S_t = l) - P(\hat{S}_t = j \mid S_t = i)\Big] \cdot \langle x_t, c_j \rangle$$
$$= \sum_{j=1}^{\hat{K}} \Big[P(\hat{S}_t = j \mid S_t = l) - P(\hat{S}_t = j \mid S_t = i)\Big] \cdot \|c_j\|^2\}$$

which is a hyper-plane in R^n. □

Remark 4.5. Note when the source is scalar, the optimal encoder separates the range of the source into continuous intervals, and maps the points in each interval into a different symbol. That is, the optimal encoder for the scalar source is a threshold encoder.

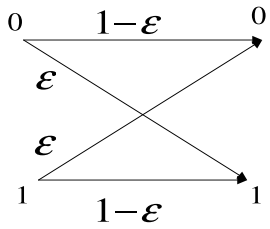

Figure 4.2: A Binary Symmetric Channel

4.4 The Algorithm to Find the Optimal Threshold of A Scalar Encoder for A Binary Symmetric Channel

In this section we focus on the special case of the binary symmetric channel and the scalar Markov source.

$$\begin{cases} P(\hat{S}_t = S_t) = 1 - \varepsilon \\ P(\hat{S}_t = 1 - S_t) = \varepsilon \end{cases} \tag{4.7}$$

where $S_t, \hat{S}_t \in \{0, 1\}$.

The channel is shown in Fig 4.2.

In this case the optimization problem reduces to that of finding an optimal threshold T such that

$$S_t = \begin{cases} 0 & X_t \leq T \\ 1 & X_t > T \end{cases}$$

For this special case of the original real-time estimation problem, we state a recursive algorithm to find a locally optimal solution. The algorithm is based on the one presented in [26]. But unlike in their problem, we have to consider the receiver memory in our calculation. Our approach is to recursively find the optimal encoder for a given decoder and then find the optimal decoder for a given encoder. Since each iteration reduces the mean squared error, the algorithm converges. Recursive algorithms are used in information theory to find the rate-distortion function and channel capacity [13] [16]. There the optimization is performed over convex sets, so the solution obtained is globally optimal. We on the other hand only know the algorithm converges to a locally optimal solution.

Let the reconstruction points be R_0 and R_1, both in $\mathbb{R}$, such that

$$\hat{X}_t = \begin{cases} R_0 = \Delta(\hat{S}_t = 0, M_{t-1}) \\ R_1 = \Delta(\hat{S}_t = 1, M_{t-1}) \end{cases}$$

Then the mean squared error is

$$\begin{aligned} D &= E\{|X_t - \hat{X}_t|^2\} \qquad (4.8) \\ &= P(\hat{S} = 0 \mid S = 0) \int_{-\infty}^{T} |x - R_0|^2 p_X(x) dx + P(\hat{S} = 1 \mid S = 0) \int_{-\infty}^{T} |x - R_1|^2 p_X(x) dx \\ &\quad + P(\hat{S} = 0 \mid S = 1) \int_{T}^{\infty} |x - R_0|^2 p_X(x) dx + P(\hat{S} = 1 \mid S = 1) \int_{T}^{\infty} |x - R_1|^2 p_X(x) dx \end{aligned}$$

4.4.1 The Optimal Encoder for A Fixed Decoder

For fixed R_0 and R_1, we can find the optimal threshold T^* by differentiating D with respect to T. In the following equation, let $P(A|B) \triangleq P(\hat{S} = A|S = B)$, where $A, B \in \{0, 1\}$, then we have

$$\begin{aligned}
\frac{dD}{dT} &= 0 \Rightarrow \\
T &= \frac{1}{2}\frac{(P(0|1) - P(0|0))\,R_0^2 + (P(1|1) - P(1|0))\,R_1^2}{(P(0|1) - P(0|0))\,R_0 + (P(1|1) - P(1|0))\,R_1} \\
&= \frac{1}{2} \cdot \frac{(2\epsilon - 1)(R_0^2 - R_1^2)}{(2\epsilon - 1)(R_0 - R_1)} \\
&= \frac{1}{2}(R_0 + R_1) \qquad (4.9)
\end{aligned}$$

To minimize mean squared error for fixed R_0 and R_1 we also need

$$\frac{d^2D}{dT^2} = 2(2\epsilon - 1)(R_0 - R_1) > 0 \qquad (4.10)$$

Therefore

$$\frac{d^2D}{dT^2} > 0 \Leftrightarrow \begin{cases} R_0 < R_1 & \text{when } \epsilon < \frac{1}{2} \\ R_0 \geq R_1 & \text{when } \epsilon \geq \frac{1}{2} \end{cases} \qquad (4.11)$$

Therefore for given R_0 and R_1 (hence a given decoder), the optimal encoder puts the threshold at the mid-point of the two reconstruction points. In addition, equation (4.11) must be satisfied. We will further discuss this point in the next subsection.

4.4.2 The Optimal Decoder for A Fixed Encoder

For fixed encoder, the optimal decoder is the conditional expectation.

$$\hat{X}_t = \begin{cases} R_0 = E\{X_t \mid \hat{S}_t = 0, M_{t-1}\} \\ R_1 = E\{X_t \mid \hat{S}_t = 1, M_{t-1}\} \end{cases} \tag{4.12}$$

where M_{t-1} is the known receiver memory from the last step.

Now once the optimal decoder for a fixed encoder is given by (4.12), we can go back to check the optimality condition given by (4.11).

We notice first, for the threshold given in (4.9) to be optimal, (4.11) must be true, but this is not guaranteed by (4.12), i.e., there may be solutions of (4.12) that violate (4.11).

Secondly, if we flip the areas encoded to 0 and 1, R_0 and R_1 will also flip since

$$\begin{aligned} R_0 &= E\{X_t \mid \hat{S}_t = 0, M_{t-1}\} \\ &= E\{X_t \mid S_t = 0, M_{t-1}\} \cdot \frac{(1-\epsilon)P(S_t=0)}{(1-\epsilon)P(S_t=0)+\epsilon P(S_t=1)} + \\ &\quad E\{X_t \mid S_t = 1, M_{t-1}\} \cdot \frac{\epsilon P(S_t=1)}{(1-\epsilon)P(S_t=0)+\epsilon P(S_t=1)} \end{aligned}$$

and

$$\begin{aligned} R_1 &= E\{X_t \mid \hat{S}_t = 0, M_{t-1}\} \\ &= E\{X_t \mid S_t = 0, M_{t-1}\} \cdot \frac{\epsilon P(S_t=0)}{\epsilon P(S_t=0)+(1-\epsilon)P(S_t=1)} + \\ &\quad E\{X_t \mid S_t = 1, M_{t-1}\} \cdot \frac{(1-\epsilon)P(S_t=1)}{\epsilon P(S_t=0)+(1-\epsilon)P(S_t=1)} \end{aligned}$$

Hence if we have $S'_t = \begin{cases} 0 & X_t > T \\ & \\ 1 & X_t \leq T \end{cases}$, then $R'_0 = R_1$ and $R'_1 = R_0$. But the derivation of (4.9) is not affected by this flip. Therefore by simply exchanging the areas coded to 1 and 0 we can always make (4.11) true and thus make the threshold given by (4.9) optimal.

4.4.3 The Algorithm To Jointly Find The Optimal Encoder And Decoder

In summary, we obtain the following recursive algorithm to find an encoder and decoder for transmission of a Markov process over a binary symmetric channel:

- Step 1: Set $\{R_0, R_1\} = \{R_0^{(0)}, R_1^{(0)}\}$, the initial reconstruction levels. They must satisfy (4.11) but are otherwise arbitrary.
- Step 2: Set $k = 0$ (the iteration index), and $D^{(0)} = \infty$.
- Step 3: Use (4.9) to determine the best threshold $T^{(k)}$.
- Step 4: Set $k = k+1$. Use (4.12) to find the best reconstruction levels $R_0^{(k)}$ and $R_1^{(k)}$.
- Step 5: Check if (4.11) is satisfied. If not, flip the areas encoded to 0 and 1, and therefore flip $R_0^{(k)}$ and $R_1^{(k)}$.

- Step 6: Compute the MSE $D^{(k)}$. If $\frac{D^{(k-1)}-D^{(k)}}{D^{(k)}} < \delta$, where δ is a preset positive fraction, go to step 7, otherwise go to step 3.

- Step 7: End the algorithm.

Remark 4.6. 1. With each iteration the MSE always decreases. From (4.8), the mean squared error is differentiable as a function of T, R_0 and R_1. Therefore we know the algorithm converges to a local optima.

2. The role played by memory in the system is in (4.12), which further affects the solution of (4.9).

4.5 Optimal estimation of memoryless Gaussian random vector source over binary symmetric channel

In this section we discuss the special case of the memoryless source. We are able to analytically characterize the optimal encoder and the minimum mean square error in this case. The optimal encoding strategy is to encode the principal component of the source. Lemma 4.8 asserts this for a random vector with independent components. Theorem 4.17 asserts the same for a source vector with correlated components.

4.5.1 System Description

Let $\mathbf{X} \in \mathbb{R}^n$ and $\mathbf{X} \sim \mathrm{N}(\mathbf{0}_n, \mathbf{K}_\mathbf{x})$, where $\mathbf{K}_\mathbf{x} \in \mathbb{R}^{n \times n}$. $\mathbf{X}$ is encoded with

$$S = G(\mathbf{X}) \tag{4.13}$$

where $S \in \{0, 1\}$. K_x is a symmetric positive definite matrix.

S is transmitted through a memoryless channel. From now on assume the channel is binary symmetric, i.e.

$$P(\hat{S} = 0|S = 0) = P(\hat{S} = 1|S = 1) = 1 - \epsilon$$

$$P(\hat{S} = 0|S = 1) = P(\hat{S} = 1|S = 0) = \epsilon$$

The decoder is

$$\hat{\mathbf{X}} \triangleq [\hat{X}_1 \ \hat{X}_2 \dots \hat{X}_n]^T = \Delta(\hat{S}) \tag{4.14}$$

The objective is to estimate $\mathbf{X}$ with minimum mean squared error, i.e. to design $G^*(\cdot)$ and $\Delta^*(\cdot)$ to minimize $E\{(\mathbf{X} - \hat{\mathbf{X}})^T(\mathbf{X} - \hat{\mathbf{X}})\}$.

For any given $G(\cdot)$, the optimal decoder is the conditional expectation, i.e. $\hat{\mathbf{X}} = E\{\mathbf{X}|\hat{S}\} = \Big[E\{X_1|\hat{S}\} \ E\{X_2|\hat{S}\} \dots E\{X_n|\hat{S}\}\Big]^T$.

4.5.2 The Optimal Vector Encoder for Binary Symmetric Channel: Independent Gaussian Noise Case

Since in section 4.3 it is shown that the optimal vector encoder over noisy channel partitions the vector space with hyper-planes, we search for our optimal design within this class of encoders. The following two lemmas provide the optimal encoder among all the encoders that partition the $\mathbb{R}^n$ space with a plane. In this subsection we derive the optimal encoder design when the components of the Gaussian random vector are mutually independent. We discuss the case of correlated components in the next subsection.

Lemma 4.7. *Let* $\mathbf{X} \in \mathbb{R}^n$ *and* $\mathbf{X} \sim \mathrm{N}(\mathbf{0}_n, \mathbf{K_x})$*, and* $\mathbf{K_x} = diag(\sigma_1^2, \sigma_2^2, \dots, \sigma_n^2)$*. Let* $\mathbf{w} \in \mathbb{R}^n$*,* $\|\mathbf{w}\| = 1$ *and* $b \in (-\infty, \infty)$*. Define a encoder such that*

$$S = G(\mathbf{X}) = \begin{cases} Y & \text{if } \mathbf{w^T X} \geq b \\ 1 - Y & \text{otherwise} \end{cases}$$

where $Y \in \{0, 1\}$. *Then for any binary symmetric channel, among all encoders with the same* $\mathbf{w}$, *the encoder with* $b = 0$, *i.e. when the plane passes through the origin, is optimal.*

Lemma 4.8. *Let* $\mathbf{X} \in \mathbb{R}^n$ *and* $\mathbf{X} \sim \mathrm{N}(\mathbf{0}_n, \mathbf{K_x})$ *and* $\mathbf{K_x} = diag(\sigma_1^2, \sigma_2^2, \ldots, \sigma_n^2)$. *Consider the encoder* $G^*(\cdot)$ *defined as below*

$$S = G^*(\mathbf{X}) = \begin{cases} Y & \text{if } \mathbf{w^{*T} X} \geq 0 \\ 1 - Y & \text{otherwise} \end{cases}$$

where $Y \in \{0, 1\}$, $\mathbf{w}^* \in \mathbb{R}^n$, $\|\mathbf{w}^*\| = 1$ *is chosen as below.*

1. *If* $\sigma_1 = \sigma_2 = \cdots = \sigma_n = \sigma$, *i.e. all the* n *directions are equally noisy, let* $\mathbf{w}^*$ *be any vector in* $\mathbb{R}^n$.

2. *Let* $\sigma_m = \max\{\sigma_1, \sigma_2, \ldots, \sigma_n\}$, *with* $m \in \{1, 2, \ldots, n\}$, *let* $\mathbf{w}^*$ *be the unit vector in the* m*-th direction.*

Then $G^*(\cdot)$ *is optimal, i.e., the optimal encoder only encodes the most noisy direction with one bit.*

To prove Lemmas 4.7 and 4.8 we prove lemmas 4.9 to 4.14.

Lemma 4.9. *Minimizing the mean squared error* $E\{(\mathbf{X}-\hat{\mathbf{X}})^T(\mathbf{X}-\hat{\mathbf{X}})\}$ *is equivalent to maximizing*

$$\left\|E\{\mathbf{X}|\hat{S}=0\}\right\|^2 P(\hat{S}=0) + \left\|E\{\mathbf{X}|\hat{S}=1\}\right\|^2 P(\hat{S}=1) \tag{4.15}$$

Proof. Since $\hat{\mathbf{X}} = E\{\mathbf{X}|\hat{S}\}$

we have

$$\begin{aligned}
& E\{(\mathbf{X}-\hat{\mathbf{X}})^T(\mathbf{X}-\hat{\mathbf{X}})\} \\
= \; & E\{\left\|\mathbf{X}-E\{\mathbf{X}|\hat{S}\}\right\|^2\} \\
= \; & E\left\{\left\|\mathbf{X}-E\{\mathbf{X}|\hat{S}=0\}\right\|^2|\hat{S}=0\right\}P(\hat{S}=0) + E\left\{\left\|\mathbf{X}-E\{\mathbf{X}|\hat{S}=1\}\right\|^2|\hat{S}=1\right\}P(\hat{S}=1) \\
= \; & \Big(E\{\mathbf{X}^T\mathbf{X}|\hat{S}=0\} - 2E\{\mathbf{X}^T|\hat{S}=0\}E\{\mathbf{X}|\hat{S}=0\} + \left\|E\{\mathbf{X}|\hat{S}=0\}\right\|^2) \cdot P(\hat{S}=0\Big) \\
& + \Big(E\{\mathbf{X}^T\mathbf{X}|\hat{S}=1\} - 2E\{\mathbf{X}^T|\hat{S}=1\}E\{\mathbf{X}|\hat{S}=1\} + \left\|E\{\mathbf{X}|\hat{S}=1\}\right\|^2) \cdot P(\hat{S}=1\Big) \\
= \; & E\{\mathbf{X}^T\mathbf{X}|\hat{S}=0\}P(\hat{S}=0) - \left\|E\{\mathbf{X}|\hat{S}=0\}\right\|^2 P(\hat{S}=0) \\
& + E\{\mathbf{X}^T\mathbf{X}|\hat{S}=1\}P(\hat{S}=1) - \left\|E\{\mathbf{X}|\hat{S}=1\}\right\|^2 P(\hat{S}=1) \\
= \; & E\{\mathbf{X}^T\mathbf{X}\} - \left\|E\{\mathbf{X}|\hat{S}=0\}\right\|^2 P(\hat{S}=0) - \left\|E\{\mathbf{X}|\hat{S}=1\}\right\|^2 P(\hat{S}=1) \\
= \; & \sum_{i=1}^{n}\sigma_i^2 - \left\|E\{\mathbf{X}|\hat{S}=0\}\right\|^2 P(\hat{S}=0) - \left\|E\{\mathbf{X}|\hat{S}=1\}\right\|^2 P(\hat{S}=1)
\end{aligned}$$

Thus the lemma is true. □

Below we define the probability mass function of the section of $\mathbb{R}^n$ mapped to 0 and 1 respectively.

$$P_0(\mathbf{w},b) \triangleq P(S=0) = \frac{1}{\sqrt{(2\pi)^n det(\mathbf{K_x})}} \int_{\mathbf{w^T x}<b} e^{-\frac{1}{2}\mathbf{x^T K_x^{-1} x}} d\mathbf{X}$$
$$= \frac{1}{\sqrt{(2\pi)^n} \prod_{i=1}^n \sigma_i} \int_{\mathbf{w^T x}<b} e^{-\frac{1}{2}\mathbf{x^T K_x^{-1} x}} d\mathbf{X}$$

and

$$\begin{aligned} P_1(\mathbf{w},b) &\triangleq P(S=1) \\ &= 1 - P_0(\mathbf{w},b) \\ &= \frac{1}{\sqrt{(2\pi)^n det(\mathbf{K_x})}} \int_{\mathbf{w^T x}<b} e^{-\frac{1}{2}\mathbf{x^T K_x^{-1} x}} d\mathbf{X} \\ &= \frac{1}{\sqrt{(2\pi)^n} \prod_{i=1}^n \sigma_i} \int_{\mathbf{w^T x}<b} e^{-\frac{1}{2}\mathbf{x^T K_x^{-1} x}} d\mathbf{X} \end{aligned}$$

In above equations, the special case where $b = 0$ is included. Obviously, when $b = 0$, $P_0(\mathbf{w}, 0) = P_1(\mathbf{w}, 0) = \frac{1}{2}$. Hereafter we drop the arguments of $P_0(\mathbf{w}, b)$ and $P_1(\mathbf{w}, b)$ and simply write them as P_0 and P_1.

Lemma 4.10. *For any $i \in \{1, 2, \ldots, n\}$, define*

$$\begin{aligned} \bar{X}_i(0) &\triangleq E\{X_i | S=0\} \\ &= \frac{1}{P_0\sqrt{(2\pi)^n det(\mathbf{K_x})}} \int_{\mathbf{w^T x}<b} x_i e^{-\frac{1}{2}\mathbf{x^T K_x^{-1} x}} d\mathbf{X} \end{aligned}$$

$$\begin{aligned} \bar{X}_i(1) &\triangleq E\{X_i | S=1\} \\ &= \frac{1}{P_1\sqrt{(2\pi)^n det(\mathbf{K_x})}} \int_{\mathbf{w^T x}\geq b} x_i e^{-\frac{1}{2}\mathbf{x^T K_x^{-1} x}} d\mathbf{X} \end{aligned}$$

and

$$\bar{\mathbf{X}}(j) = [\bar{X}_1(j)\ \bar{X}_2(j) \dots \bar{X}_n(j)]^T \tag{4.16}$$

for $j \in \{0, 1\}$.

Then we have

$$E\{X_i|\hat{S} = 0\} = \frac{(1-\epsilon)P_0\bar{X}_i(0) + \epsilon P_1\bar{X}_i(1)}{(1-\epsilon)P_0 + \epsilon P_1} \tag{4.17}$$

$$E\{X_i|\hat{S} = 1\} = \frac{\epsilon P_0\bar{X}_i(0) + (1-\epsilon)P_1\bar{X}_i(1)}{\epsilon P_0 + (1-\epsilon)P_1} \tag{4.18}$$

Proof.

$$\begin{aligned} E\{X_i|\hat{S} = 0\} &= E\{X_i|S = 0, \hat{S} = 0\}P(S = 0|\hat{S} = 0) + E\{X_i|S = 1, \hat{S} = 0\}P(S = 1|\hat{S} = 0) \\ &= E\{X_i|S = 0\}P(S = 0|\hat{S} = 0) + E\{X_i|S = 1\}P(S = 1|\hat{S} = 0) \\ &= \frac{(1-\epsilon)P_0}{(1-\epsilon)P_0 + \epsilon P_1}\bar{X}_i(0) + \frac{\epsilon P_1}{(1-\epsilon)P_0 + \epsilon P_1}\bar{X}_i(1) \end{aligned}$$

The second equation above is because that $X_i \to S \to \hat{S}$ is a Markov chain. The third equation is because of Bayes Rule.

Changing $\hat{S} = 0$ to $\hat{S} = 1$, we can prove equation (4.18) in the same way. □

Lemma 4.11.

$$P_0\bar{X}_i(0) + P_1\bar{X}_i(1) = E\{X_i\} = 0, \forall i \in \{1, 2, \cdots, n\} \tag{4.19}$$

Proof. The proof is straightforward and omitted. □

Lemma 4.12. *Define for all* $j \in \{1, 2, \cdots, n\}$

$$\begin{aligned} I_j(b) &\triangleq \int_{\mathbf{w^T x}<b} x_j p_{\mathbf{X}}(\mathbf{x}) d\mathbf{x}, \forall j \in \{1, 2, \cdots, n\} \\ &= \frac{1}{(2\pi)^{\frac{n}{2}} \prod_{i=1}^n \sigma_i} \int_{\mathbf{w^T x}<b} x_j e^{-\frac{1}{2}\mathbf{x^T K_x^{-1} x}} d\mathbf{X} \end{aligned} \tag{4.20}$$

where $p_{\mathbf{X}}(\cdot)$ *is the probability density function of random vector* $\mathbf{X}$*. Then*

$$\begin{aligned} &\left\| E\{\mathbf{X}|\hat{S}=0\} \right\|^2 P(\hat{S}=0) + \left\| E\{\mathbf{X}|\hat{S}=1\} \right\|^2 P(\hat{S}=1) \\ = \; & \frac{(2\epsilon-1)^2 \sum_{j=1}^n I_j(b)^2}{-(2\epsilon-1)^2 P_0^2 + (2\epsilon-1) P_0 + \epsilon(1-\epsilon)} \end{aligned} \tag{4.21}$$

Proof. From Lemma 4.10, we know that

$$\begin{aligned} &\left\| E\{\mathbf{X}|\hat{S}=0\} \right\|^2 P(\hat{S}=0) + \left\| E\{\mathbf{X}|\hat{S}=1\} \right\|^2 P(\hat{S}=1) \\ = \; & \sum_{j=1}^n \left(E\{X_j|\hat{S}=0\} \right)^2 P(\hat{S}=0) + \sum_{j=1}^n \left(E\{X_j|\hat{S}=1\} \right)^2 P(\hat{S}=1) \\ = \; & \sum_{j=1}^n \frac{\left((1-\epsilon)P_0 \bar{X}_j(0) + \epsilon P_1 \bar{X}_j(1)\right)^2}{(1-\epsilon)P_0 + \epsilon P_1} + \sum_{j=1}^n \frac{\left(\epsilon P_0 \bar{X}_j(0) + (1-\epsilon) P_1 \bar{X}_j(1)\right)^2}{\epsilon P_0 + (1-\epsilon) P_1} \\ = \; & (2\epsilon-1)^2 \sum_{j=1}^n \left(P_0 \bar{X}_j(0)\right)^2 \left(\frac{1}{(1-\epsilon)P_0 + \epsilon P_1} + \frac{1}{\epsilon P_0 + (1-\epsilon) P_1} \right) \\ = \; & (2\epsilon-1)^2 \sum_{j=1}^n \left(P_0 \bar{X}_j(0)\right)^2 \left(\frac{1}{(1-2\epsilon)P_0 + \epsilon} + \frac{1}{(2\epsilon-1)P_0 + 1 - \epsilon} \right) \\ = \; & \frac{(2\epsilon-1)^2}{-(2\epsilon-1)^2 P_0^2 + (2\epsilon-1) P_0 + \epsilon(1-\epsilon)} \sum_{j=1}^n \left(P_0 \bar{X}_j(0)\right)^2 \\ = \; & \frac{(2\epsilon-1)^2}{-(2\epsilon-1)^2 P_0^2 + (2\epsilon-1) P_0 + \epsilon(1-\epsilon)} \sum_{j=1}^n \left(\frac{1}{\sqrt{(2\pi)^n det(\mathbf{K_x})}} \int_{\mathbf{w^T x}<b} x_j e^{-\frac{1}{2}\mathbf{x^T K_x^{-1} x}} d\mathbf{X} \right)^2 \\ = \; & \frac{(2\epsilon-1)^2 \sum_{j=1}^n I_j(b)^2}{-(2\epsilon-1)^2 P_0^2 + (2\epsilon-1) P_0 + \epsilon(1-\epsilon)} \end{aligned} \tag{4.22}$$

The second equation comes from Lemmas 4.10, the third equation from (4.19), the fourth equation is true because $P_0 + P_1 = 1$, and the sixth equation is due to the definition of $\bar{X}_i(0)$.

□

Since $P_0 = \frac{1}{2}$ when $b = 0$, by Lemma 4.12, to prove Lemma 4.7 we need to show

$$\begin{aligned} & \frac{\sum_{j=1}^{n} I_j^2(b)}{-(2\epsilon-1)^2 P_0^2 + (2\epsilon-1) P_0 + \epsilon(1-\epsilon)} \\ \leq & \frac{\sum_{j=1}^{n} I_j^2(0)}{-(2\epsilon-1)^2 \left(\frac{1}{2}\right)^2 + (2\epsilon-1)\left(\frac{1}{2}\right) + \epsilon(1-\epsilon)} \\ = & \frac{\sum_{j=1}^{n} I_j^2(0)}{\frac{1}{4}} \end{aligned} \tag{4.23}$$

We have the following lemma regarding $I_j(b)$.

Lemma 4.13. *Let* $\mathbf{w} = [\ w_1 \quad w_2 \quad \cdots \quad w_n\ ]^T$, $\Omega_{\mathbf{w}}^2 = \sum_{j=1}^{n} w_i^2 \sigma_i^2$

$$I_j(b) = R_j(\mathbf{w}) e^{-\frac{b^2}{2\Omega_{\mathbf{w}}^2}}, \forall j \in \{1, 2, \cdots, n\} \tag{4.24}$$

where $R_j(\mathbf{w})$ *is independent of* b.

Proof. Let

$$\mathbf{P}_1 = \begin{bmatrix} P_{11} & P_{12} & \cdots & P_{1n} \\ P_{21} & P_{22} & \cdots & P_{2n} \\ \vdots & \vdots & \ddots & \vdots \\ P_{n1} & P_{n2} & \cdots & P_{nn} \end{bmatrix}$$

be a rotation matrix such that

$$\mathbf{P}_1 \begin{pmatrix} 1 \\ 0 \\ \vdots \\ 0 \end{pmatrix} = \begin{pmatrix} w_1 \\ w_2 \\ \vdots \\ w_n \end{pmatrix}$$

Then the original random vector $\mathbf{w} = \begin{pmatrix} w_1 \\ w_2 \\ \vdots \\ w_n \end{pmatrix}$ is rotated to $\mathbf{Z} = \begin{pmatrix} 1 \\ 0 \\ \vdots \\ 0 \end{pmatrix}$. Since x_i's are orthogonal, the variance of z_1, which is in the direction of $\mathbf{w}$ in the original coordinate system and the first basic direction of the transformed coordinate, is the following:

$$\begin{aligned} \sigma_{z_1}^2 &= \Omega_{\mathbf{w}}^2 \\ &= \sum_{j=1}^{n} w_i^2 \sigma_i^2 \end{aligned} \tag{4.25}$$

The probability density function of random vector $\mathbf{Z}$ now is

$$p_{\mathbf{Z}}(\mathbf{z}) = \frac{1}{(2\pi)^{\frac{n}{2}} det(\mathbf{K_x})} e^{-\frac{1}{2}\mathbf{z^T P_1^T K_x^{-1} P_1 z}}$$

Notice since $\mathbf{P}_1$ is orthogonal, the determinant of the variance matrix is not changed.

Now we look at $I_1(b)$,

$$
\begin{aligned}
I_1(b) &\triangleq \int_{\mathbf{w^T x}<b} x_1 p_{\mathbf{X}}(\mathbf{x}) d\mathbf{x} \\
&= \int_{\mathbf{w^T x}<b} \sum_{j=1}^{n} P_{1j} z_j p_{\mathbf{Z}}(\mathbf{z}) d\mathbf{z} \\
&= P_{11} \int_{-\infty}^{b} z_1 dz_1 \int_{-\infty}^{\infty} p_{\mathbf{Z}}(\mathbf{z}) dz_2 \cdots dz_n + \sum_{j=2}^{n} P_{1j} \int_{-\infty}^{b} dz_1 \int_{-\infty}^{\infty} z_j p_{\mathbf{Z}}(\mathbf{z}) dz_2 \cdots dz_n \\
&= \frac{P_{11}}{\sqrt{2\pi}\sigma_{z_1}} \int_{-\infty}^{b} z_1 e^{-\frac{z_1^2}{2\sigma_1^2}} dz_1 \\
&\quad + \sum_{j=2}^{n} \frac{P_{1j}}{2\pi\sqrt{\sigma_{z_1}^2\sigma_{z_j}^2 - \sigma_{z_1 z_j}^2}} \int_{-\infty}^{b}\int_{-\infty}^{\infty} z_j e^{-\frac{1}{2}\begin{pmatrix} z_1 & z_j \end{pmatrix}\begin{pmatrix} \sigma_{z_1}^2 & \sigma_{z_1 z_j} \\ \sigma_{z_1 z_j} & \sigma_{z_j}^2 \end{pmatrix}^{-1}\begin{pmatrix} z_1 \\ z_j \end{pmatrix}} dz_j dz_1 \\
&= -P_{11}\sigma_{z_1} e^{-\frac{b^2}{2\sigma_{z_1}^2}} \\
&\quad + \sum_{j=2}^{n} \frac{P_{1j}}{2\pi\sqrt{\sigma_{z_1}^2\sigma_{z_j}^2 - \sigma_{z_1 z_j}^2}} \int_{-\infty}^{b}\int_{-\infty}^{\infty} z_j e^{-\frac{1}{2}\begin{pmatrix} z_1 & z_j \end{pmatrix}\begin{pmatrix} \sigma_{z_1}^2 & \sigma_{z_1 z_j} \\ \sigma_{z_1 z_j} & \sigma_{z_j}^2 \end{pmatrix}^{-1}\begin{pmatrix} z_1 \\ z_j \end{pmatrix}} dz_j dz_1
\end{aligned}
$$

Now we analyze the second term. Without loss of generality, let $j = 2$. Define

$$a \triangleq \frac{\sigma_{z_2}}{\sqrt{\sigma_{z_1}^2\sigma_{z_2}^2 - \sigma_{z_1 z_2}^2}} \tag{4.26}$$

$$f \triangleq \frac{\sigma_{z_1}}{\sqrt{\sigma_{z_1}^2\sigma_{z_2}^2 - \sigma_{z_1 z_2}^2}} \tag{4.27}$$

$$c \triangleq \frac{-\sigma_{z_1 z_2}}{\sigma_{z_1}^2\sigma_{z_2}^2 - \sigma_{z_1 z_2}^2} \tag{4.28}$$

and

$$g \triangleq \frac{c}{f} = \frac{-\sigma_{z_1 z_2}}{\sigma_{z_1}\sqrt{\sigma_{z_1}^2\sigma_{z_2}^2 - \sigma_{z_1 z_2}^2}} \tag{4.29}$$

Notice

$$a^2 - g^2 = \frac{1}{\sigma_{z_1}^2}$$

Then we have

$$\begin{aligned}
& \int_{-\infty}^{b}\int_{-\infty}^{\infty} z_2 e^{-\frac{1}{2}\begin{pmatrix} z_1 & z_2 \end{pmatrix}\begin{pmatrix} \sigma_{z_1}^2 & \sigma_{z_1 z_2} \\ \sigma_{z_1 z_2} & \sigma_{z_2}^2 \end{pmatrix}^{-1}\begin{pmatrix} z_1 \\ z_2 \end{pmatrix}} dz_2 dz_1 \\
= & \int_{-\infty}^{b}\int_{-\infty}^{\infty} z_2 e^{-\frac{1}{2}\left(a^2 z_1^2 + f^2 z_2^2 + 2c z_1 z_2\right)} dz_2 dz_1 \\
= & \int_{-\infty}^{b} e^{-\frac{a^2 z_1^2}{2}} \int_{-\infty}^{\infty} z_2 e^{-\frac{1}{2}\left(f^2 z_2^2 + 2c z_1 z_2\right)} dz_2 dz_1 \\
= & \int_{-\infty}^{b} e^{-\frac{1}{2}(a^2 - g^2) z_1^2} \int_{-\infty}^{\infty} z_2 e^{-\frac{1}{2}\left(f^2 z_2^2 + 2c z_1 z_2 + g^2 z_1^2\right) + \frac{1}{2} g^2 z_1^2} dz_2 dz_1 \\
= & \int_{-\infty}^{b} e^{-\frac{1}{2}(a^2 - g^2) z_1^2} \int_{-\infty}^{\infty} z_2 e^{-\frac{1}{2}(f z_2 + g z_1)^2} dz_2 dz_1 \\
= & -\frac{\sqrt{2\pi} g}{f^2} \int_{-\infty}^{b} z_1 e^{-\frac{1}{2}(a^2 - g^2) z_1^2} dz_1 \\
= & -\frac{\sqrt{2\pi} g}{f^2} \int_{-\infty}^{b} z_1 e^{-\frac{z_1^2}{2\sigma_{z_1}^2}} dz_1 \\
= & \frac{\sqrt{2\pi} g \sigma_{z_1}}{f^2} e^{-\frac{b^2}{2\sigma_{z_1}^2}} \\
= & \; r_{12} e^{-\frac{b^2}{2\sigma_{z_1}^2}}
\end{aligned} \tag{4.30}$$

where $r_{12} = \frac{\sqrt{2\pi} g \sigma_{z_1}}{f^2}$ is independent of b. Similarly it can be shown that the j-th term in the summation in equation 4.26 can be written as $r_{1j} e^{-\frac{b^2}{2\sigma_{z_1}^2}}$ where r_{1j} is

independent of b. It follows that

$$\begin{aligned} I_1(b) &= \sum_{j=1}^{n} r_{1j} e^{-\frac{b^2}{2\sigma_{z_1}^2}} \\ &\triangleq R_1 e^{-\frac{b^2}{2\Omega_{\mathbf{w}}^2}} \end{aligned} \tag{4.31}$$

where R_1 is independent of b and can be obtained from equations (4.26) and (4.30).

To show $I_j(b) = R_j e^{-\frac{b^2}{2\Omega_{\mathbf{w}}^2}}$, repeat the analysis with

$$\mathbf{P}_1 \begin{pmatrix} 0 \\ \vdots \\ 0 \\ 1 \\ 0 \\ \vdots \\ 0 \end{pmatrix} = \begin{pmatrix} w_1 \\ w_2 \\ \vdots \\ \vdots \\ \vdots \\ w_n \end{pmatrix}$$

where $\begin{pmatrix} 0 & \cdots & 0 & 1 & 0 & \cdots & 0 \end{pmatrix}^T$ is the j-th basis vector. □

Lemma 4.14.

$$\frac{\sqrt{1-e^{-\varphi^2}}}{2} \geq \frac{1}{\sqrt{2\pi}} \int_0^{\varphi} e^{-\frac{y^2}{2}} dy, \ \forall \varphi \geq 0 \tag{4.32}$$

where the equality is true when $\varphi = 0$ *or* $\varphi \to \infty$.

Proof. See Appendix C.

□

With lemmas 4.9— 4.14, we prove Lemma 4.7 as follows.

- *Proof of Lemma 4.7*

  Lemma 4.13 tells us that

$$\begin{aligned} \sum_{j=1}^{n} I_j^2(b) &= \sum_{j=1}^{n} R_j^2 e^{-\frac{b^2}{\Omega_{\mathbf{w}}^2}} \\ &= F(\mathbf{w}) e^{-\frac{b^2}{\Omega_{\mathbf{w}}^2}} \end{aligned} \tag{4.33}$$

  where $F(\mathbf{w})$ does not depend on b.

  Hence (4.23) becomes

$$\frac{\sum_{j=1}^{n} F(\mathbf{w}) e^{-\frac{b^2}{\Omega_{\mathbf{w}}^2}}}{-\left(2\epsilon-1\right)^2 P_0^2 + \left(2\epsilon-1\right) P_0 + \epsilon(1-\epsilon)} \leq \frac{\sum_{j=1}^{n} F(\mathbf{w})}{\frac{1}{4}} \tag{4.34}$$

  Define

$$\alpha \triangleq \frac{1}{\sqrt{2\pi}\Omega_{\mathbf{w}}} \int_0^b e^{-\frac{z_1^2}{2\Omega_{\mathbf{w}}^2}} dz_1 \tag{4.35}$$

  Then

$$\begin{aligned} P_0 &= \frac{1}{\sqrt{2\pi}\Omega_{\mathbf{w}}} \int_{-\infty}^{b} e^{-\frac{z_1^2}{2\Omega_{\mathbf{w}}^2}} dz_1 \\ &= \frac{1}{2} + \alpha \end{aligned}$$

Continuing with (4.34), since $P_0 = \frac{1}{2} + \alpha$, we get

$$\begin{aligned} & \frac{\sum_{j=1}^{n} F(\mathbf{w}) e^{-\frac{b^2}{\Omega_{\mathbf{w}}^2}}}{-(2\epsilon-1)^2 P_0^2 + (2\epsilon-1) P_0 + \epsilon(1-\epsilon)} \\ \leq & \frac{\sum_{j=1}^{n} F(\mathbf{w})}{\frac{1}{4}} \\ \Leftrightarrow & -(2\epsilon-1)^2 P_0^2 + (2\epsilon-1) P_0 + \epsilon(1-\epsilon) \geq \frac{e^{-\frac{b^2}{\Omega_{\mathbf{w}}^2}}}{4} \\ \Leftrightarrow & \frac{1}{4} - (2\epsilon-1)^2 \alpha^2 \geq \frac{e^{-\frac{b^2}{\Omega_{\mathbf{w}}^2}}}{4} \end{aligned}$$

Since $(2\epsilon-1)^2 \leq 1$ it suffices to prove

$$\frac{1}{4} - \alpha^2 \geq \frac{e^{-\frac{b^2}{\Omega_{\mathbf{w}}^2}}}{4}$$

i.e.

$$\begin{aligned} \alpha &= \frac{1}{\sqrt{2\pi}\Omega_{\mathbf{w}}} \int_0^b e^{-\frac{z_1^2}{2\Omega_{\mathbf{w}}^2}} dz_1 \\ &\leq \frac{\sqrt{1 - e^{-\frac{b^2}{\Omega_{\mathbf{w}}^2}}}}{2} \end{aligned} \tag{4.36}$$

By Lemma 4.14,

$$\frac{1}{\sqrt{2\pi}} \int_0^{\varphi} e^{-\frac{y^2}{2}} dy \leq \frac{\sqrt{1 - e^{-\varphi^2}}}{2}, \ \forall \varphi \geq 0$$

Putting $y = \frac{z_1}{\Omega_{\mathbf{w}}}$ in (4.36), the lemma follows.

We prove one more lemma before using Lemma 4.7 to prove Lemma 4.8.

Lemma 4.15. *For $w_1 \neq 0$ and* $\mathbf{K}$ *non-singular,*

$$\begin{aligned} & det\left[\frac{1}{\sigma_1^2 w_1^2}\begin{pmatrix} w_2^2 & w_2w_3 & \cdots & w_2w_n \\ w_3w_2 & w_3^2 & \cdots & w_3w_n \\ \vdots & \vdots & \ddots & \vdots \\ w_nw_2 & w_nw_3 & \cdots & w_n^2 \end{pmatrix} + diag\left(\frac{1}{\sigma_2^2}, \frac{1}{\sigma_3^2}, \cdots, \frac{1}{\sigma_n^2}\right)\right] \\ = & \frac{\sigma_1^2 w_1^2 + \sigma_2^2 w_2^2 + \cdots + \sigma_n^2 w_n^2}{w_1^2 \sigma_1^2 \sigma_2^2 \cdots \sigma_n^2} \\ = & \frac{\sum_{i=1}^n \sigma_i^2 w_i^2}{w_1^2 \prod_{i=1}^n \sigma_i^2} \end{aligned} \tag{4.37}$$

Proof. See Appendix D

□

With Lemma 4.7 and Lemma 4.15, we prove Lemma 4.8 as follows.

- *Proof of Lemma 4.8*

From Lemmas 4.9, 4.12 and Lemma 4.7, we want to maximize the following expression when $b = 0$.

$$\begin{aligned} & \frac{\sum_{i=1}^n \left(\frac{1}{(2\pi)^{\frac{n}{2}} \prod_{j=1}^n \sigma_j} \int_{\mathbf{w^T x}<b} x_i e^{-\frac{1}{2}\sum_{j=1}^n \frac{x_j^2}{\sigma_j^2}} d\mathbf{x}\right)^2}{-(2\epsilon-1)^2 P_0^2 + (2\epsilon-1) P_0 + \epsilon(1-\epsilon)} \\ = & \left(\frac{4}{(2\pi)^{\frac{n}{2}} \prod_{j=1}^n \sigma_j}\right)^2 \sum_{i=1}^n \left(\int_{\mathbf{w^T x}<0} x_i e^{-\frac{1}{2}\sum_{j=1}^n \frac{x_j^2}{\sigma_j^2}} d\mathbf{x}\right)^2 \end{aligned} \tag{4.38}$$

Look at the term with $i = 1$,

$$
\begin{aligned}
& \frac{1}{(2\pi)^{\frac{n}{2}}\prod_{j=1}^{n}\sigma_j}\int_{\mathbf{w^T x}<0} x_1 e^{-\frac{1}{2}\sum_{j=1}^{n}\frac{x_j^2}{\sigma_j^2}}d\mathbf{X} \\
= & \frac{1}{(2\pi)^{\frac{n}{2}}\prod_{j=1}^{n}\sigma_j}\int_{-\infty}^{\infty}\cdots\int_{-\infty}^{\infty}\int_{-\infty}^{-\frac{\sum_{k=2}^{n}w_k x_k}{w_1}} x_1 e^{-\frac{1}{2}\sum_{j=1}^{n}\frac{x_j^2}{\sigma_j^2}}dx_1dx_2\cdots dx_n \\
= & \frac{1}{(2\pi)^{\frac{n}{2}}\prod_{j=1}^{n}\sigma_j}\int_{-\infty}^{\infty}e^{-\frac{x_n^2}{2\sigma_n^2}}\int_{-\infty}^{\infty}e^{-\frac{x_{n-1}^2}{2\sigma_{n-1}^2}}\int_{-\infty}^{\infty}e^{-\frac{x_2^2}{2\sigma_2^2}}\int_{-\infty}^{-\frac{\sum_{k=2}^{n}w_k x_k}{w_1}} x_1 e^{-\frac{x_1^2}{2\sigma_1^2}}dx_1dx_2\cdots dx_n \\
= & -\frac{\sigma_1}{(2\pi)^{\frac{n}{2}}\prod_{j=2}^{n}\sigma_j}\int_{-\infty}^{\infty}\cdots\int_{-\infty}^{\infty}e^{-\frac{1}{2}\sum_{j=2}^{n}\frac{x_j^2}{\sigma_j^2}}e^{-\frac{(\sum_{k=2}^{n}w_k x_k)^2}{2\sigma_1^2 w_1^2}}dx_2dx_3\cdots dx_n
\end{aligned}
$$

If $w_1 = 0$, the innermost integration has limits from $-\infty$ to $+\infty$. Since random vector $\mathbf{X}$ is zero mean, we know the integral is 0.

Now assuming $w_1 \neq 0$, continuing from above equation we have

$$
\begin{aligned}
& -\frac{\sigma_1}{(2\pi)^{\frac{n}{2}}\prod_{j=2}^{n}\sigma_j}\cdot \\
& \int_{-\infty}^{\infty}\cdots\int_{-\infty}^{\infty}e^{-\frac{1}{2}\sum_{j=2}^{n}\frac{x_j^2}{\sigma_j^2}}e^{-\frac{(\sum_{k=2}^{n}w_k x_k)^2}{2\sigma_1^2 w_1^2}}dx_2dx_3\cdots dx_n \\
= & -\frac{(2\pi)^{\frac{n-1}{2}}\sigma_1}{(2\pi)^{\frac{n}{2}}\prod_{j=2}^{n}\sigma_j}(det[\frac{1}{\sigma_1^2 w_1^2}\begin{pmatrix} w_2^2 & w_2w_3 & \cdots & w_2w_n \\ w_3w_2 & w_3^2 & \cdots & w_3w_n \\ \vdots & \vdots & \ddots & \vdots \\ w_nw_2 & w_nw_3 & \cdots & w_n^2 \end{pmatrix} \\
& +diag\left(\frac{1}{\sigma_2^2},\frac{1}{\sigma_3^2},\cdots,\frac{1}{\sigma_n^2}\right)])^{-\frac{1}{2}}
\end{aligned}
$$

$$= -\frac{\sigma_1}{(2\pi)^{\frac{1}{2}}\prod_{j=2}^{n}\sigma_j}\frac{w_1\prod_{i=1}^{n}\sigma_i}{\sqrt{\sum_{i=1}^{n}\sigma_i^2 w_i^2}} \tag{4.39}$$

$$= -\frac{\sigma_1^2 w_1}{\sqrt{2\pi\sum_{i=1}^{n}\sigma_i^2 w_i^2}} \tag{4.40}$$

where (4.39) comes from lemma 4.15.

Similarly we can show the j-th term is $\frac{-\sigma_j^2 w_j}{\sqrt{2\pi\sum_{i=1}^{n}\sigma_i^2 w_i^2}}$.

Thus (4.38) becomes

$$(2\varepsilon-1)^2\frac{2}{\pi}\cdot\frac{\sum_{j=1}^{n}\sigma_j^4 w_j^2}{\sum_{j=1}^{n}\sigma_j^2 w_j^2} \tag{4.41}$$

Without loss of generality, let $\sigma_k = \max\{\sigma_i : w_i \neq 0\}$, then

$$\frac{\sum_{j=1}^{n}\sigma_j^4 w_j^2}{\sum_{j=1}^{n}\sigma_j^2 w_j^2} = \sigma_k^2 - \frac{\sum_{j=1,j\neq k}^{n}(\sigma_1^2-\sigma_j^2)\sigma_j^2 w_j^2}{\sum_{j=2}^{n}\sigma_j^2 w_j^2} \tag{4.42}$$

The second term in (4.42) is non-negative. There are two possible cases.

1. $\sigma_1 = \sigma_2 = \cdots = \sigma_n = \sigma$, i.e. the n directions are equally noisy. In this case the mean squared error is constant for all $\mathbf{w}$, thus any $\mathbf{w}$ is optimal.

2. Otherwise, (4.38) is maximized, i.e. the mean squared estimation error is minimized, if and only if $w_j = 0, \forall j \in \{2, 3, \cdots, n\}$. In this case, since $\|\mathbf{w}\| = 1$, we know that $w_1 = 1$, i.e. $\mathbf{w}$ is in the direction with the maximum noise variance.

The lemma is proved.

Remark 4.16. When the encoding is performed according to Lemma 4.8, the minimum MSE for any given binary symmetric channel can be obtained:

1. $\sigma_1 = \sigma_2 = \cdots = \sigma_n = \sigma$, i.e. the n directions are equally noisy.

   The MSE is

   $$\left(n - \frac{2(2\epsilon - 1)^2}{\pi}\right)\sigma^2$$

   When the channel has maximum entropy, i.e. $\epsilon = \frac{1}{2}$, the minimum MSE is $n\sigma^2$. Therefore no information is transmitted over the channel.

   When the channel is perfect, i.e. $\epsilon = 0$, the minimum MSE is

   $$\left(n - \frac{2}{\pi}\right)\sigma^2$$

   The reduction in MSE is due to quantization.

2. When not all variances are the same, and $\sigma_i = \max(\sigma_1, \sigma_2, \cdots, \sigma_n)$, i.e. direction i is the most noisy.

   The MSE is

   $$\sum_{j \neq i} \sigma_j^2 + \left(1 - \frac{2(2\epsilon - 1)^2}{\pi}\right)\sigma_i^2$$

   When the channel has maximum entropy, i.e. $\epsilon = \frac{1}{2}$, the minimum MSE is $\sum_{j=1}^{n} \sigma_j^2$. Therefore no information is transmitted over the channel.

   When the channel is perfect, i.e. $\epsilon = 0$, the minimum MSE is

   $$\sum_{j \neq i} \sigma_j^2 + \left(1 - \frac{2}{\pi}\right)\sigma_i^2$$

The reduction in MSE is due to quantization in the X_i direction.

4.5.3 The Optimal Vector Encoder for Binary Symmetric Channel: Correlated Gaussian Noise Case

For an n dimensional zero-mean Gaussian random vector with density

$$f_{\mathbf{X}}(\mathbf{x}) = \frac{1}{(2\pi)^{\frac{n}{2}}\sqrt{det(\mathbf{K_X})}} e^{-\frac{1}{2}\mathbf{x}^T\mathbf{K_X^{-1}}\mathbf{x}}$$

where $\mathbf{K_X}$ is the covariance matrix defined by

$$\mathbf{K_X} \triangleq E\{\mathbf{X}\mathbf{X}^T\} = E\begin{bmatrix} X_1^2 & X_1X_2 & \cdots & X_1X_n \\ X_2X_1 & X_2^2 & \cdots & X_2X_n \\ \vdots & \vdots & \ddots & \vdots \\ X_nX_1 & X_nX_2 & \cdots & X_n^2 \end{bmatrix}$$

If K_x is positive-definite then $\mathbf{K_X}$ can be diagonalized to be

$$\mathbf{M} = diag\{\sigma_1^2, \sigma_2^2, \cdots, \sigma_n^2\} = \mathbf{Q^T K_x Q}$$

where $\sigma_1^2, \sigma_2^2, \cdots, \sigma_n^2$ are the eigen-values of $\mathbf{K_X}$, with corresponding orthonormal eigen-vectors $\mathbf{v}_1, \mathbf{v}_2, \cdots, \mathbf{v}_n$ and $\mathbf{Q} \triangleq \begin{bmatrix} \mathbf{v}_1 & \mathbf{v}_2 & \cdots & \mathbf{v}_n \end{bmatrix}$ (See e.g. [30]). $\mathbf{Q}$ is an orthonormal matrix with $\mathbf{Q}^T\mathbf{Q} = \mathbf{Q}\mathbf{Q}^T = \mathbf{I}$, where $\mathbf{I}$ is the unit matrix. We also have $det[\mathbf{K_X}] = det[\mathbf{M}] = \prod_{j=1}^n \sigma_j^2$, $\mathbf{K_X^{-1}} = \mathbf{Q}\mathbf{M}^{-1}\mathbf{Q}^T$, and $det[\mathbf{Q}] = 1$..

Then we have the following theorem.

Theorem 4.17. *Let* $\mathbf{X} \in \mathbb{R}^n$ *and* $\mathbf{X} \sim \mathrm{N}(\mathbf{0}_n, \mathbf{K_x})$ *and hence* $\mathbf{K_X}$ *has orthonormal eigen-vectors* $\mathbf{v}_1, \mathbf{v}_2, \cdots, \mathbf{v}_n$ *corresponding to eigen-values* $\sigma_1^2, \sigma_2^2, \cdots, \sigma_n^2$. *Consider encoder* $G^*(\cdot)$ *defined as below*

$$S = G^*(\mathbf{X}) = \begin{cases} Y & \text{if } \mathbf{w^{*T}X} \geq 0 \\ 1 - Y & \text{otherwise} \end{cases}$$

where $Y \in \{0, 1\}$, $\mathbf{w}^* \in \mathbb{R}^n$, $\|\mathbf{w}^*\| = 1$ *and* w^* *is chosen as below. If*

1. $\sigma_1 = \sigma_2 = \cdots = \sigma_n = \sigma$, *i.e. all the* n *directions are equally noisy,* $\mathbf{w}^*$ *is any vector in* $\mathbb{R}^n$.

2. *Otherwise, let* $\sigma_m = \max\{\sigma_1, \sigma_2, \ldots, \sigma_n\}$, *with* $m \in \{1, 2, \ldots, n\}$. *Then* $\mathbf{w}^* = \mathbf{v}_m$ *is the unit vector in the direction of the m-th eigen-vector.*

Then $G^*(\cdot)$ *is optimal, i.e., the optimal encoder only encodes the most noisy direction with one bit.*

Proof. By Theorem 4.4, there is an optimal encoder of $\mathbf{X}$ within the class of encoders separating $\mathbb{R}^n$ by a hyperplane through the origin.

Consider random vector $\mathbf{Z} = \mathbf{Q}^T\mathbf{X}$, where $\mathbf{Q} = \begin{bmatrix} \mathbf{v}_1 & \mathbf{v}_2 & \cdots & \mathbf{v}_n \end{bmatrix}$. Then the covariance of $\mathbf{Z}$ satisfies

$$\mathbf{K_Z} \triangleq E\{\mathbf{Z}\mathbf{Z}^T\} = \mathbf{Q}^T\mathbf{K_X}\mathbf{Q} = \mathbf{M} = diag\{\sigma_1^2, \sigma_2^2, \cdots, \sigma_n^2\} \tag{4.43}$$

and the density of $\mathbf{Z}$ is

$$\begin{aligned} f_{\mathbf{Z}}(\mathbf{z}) &= \frac{1}{(2\pi)^{\frac{n}{2}}\sqrt{det(\mathbf{K_Z})}} e^{-\frac{1}{2}\mathbf{z}^T\mathbf{K_Z^{-1}}\mathbf{z}} \\ &= \frac{1}{(2\pi)^{\frac{n}{2}}\prod_{j=1}^{n}\sigma_j} e^{-\frac{1}{2}\mathbf{z}^T\mathbf{M^{-1}}\mathbf{z}} \end{aligned}$$

All the n components of random vector $\mathbf{Z}$ are independent. Lemma 4.8 gives an optimal encoder for such a random vector. Below we will prove there is a 1-to-1 map between the hyperplane encoders of $\mathbf{Z}$ and $\mathbf{X}$ producing the same mean squared error.

Consider the mean squared estimation error caused by the following two encoders

$$S_x = G_x(\mathbf{X}) = \begin{cases} Y & \text{if } \mathbf{w^T X} \geq 0 \\ 1-Y & \text{otherwise} \end{cases} \tag{4.44}$$

with $Y \in \{0, 1\}$.

and

$$S_z = G_z(\mathbf{Z}) = \begin{cases} Y & \text{if } (\mathbf{Q^T w})^{\mathbf{T}}\mathbf{Z} = \mathbf{w^T Q Z} \geq 0 \\ 1-Y & \text{otherwise} \end{cases} \tag{4.45}$$

with $Y \in \{0, 1\}$.

The encoder $G_z(\cdot)$ encodes the random vector $\mathbf{Z}$, which is rotated from $\mathbf{X}$ by $\mathbf{Q^T}$, with hyper-plane $\mathbf{Q^T w}$, which is rotated by $\mathbf{Q^T}$ from the hyper-plane $\mathbf{w}$ used by $G_x(\cdot)$.

Let $P_{x0} \triangleq P(S_x = 0)$ and $P_{x1} \triangleq P(S_x = 1)$. From Lemma 4.10, the outputs of

the decoder in estimating X when the encoder is $G_x(\cdot)$ are

$$E\{\mathbf{X}|\hat{S}_x = 0\} = \frac{(1-\epsilon)P_{x0}E\{\mathbf{X}|S_x = 0\} + \epsilon P_{x1}E\{\mathbf{X}|S_x = 1\}}{(1-\epsilon)P_{x0} + \epsilon P_{x1}} \tag{4.46}$$

and

$$E\{\mathbf{X}|\hat{S}_x = 1\} = \frac{\epsilon P_{x0}E\{\mathbf{X}|S_x = 0\} + (1-\epsilon)P_{x1}E\{\mathbf{X}|S_x = 1\}}{\epsilon P_{x0} + (1-\epsilon)P_{x1}} \tag{4.47}$$

where $\epsilon = P(\hat{S} = 0 \mid S = 1) = P(\hat{S} = 1 \mid S = 0)$. Define $P_{z0} \triangleq P(S_z = 0)$ and $P_{z1} \triangleq P(S_z = 1)$. Again by Lemma 4.10, the outputs of the decoder in estimating $\mathbf{Z}$ when the encoder is $G_z(\cdot)$ are

$$E\{\mathbf{Z}|\hat{S}_z = 0\} = \frac{(1-\epsilon)P_{z0}E\{\mathbf{X}|S_z = 0\} + \epsilon P_{z1}E\{\mathbf{Z}|S_z = 1\}}{(1-\epsilon)P_{z0} + \epsilon P_{z1}} \tag{4.48}$$

and

$$E\{\mathbf{Z}|\hat{S}_z = 1\} = \frac{\epsilon P_{z0}E\{\mathbf{Z}|S_z = 0\} + (1-\epsilon)P_{z1}E\{\mathbf{Z}|S_z = 1\}}{\epsilon P_{z0} + (1-\epsilon)P_{z1}} \tag{4.49}$$

With encoder as $G_x(\cdot)$, the expectation of $\mathbf{X}$ conditioned on $S_x = 0$ is

$$\begin{aligned} & E\{\mathbf{X}|S_x = 0\} \\ = \; & \frac{1}{P_{x0}\sqrt{(2\pi)^n det(\mathbf{K_x})}} \int_{\mathbf{w^T x}<0} \mathbf{x} e^{-\frac{1}{2}\mathbf{x^T K_x^{-1} x}} d\mathbf{X} \\ = \; & \frac{1}{P_{x0}\sqrt{(2\pi)^n}\prod_{i=1}^n \sigma_i} \int_{\mathbf{w^T x}<0} \mathbf{x} e^{-\frac{1}{2}\mathbf{x^T K_x^{-1} x}} d\mathbf{X} \end{aligned}$$

and

$$\begin{aligned} P_{x0} &= \frac{1}{\sqrt{(2\pi)^n det(\mathbf{K_x})}} \int_{\mathbf{w^T x}<0} e^{-\frac{1}{2}\mathbf{x^T K_x^{-1} x}} d\mathbf{X} \\ &= \frac{1}{\sqrt{(2\pi)^n \prod_{i=1}^n \sigma_i}} \int_{\mathbf{w^T x}<0} e^{-\frac{1}{2}\mathbf{x^T K_x^{-1} x}} d\mathbf{X} \end{aligned}$$

On the other hand, when the encoder is $G_z(\cdot)$ the expectation of $\mathbf{Z}$ conditioned on $S_z = 0$ is

$$\begin{aligned} & E\{\mathbf{Z}|S_z = 0\} \\ = & \frac{1}{P_{z0}\sqrt{(2\pi)^n det(\mathbf{M})}} \int_{\mathbf{w^T Q z}<0} \mathbf{z} e^{-\frac{1}{2}\mathbf{z^T M^{-1} z}} d\mathbf{Z} \\ = & \frac{1}{P_{z0}\sqrt{(2\pi)^n \prod_{i=1}^n \sigma_i}} \int_{\mathbf{w^T Q z}<0} \mathbf{z} e^{-\frac{1}{2}\mathbf{z^T M^{-1} z}} d\mathbf{Z} \end{aligned}$$

and

$$\begin{aligned} P_{z0} &= \frac{1}{\sqrt{(2\pi)^n det(\mathbf{M})}} \int_{\mathbf{w^T Q z}<0} e^{-\frac{1}{2}\mathbf{z^T M^{-1} z}} d\mathbf{Z} \\ &= \frac{1}{\sqrt{(2\pi)^n \prod_{i=1}^n \sigma_i}} \int_{\mathbf{w^T Q z}<0} e^{-\frac{1}{2}\mathbf{z^T M^{-1} z}} d\mathbf{Z} \end{aligned}$$

Since $\mathbf{Z} = \mathbf{Q^T X}$ and $\mathbf{M} = \mathbf{Q^T K_x Q}$, we know

$$\begin{aligned} P_{z0} &= \frac{1}{\sqrt{(2\pi)^n \prod_{i=1}^n \sigma_i}} \int_{\mathbf{w^T Q z}<0} e^{-\frac{1}{2}\mathbf{z^T M^{-1} z}} d\mathbf{Z} \\ &= \frac{1}{\sqrt{(2\pi)^n \prod_{i=1}^n \sigma_i}} \int_{\mathbf{w^T x}<0} e^{-\frac{1}{2}\mathbf{x^T Q M^{-1} Q^T x}} det[Q] d\mathbf{X} \\ &= \frac{1}{\sqrt{(2\pi)^n \prod_{i=1}^n \sigma_i}} \int_{\mathbf{w^T x}<0} e^{-\frac{1}{2}\mathbf{x^T K_x^{-1} x}} d\mathbf{X} \\ &= P_{x0} \end{aligned}$$

since $det[Q] = 1$. Also

$$\begin{aligned}
& E\{\mathbf{Z}|S_z = 0\} \\
= & \frac{1}{P_{z0}\sqrt{(2\pi)^n}\prod_{i=1}^n \sigma_i} \int_{\mathbf{w^T Qz}<0} \mathbf{z} e^{-\frac{1}{2}\mathbf{z^T M^{-1} z}} d\mathbf{Z} \\
= & \frac{1}{P_{x0}\sqrt{(2\pi)^n}\prod_{i=1}^n \sigma_i} \int_{\mathbf{w^T x}<0} \mathbf{Q^T x} e^{-\frac{1}{2}\mathbf{x^T Q M^{-1} Q^T x}} det[\mathbf{Q}] d\mathbf{X} \\
= & \frac{1}{P_{x0}\sqrt{(2\pi)^n}\prod_{i=1}^n \sigma_i} \int_{\mathbf{w^T x}<0} \mathbf{Q^T x} e^{-\frac{1}{2}\mathbf{x^T K_x^{-1} x}} d\mathbf{X} \\
= & \mathbf{Q^T} E\{\mathbf{X}|S_x = 0\}
\end{aligned}$$

Similarly we can prove $E\{\mathbf{Z}|S_z = 1\} = \mathbf{Q^T} E\{\mathbf{X}|S_x = 1\}$ and therefore by (4.48) and (4.49)

$$E\{\mathbf{Z}|\hat{S}_z = 0\} = \mathbf{Q^T} E\{\mathbf{X}|\hat{S}_x = 0\}$$

and

$$E\{\mathbf{Z}|\hat{S}_z = 1\} = \mathbf{Q^T} E\{\mathbf{X}|\hat{S}_x = 1\}$$

Moreover,

$$\begin{aligned}
& E_{G_z}\left\{\left(\mathbf{Z} - \hat{\mathbf{Z}}\right)^T \left(\mathbf{Z} - \hat{\mathbf{Z}}\right)\right\} \\
= & E_{G_x}\left\{\left(\mathbf{Q^T X} - \mathbf{Q^T}\hat{\mathbf{X}}\right)^T \left(\mathbf{Q^T X} - \mathbf{Q^T}\hat{\mathbf{X}}\right)\right\} \\
= & E_{G_x}\left\{\left(\mathbf{X} - \hat{\mathbf{X}}\right)^T \mathbf{Q}\mathbf{Q}^T \left(\mathbf{X} - \hat{\mathbf{X}}\right)\right\} \\
= & E_{G_x}\left\{\left(\mathbf{X} - \hat{\mathbf{X}}\right)^T \left(\mathbf{X} - \hat{\mathbf{X}}\right)\right\}
\end{aligned}$$

The mean squared error achieved by $G_x(\cdot)$ in estimating $\mathbf{X}$ and the mean squared error achieved by $G_z(\cdot)$ in estimating $\mathbf{Z}$ are the same.

Thus for every encoder of $\mathbf{X}$ of the form (4.44), we can find an encoder of $\mathbf{Z}$ of the form (4.45), such that the error in estimating $\mathbf{X}$ and $\mathbf{Z}$ are the same, and vice versa.

Therefore if $\mathbf{w}^*$ in (4.44) is optimal, $\mathbf{Q^T w}$ in (4.45) is also optimal, and vice versa.

From Lemma 4.8, if $\sigma_m = \max\{\sigma_1, \sigma_2, \cdots, \sigma_n\}$, an optimal encoder for $\mathbf{Z}$ is in the form (4.45) with $\mathbf{Q^T w} = [\ 0 \ \cdots \ 0 \ 1 \ 0 \ \cdots \ 0\ ]^T$, where the 1 is the m-th component. Then an optimal encoder for $\mathbf{X}$ is in the form (4.44) with

$$\begin{aligned}
\mathbf{w} &= Q \begin{bmatrix} 0 & \cdots & 0 & 1 & 0 & \cdots & 0 \end{bmatrix}^T \\
&= \begin{bmatrix} \mathbf{v}_1 & \mathbf{v}_2 & \cdots & \mathbf{v}_n \end{bmatrix} \begin{bmatrix} 0 & \cdots & 0 & 1 & 0 & \cdots & 0 \end{bmatrix}^T \\
&= \mathbf{v}_m
\end{aligned}$$

□

4.6 Summary

We study the real-time estimation of a Markov process over a memoryless noisy digital communication channel to minimize the mean squared estimation error. We first show the optimal encoder can be a function of the current state of the Markov process and the probability mass function of the state of the memory of the receiver given the current state. We then prove the optimal encoder separates the state space with hyper-planes. A recursive algorithm is then given to jointly find the locally

optimal encoder and decoder for the special case of the binary symmetric channel and scalar source. For memoryless Gaussian vector source and binary symmetric channel we analytically derive the global joint optimal encoder and decoder. This turns out to be an encoding of the principal component of the source vector. We derive the minimum mean squared error as a function of the variance of source and the channel noise.

Many problems remain open. The recursive relation between the optimal design across time steps needs to be found. The recursive algorithm to find optimal encoder and decoder needs to be generalized to channels other than the binary symmetric channel. For the memoryless Gaussian vector case, we also need to find the optimal designs for more practical channels. The memory state update is given in our problem. The optimal joint design of encoder, decode, and memory update is another interesting problem.

Chapter 5

Conclusion and Future Work

This thesis studies design and analysis of integrated control, estimation, and communication systems. The application focus has been active vehicle safety systems. We have shown in Chapter 2 that the vehicle safety communication could bring benefit to traffic safety and efficiency. The results motivated us to design a system to realize such communication. In Chapter 3, we have designed vehicle-vehicle/roadside-vehicle communication protocols that satisfy the reliability and latency demands of vehicle safety messaging. Implementation of our ad hoc protocol does not require infrastructure. The protocols comply with the architecture of the proposed DSRC standard. We have studied the real-time estimation of a Markov process over noisy digital communication channel in Chapter 4. We have derived some structural results for the optimal encoder and decoder, proposed an iterative algorithm to find a locally optimal encode/decoder pair, and derived the global optimal encoder and decoder for

a memoryless Gaussian source transmitted over binary symmetric channel. Some of the future works besides those mentioned in the summary of each chapter are listed below.

1. Design of CACC system

   Our simulation of the *braking* scenario in OVC does not show the benefit of communication. However an idealized sensor model was used in the simulation. If after realistic sensor models are implemented a negative results is still obtained, braking warning should not be the focus of future analytical and experimental work. Other future work could include enhancement of the warning message response methodology, the systematic adjustment of controller aggressiveness, and quantitative study of shock wave smoothing.

2. MAC protocol design for vehicle safety communications

   The environment faced by vehicle safety communication is heterogeneous. We believe in such settings transmission power and data rate need to be adapted to the environment. For example, when traffic density is high, vehicles should transmit at a lower power to reduce the interference to neighboring vehicles. At the same time since the density is high, packets transmitted at low power can reach enough neighboring vehicles for safety. On the other hand when the density is low, the transmission power should be increased to reach the same number of vehicles. This is also necessary, because when the density is low,

the velocity is high and louder communication is needed to ensure safety. Such adaptive system could be designed based on current results. Applying more efficient coding schemes than repetition coding could be another direction of study, e.g., erasure coding [73]. We need to design the system considering both the communication and computation components. In the simulation, we used a deterministic channel model. The wireless V-V communication channel should be better understood and modelled. We should repeat the simulations with the enhanced model.

3. State estimation over wireless channel

   There are many open problems in the field of real-time estimation over wireless communication channels. In this thesis we only study the estimation of a Markov process, and some results apply to the binary symmetric channel only. Some possible extensions to our work include the real-time estimation of non-Gaussian sources and over more general channels, e.g., M-ary symmetric channels, AWGN channels with transmission power constraints, channels with memory, and combinations of these. Relations of our findings with existing results in related fields should be further explored. For example, in information theory, the "anytime capacity" of a channel [61] [22] [62] [77] [63] is a recently discovered property relating the decoding delay with the probability of error. Such a property could be very important for estimation over a noisy channel. Relevant results about packet erasure channel could also be linked to our work

on protocol design in Chapter3. Collisions of packets could be modelled as erasures.

Appendix A

Proofs of the Lemmas in Section 3.4

A.1 Proof of Lemma 3.3

Proof. There are two methods to prove this lemma.

1. $P(\neg S_j) = 1 - P(S_j)$

   Let E_l be the event that there are l messages generated by all transmitters within interference range of the receiver in $(t_j - \tau, t_j]$. Since one message can only affect a time period of length τ after the message's generation, these l messages are all the messages whose repetitions could interfere with repetition p_j. The probability that any one of the l messages selects the slot occupied by p_j (to transmit its own repetition) is $\frac{k}{n}$. Repetition p_j is received successfully if

and only if none of the l messages selects p_j's time slot. Formally we have

$$\begin{aligned} P(S_j) &= \sum_{l=0}^{\infty} P(S_j|E_l)P(E_l) \\ &= \sum_{l=0}^{\infty} \left(1 - \frac{k}{n}\right)^l \cdot e^{-m\lambda\tau} \frac{(m\lambda\tau)^l}{l!} \\ &= e^{-m\lambda\tau} \sum_{l=0}^{\infty} \frac{[m\lambda\tau(1-\frac{k}{n})]^l}{l!} \\ &= e^{-m\lambda\tau} e^{m\lambda\tau(1-\frac{k}{n})} \\ &= e^{-m\lambda\tau\frac{k}{n}} \end{aligned}$$

In above derivation we used the fact that the repetitions of different messages are independent and the total message generation process is Poisson.

Therefore $P(\neg S_j) = 1 - P(S_j) = 1 - e^{-m\lambda\tau\frac{k}{n}}$

2. Prove using the theory of compound Poisson distribution. Let l be the total number of message generated in the interference range of the receiver in $(t_j - \tau, t_j]$. For each of these messages define a Bernoulli variable X_i corresponding to the time slot occupied by p_j, where $X_i = 1$ means that there is a repetition of the i-th message in the time slot and $X_i = 0$ means the time slot is not selected by this message. We then have $P(X_i = 1) = \frac{k}{n}$ and $P(X_i = 0) = 1 - \frac{k}{n}$. Since all $X_i's$ are i.i.d from the design of the protocol, $X = \sum_{i=1}^{L} X_i$ is the sum of L random variables, where L itself is a Poisson distributed random variable with $P(L = l) = e^{-m\lambda\tau}\frac{(m\lambda\tau)^l}{l!}$. According to the theory of compound Poisson

distribution (see e.g. [28]), X also has a Poisson distribution with $P(X = l) = e^{-m\lambda\tau\frac{n}{k}}\frac{(m\lambda\tau\frac{n}{k})^l}{l!}$. Therefore

$$\begin{aligned} P(\neg S_j) &= 1 - P(S_j) \\ &= 1 - P(X = 0) \\ &= 1 - e^{-m\lambda\tau\frac{n}{k}} \end{aligned}$$

□

A.2 Proof of Lemma 3.4

Proof. We prove using induction.

1. For $k = 2$, we need to prove that for any i, j, $1 \leq i, j \leq n$

$$P(\neg S_i \wedge \neg S_j) > P(\neg S_i)P(\neg S_j)$$

First observe

$$\begin{aligned} P(\neg S_i \wedge \neg S_j) &= 1 - P(S_i \vee S_j) \\ &= 1 - P(S_i) - P(S_j) + P(S_i \wedge S_j) \end{aligned}$$

Lemma 3.3 states

$$P(S_i) = P(S_j) = e^{-m\lambda\tau\frac{k}{n}}$$

Next we analyze $P(S_i \wedge S_j)$.

Suppose that p_i starts at t_i and p_j starts at t_j, and assume $t_j > t_i$ without loss of generality. Then p_i can potentially interfere with messages generated in $(t_i - \tau, t_i]$ only, and p_j with messages generated in $(t_j - \tau, t_j]$ only.

Since p_i and p_j are known to be selected by the same one message, we have

$$t_i - \tau < t_j - \tau < t_i < t_j.$$

Let $\tau_1 = t_i - (t_j - \tau) = \tau - (t_j - t_i)$, and $\tau_0 = \tau - \tau_1 = t_j - t_i$. Then the time period $(t_i - \tau, t_j]$ is divided into three time intervals, $I_1 = (t_i - \tau, t_j - \tau]$, $I_2 = (t_j - \tau, t_i]$, and $I_3 = (t_i, t_j]$. I_1 and I_3 both have length τ_0 while the length of I_2 is τ_1. Messages generated in I_1 can only interfere with p_i, and messages generated in I_3 can only interfere with p_j. However messages generated in I_2 can interfere with both p_i and p_j. We also observe that the behavior of messages generated in different intervals is independent. $P(S_i \wedge S_j)$ is the probability that neither p_i nor p_j are collided. With the same assumptions as used in the proof

of lemma 3.3, we have

$$P(S_i \wedge S_j) = \left(\sum_{l_1=0}^{\infty}\left(1-\frac{k}{n}\right)^{l_1}\cdot e^{-m\lambda\tau_0}\frac{(m\lambda\tau_0)^{l_1}}{l_1!}\right)\cdot\left(\sum_{l_2=0}^{\infty}\left(1-\frac{k}{n}\right)^{2l_2}\cdot e^{-m\lambda\tau_1}\frac{(m\lambda\tau_1)^{l_2}}{l_2!}\right)\cdot$$
$$\left(\sum_{l_3=0}^{\infty}\left(1-\frac{k}{n}\right)^{l_3}\cdot e^{-m\lambda\tau_0}\frac{(m\lambda\tau_0)^{l_3}}{l_3!}\right)$$
$$= e^{-m\lambda\tau_0\frac{k}{n}}\cdot e^{m\lambda\tau_1[\left(1-\frac{k}{n}\right)^2-1]}\cdot e^{-m\lambda\tau_0\frac{k}{n}}$$
$$= e^{-2m\lambda\tau\frac{k}{n}+m\lambda\tau_1\frac{k^2}{n^2}}$$
$$> e^{-2m\lambda\tau\frac{k}{n}}$$
$$= P(S_i)P(S_j)$$

where the last equation comes from lemma 3.3.

Therefore

$$P(\neg S_i \wedge \neg S_j) = 1 - P(S_i \vee S_j)$$
$$= 1 - P(S_i) - P(S_j) + P(S_i \wedge S_j)$$
$$> 1 - P(S_i) - P(S_j) + P(S_i)P(S_j)$$
$$= [1 - P(S_i)][1 - P(S_j)]$$
$$= P(\neg S_i)P(\neg S_j)$$

The above inequality holds for all i, j,$1 \leq i, j \leq n$. Since order does not matter in equation (3.2), we can arbitrarily let $p_1 = p_i$ and $p_2 = p_j$. The lemma is thus proved for the case of $r = 2$.

2. Assume equation (3.2) holds for all of j satisfying $1 < j \leq r - 1 \leq n - 1$, then

we have

$$P(\neg S_1 \wedge \ldots \wedge \neg S_{r-1}) > (\prod_{j=1}^{r-1} P(\neg S_j))$$

Let t_i be the starting time of repetition p_i for any $1 \leq i \leq r$. Since the order does not matter in equation (3.2), we can always rearrange the repetitions such that $t_1 < t_2 < \ldots < t_{r-1} < t_r$. Therefore we can assume this ordering without loss of generality.

Now let B_i be the event that there are i other messages generated in the time period $(t_1 - \tau, t_{r-1}]$.

$$\begin{aligned} P(\neg S_1 \wedge \ldots \wedge \neg S_{r-1} | \neg S_r) &= \sum_{i=0}^{\infty} P(\neg S_1 \wedge \ldots \wedge \neg S_{r-1} | B_i, \neg S_r) P(B_i | \neg S_r) \\ &= \sum_{i=0}^{\infty} P(\neg S_1 \wedge \ldots \wedge \neg S_{r-1} | B_i) P(B_i | \neg S_r) \\ &\geq \sum_{i=0}^{\infty} P(\neg S_1 \wedge \ldots \wedge \neg S_{r-1} | B_i) P(B_i) \\ &= P(\neg S_1 \wedge \ldots \wedge \neg S_{r-1}) \end{aligned}$$

In above derivation, the second equation is obtained because the slots are chosen independently. Therefore event that p_r fails affects the probability of failure of another packet only by saying that there might be other interfering messages for the second packet. If all the interfering messages are known, the failure of one packet says nothing more about the failure of the other. $P(B_i|\neg S_r) \geq P(B_i)$

because when packet p_r fails, there are surely some other messages generated in $(t_r - \tau, t_r]$. Therefore it is more probable there are interfering messages in $(t_r - \tau, t_{r-1}]$ and thus in $(t_1 - \tau, t_{r-1}]$.

From above inequality we have

$$\begin{aligned} P(\neg S_1 \wedge \ldots \wedge \neg S_{r-1} \wedge \neg S_r) &= P(\neg S_1 \wedge \ldots \wedge \neg S_{r-1} | \neg S_r) P(\neg S_r) \\ &\geq P(\neg S_1 \wedge \ldots \wedge \neg S_{r-1}) P(\neg S_r) \\ &> (\prod_{j=1}^{r-1} P(\neg S_j)) P(\neg S_r) \\ &= \prod_{j=1}^{r} P(\neg S_j) \end{aligned}$$

The first inequality holds for the same reasons $P(B_i|\neg S_r) \geq P(B_i)$. Hence equation (3.2) also holds for r, and the lemma is proved.

□

A.3 Proof of Lemma 3.5

Proof. Following the same arguments as in the proof of Lemma 3.3, let E_l be the event that there are l messages generated by all transmitters in $(t_j - \tau, t_j]$. Then $l \geq 1$ since T_j has occurred. Thus

$$
\begin{aligned}
P(S_j|T_j) &= \sum_{l=1}^{\infty} P(S_j|E_l)P(E_l) \\
&= \sum_{l=1}^{\infty} \left(1 - \frac{k}{n}\right)^l \cdot e^{-m\lambda\tau} \frac{(m\lambda\tau)^l}{l!} \\
&= e^{-m\lambda\tau} \sum_{l=1}^{\infty} \frac{[m\lambda\tau(1-\frac{k}{n})]^l}{l!} \\
&= e^{-m\lambda\tau}(e^{m\lambda\tau(1-\frac{k}{n})} - 1) \\
&= e^{-m\lambda\tau\frac{k}{n}} - e^{-m\lambda\tau}
\end{aligned}
$$

Therefore

$$P(\neg S_j|T_j) = 1 - P(S_j|T_j) = 1 - e^{-m\lambda\tau\frac{k}{n}} + e^{-m\lambda\tau}$$

□

A.4 Proof of Lemma 3.7

Proof.

$$
\begin{aligned}
P(\neg S_r|\neg S_1 \wedge \ldots \wedge \neg S_{r-1}) &= P(\neg S_r|\neg S_1 \wedge \ldots \wedge \neg S_{r-1} \wedge T_r)P(T_r|\neg S_1 \wedge \ldots \wedge \neg S_{r-1}) \\
&\quad + P(\neg S_r|\neg S_1 \wedge \ldots \wedge \neg S_{r-1} \wedge \neg T_r)P(\neg T_r|\neg S_1 \wedge \ldots \wedge \neg S_{r-1}) \\
&= P(\neg S_r|\neg S_1 \wedge \ldots \wedge \neg S_{r-1} \wedge T_r)P(T_r|\neg S_1 \wedge \ldots \wedge \neg S_{r-1}) + 0 \\
&\leq P(\neg S_r|\neg S_1 \wedge \ldots \wedge \neg S_{r-1} \wedge T_r) \\
&= P(\neg S_r|T_r)
\end{aligned}
$$

The last equation comes from the fact that a message selects different time slots in its lifetime to transmit packets independently. Therefore the failure of p_j says nothing about p_k for $k \neq j$ other than that there may be messages from other transmitters in $(t_j, t_k]$, the lifetime period shared by the two repetitions.

□

Appendix B

Calculation of the Interference Range

The procedure to calculate the interference range r_i, given the distance between transmitter and receiver r, the message range R, and the date rate, is as follows. We need to first calculate the transmission power P_t required of R, and then the interference range r_i for r.

There is a Signal to Interference+Noise Ratio (SINR) threshold for a radio to receive data at a given data rate. The higher the data rate, the higher the threshold. Specific values of the thresholds depend on the radio design. In our simulation we use the SINR threshold values of a commercial off-the-self 802.11a radio product.

The procedure to calculate transmission power P_t of a message to reach a message range R at a given data rate is the following.

1. **Find the SINR threshold β corresponding to the data rate.**

   The ratio between the reception power P_r and thermal noise N is β in dB.

2. **Calculate the reception power**

   $P_r = N \cdot 10^{\frac{\beta}{10}}$.

3. **Calculate the transmission power**

   Use the path-loss channel model, P_r, and R to calculate P_t. If the free-space model is used, $P_t = P_r \cdot \frac{R^2}{A}$, with A being some constant depending on the signal wavelength and the gains of transmit and receive antennas.

Given the transmission power P_t, the TX/RX distance $r \leq R$, and the data rate, the procedure to calculate the interference range r_i of the receiver is the following.

1. **Find the SINR threshold β corresponding to the data rate**.

2. **Calculate the power of the signal at the receiver P_r**

   If the free-space model is used, $P_r = P_t \cdot \frac{A}{r^2}$.

3. **Calculate the minimum power required to interfere**

   The ratio between P_r and the interference power P_i is equal to or lower than β in dB, hence, $P_i = 10^{\frac{\beta}{10}} P_r$.

4. **Calculate r_i**

Use the channel model, P_t, and P_i to calculate r_i. If the free-space mode is used, $r_i = \sqrt{\frac{AP_i}{P_t}}$. All nodes closer than r_i from the receiver can interfere.

The interference range depends on the TX/RX distance. If free-space channel model is used, we have the following relation.

$$r_i = 10^{\frac{\beta}{20}} \cdot r \tag{B.1}$$

Hence, the interference range as well as the number of interferers of a receiver is a linearly increasing function of its distance to the transmitter[1]. All the following results were taken when the distance between the transmitter and receiver is the message range. So all the results are for the worst case.

[1]Although the communication region increases quadratically with the transmitter-receiver distance, the number of the interference only increases linearly because the network topology is constrained by road paths

Appendix C

Proof of Lemma 4.14

Proof. When $\varphi = 0$, both sides of (4.32) equal to 0. When $\varphi \to +\infty$, both sides are equal to $\frac{1}{2}$. Hence inequality holds at both 0 and ∞.

We will show for all $\varphi \in (0, \infty)$, the left side of (4.32) is greater than the right side. Since both sides are positive, (4.32) is equivalent to

$$V(\varphi) \triangleq \frac{1 - e^{-\varphi^2}}{4} - \frac{1}{2\pi}\left(\int_0^{\varphi} e^{-\frac{y^2}{2}} dy\right)^2 \geq 0 \tag{C.1}$$

We differentiate $V(\varphi)$ with φ and get

$$\frac{dV}{d\varphi} = \frac{\varphi e^{-\varphi^2}}{2} - \frac{1}{\pi} e^{-\frac{\varphi^2}{2}} \int_0^{\varphi} e^{-\frac{y^2}{2}} dy \tag{C.2}$$

Clearly, $\frac{dV}{d\varphi}$ is zero when either $\varphi = 0$ or $\varphi \to +\infty$. We study its sign in $(0, +\infty)$

For all $\varphi \in (0, \infty)$, define $W(\varphi) \triangleq e^{\frac{\varphi^2}{2}}\left(\frac{dV}{d\varphi}\right)$. Therefore

$$W(\varphi) = \frac{\varphi e^{-\frac{\varphi^2}{2}}}{2} - \frac{1}{\pi}\int_0^{\varphi} e^{-\frac{y^2}{2}} dy \tag{C.3}$$

$W(\varphi)$ and $\frac{dV}{d\varphi}$ have the same sign when $\varphi > 0$ and is finite. We can study the sign of $\frac{dV}{d\varphi}$ using $W(\varphi)$.

$W(0) = 0$ and $W(+\infty) = -\frac{1}{\sqrt{2\pi}} < 0$. The first term in (C.3) first increases from 0 with φ, then decreases until it converges to 0. The second term on the other hand keeps increasing from 0 with φ, so the sign of $W(\varphi)$, therefore the sign of $\frac{dV}{c\varphi}$, must be negative for large φ. Now we analyze the change trend of the sign of $W(\varphi)$ with φ by differentiating it.

$$\frac{dW}{d\varphi} = e^{-\frac{\varphi^2}{2}}\left(\frac{1}{2} - \frac{1}{\pi} - \frac{\varphi^2}{2}\right) \tag{C.4}$$

Clearly, $\frac{dW}{d\varphi} \geq 0$, if $\varphi \leq \sqrt{1-\frac{2}{\pi}}$. Since $W(0) = 0$, we have $W(\varphi) > 0$ in $\left(0, \sqrt{1-\frac{2}{\pi}}\right]$. On the other hand, $\frac{dW}{d\varphi} < 0$, if $\varphi > \sqrt{1-\frac{2}{\pi}}$. Therefore in $(\sqrt{1-\frac{2}{\pi}}, \infty)$ $W(\varphi)$ keeps decreasing, going from positive to negative. Since $W(\varphi)$ and $\frac{dV}{d\varphi}$ have the same sign except for $\varphi \to +\infty$, we know the following about $\frac{dV}{d\varphi}$:

$$\frac{dV}{d\varphi}\begin{cases} = 0 & \varphi = 0 \\ > 0 \text{ and increasing} & \varphi \in (0, \sqrt{1-\frac{2}{\pi}}] \\ > 0 \text{ and decreasing} & \varphi \in (\sqrt{1-\frac{2}{\pi}}, \varphi^*] \\ < 0 \text{ and decreasing} & \varphi > \varphi^* \text{ and finite} \\ = 0 & \varphi \to +\infty \end{cases}$$

where $\varphi*$ is a finite positive number in $(1-\frac{2}{\pi}, +\infty)$ whose exact value is not important to us.

From the sign of $\frac{dV}{d\varphi}$ we can see that $V(\varphi)$ starts from 0 when $\varphi = 0$. It first increases then decreases monotonically with φ, and converges to zero when $\varphi \to +\infty$. Hence it can never be negative. The only possibility is $V(\varphi)$ first increases with φ from 0 to be positive , then decreases while still being positive, and eventually goes back to 0. Figure C.1 confirms our analysis.

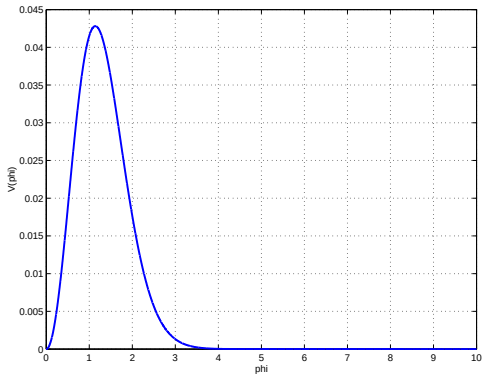

Figure C.1: V as a function of φ

Therefore we have proved that $V(\varphi) \geq 0$, $\forall \varphi \in (0, +\infty)$, and the lemma is proved. □

Appendix D

Proof of Lemma 4.15

Proof. We prove by induction.

When $n = 2$, $det\left[\frac{w_2^2}{\sigma_1^2 w_1^2} + \frac{1}{\sigma_2^2}\right] = \frac{\sigma_1^2 w_1^2 + \sigma_2^2 w_2^2}{w_1^2 \sigma_1^2 \sigma_2^2}$. This establishes a base case.

Suppose the lemma holds for all matrices of the above form of size $(k-1)\times(k-1)$, then observe that

$$det\left[\frac{1}{\sigma_1^2 w_1^2}\begin{pmatrix} w_2^2 & w_2 w_3 & \cdots & w_2 w_k \\ w_3 w_2 & w_3^2 & \cdots & w_3 w_k \\ \vdots & \vdots & \ddots & \vdots \\ w_k w_2 & w_k w_3 & \cdots & w_k^2 \end{pmatrix} + diag\left(\frac{1}{\sigma_2^2}, \frac{1}{\sigma_3^2}, \cdots, \frac{1}{\sigma_k^2}\right)\right]$$

$$
\begin{aligned}
&= \begin{vmatrix}
\frac{w_2^2}{\sigma_1^2 w_1^2} + \frac{1}{\sigma_2^2} & \frac{w_2 w_3}{\sigma_1^2 w_1^2} & \cdots & \frac{w_2 w_k}{\sigma_1^2 w_1^2} \\
\frac{w_3 w_2}{\sigma_1^2 w_1^2} & \frac{w_3^2}{\sigma_1^2 w_1^2} + \frac{1}{\sigma_3^2} & \cdots & \frac{w_3 w_k}{\sigma_1^2 w_1^2} \\
\vdots & \vdots & \ddots & \vdots \\
\frac{w_k w_2}{\sigma_1^2 w_1^2} & \frac{w_k w_3}{\sigma_1^2 w_1^2} & \cdots & \frac{w_k^2}{\sigma_1^2 w_1^2} + \frac{1}{\sigma_k^2}
\end{vmatrix} \\
&\triangleq |A(k)|
\end{aligned}
$$

where $|M|$ stands for the determinant of matrix M.

Then

$$
\begin{aligned}
|A(k)| &= \frac{\sigma_1^2 w_1^2 + \sigma_2^2 w_2^2 + \cdots + \sigma_k^2 w_k^2}{w_1^2 \sigma_1^2 \sigma_2^2 \cdots \sigma_k^2} \\
&= \frac{\sum_{i=1}^{k} \sigma_i^2 w_i^2}{w_1^2 \prod_{i=1}^{k} \sigma_i^2}
\end{aligned}
$$

Now,

$$
|A(k+1)| = \begin{vmatrix}
\frac{w_2^2}{\sigma_1^2 w_1^2} + \frac{1}{\sigma_2^2} & \frac{w_2 w_3}{\sigma_1^2 w_1^2} & \cdots & \frac{w_2 w_k}{\sigma_1^2 w_1^2} & \frac{w_2 w_{k+1}}{\sigma_1^2 w_1^2} \\
\frac{w_3 w_2}{\sigma_1^2 w_1^2} & \frac{w_3^2}{\sigma_1^2 w_1^2} + \frac{1}{\sigma_3^2} & \cdots & \frac{w_3 w_k}{\sigma_1^2 w_1^2} & \frac{w_3 w_{k+1}}{\sigma_1^2 w_1^2} \\
\vdots & \vdots & \ddots & \vdots & \vdots \\
\frac{w_k w_2}{\sigma_1^2 w_1^2} & \frac{w_k w_3}{\sigma_1^2 w_1^2} & \cdots & \frac{w_k^2}{\sigma_1^2 w_1^2} + \frac{1}{\sigma_k^2} & \frac{w_k w_{k+1}}{\sigma_1^2 w_1^2} \\
\frac{w_{k+1} w_2}{\sigma_1^2 w_1^2} & \frac{w_{k+1} w_3}{\sigma_1^2 w_1^2} & \cdots & \frac{w_{k+1} w_k}{\sigma_1^2 w_1^2} & \frac{w_{k+1}^2}{\sigma_1^2 w_1^2} + \frac{1}{\sigma_{k+1}^2}
\end{vmatrix}
$$

We prove in two cases depending on the value of w_k, i.e. $w_k \neq 0$ and $w_k = 0$.

1. Assume $w_k \neq 0$

Then

$$
|A(k+1)| = \begin{vmatrix}
\frac{w_2^2}{\sigma_1^2 w_1^2} + \frac{1}{\sigma_2^2} & \frac{w_2 w_3}{\sigma_1^2 w_1^2} & \cdots & \frac{w_2 w_{k-1}}{\sigma_1^2 w_1^2} & \frac{w_2 w_k}{\sigma_1^2 w_1^2} & \frac{w_2 w_{k+1}}{\sigma_1^2 w_1^2} \\
\frac{w_3 w_2}{\sigma_1^2 w_1^2} & \frac{w_3^2}{\sigma_1^2 w_1^2} + \frac{1}{\sigma_3^2} & \cdots & \frac{w_2 w_{k-1}}{\sigma_1^2 w_1^2} & \frac{w_3 w_k}{\sigma_1^2 w_1^2} & \frac{w_3 w_{k+1}}{\sigma_1^2 w_1^2} \\
\vdots & \vdots & \ddots & \vdots & \vdots & \vdots \\
\frac{w_k w_2}{\sigma_1^2 w_1^2} & \frac{w_k w_3}{\sigma_1^2 w_1^2} & \cdots & \frac{w_k w_{k-1}}{\sigma_1^2 w_1^2} & \frac{w_k^2}{\sigma_1^2 w_1^2} + \frac{1}{\sigma_k^2} & \frac{w_k w_{k+1}}{\sigma_1^2 w_1^2} \\
0 & 0 & \cdots & 0 & -\frac{w_{k+1}}{\sigma_k^2 w_k} & \frac{1}{\sigma_{k+1}^2}
\end{vmatrix}
$$

$$
= \begin{vmatrix}
\frac{w_2^2}{\sigma_1^2 w_1^2} + \frac{1}{\sigma_2^2} & \frac{w_2 w_3}{\sigma_1^2 w_1^2} & \cdots & \frac{w_2 w_{k-1}}{\sigma_1^2 w_1^2} & \frac{w_2 w_k}{\sigma_1^2 w_1^2} & 0 \\
\frac{w_3 w_2}{\sigma_1^2 w_1^2} & \frac{w_3^2}{\sigma_1^2 w_1^2} + \frac{1}{\sigma_3^2} & \cdots & \frac{w_2 w_{k-1}}{\sigma_1^2 w_1^2} & \frac{w_3 w_k}{\sigma_1^2 w_1^2} & 0 \\
\vdots & \vdots & \ddots & \vdots & \vdots & \vdots \\
\frac{w_{k-1} w_2}{\sigma_1^2 w_1^2} & \frac{w_{k-1} w_3}{\sigma_1^2 w_1^2} & \cdots & \frac{w_{k-1}^2}{\sigma_1^2 w_1^2} + \frac{1}{\sigma_{k-1}^2} & \frac{w_{k-1} w_k}{\sigma_1^2 w_1^2} & 0 \\
\frac{w_k w_2}{\sigma_1^2 w_1^2} & \frac{w_k w_3}{\sigma_1^2 w_1^2} & \cdots & \frac{w_k w_{k-1}}{\sigma_1^2 w_1^2} & \frac{w_k^2}{\sigma_1^2 w_1^2} + \frac{1}{\sigma_k^2} & -\frac{w_{k+1}}{\sigma_k^2 w_k} \\
0 & 0 & \cdots & 0 & -\frac{w_{k+1}}{\sigma_k^2 w_k} & \frac{1}{\sigma_{k+1}^2} + \frac{w_{k+1}^2}{\sigma_k^2 w_k^2}
\end{vmatrix}
$$

$$
= \left|\begin{array}{ccc|c}
 & & & 0 \\
 & A(k) & & \vdots \\
 & & & 0 \\
 & & & -\frac{w_{k+1}}{\sigma_k^2 w_k} \\
\hline
0 & \cdots & 0 & \frac{1}{\sigma_{k+1}^2} + \frac{w_{k+1}^2}{\sigma_k^2 w_k^2}
\end{array}\right|
$$

$$
\begin{aligned}
&= \left(\frac{1}{\sigma_{k+1}^2} + \frac{w_{k+1}^2}{\sigma_k^2 w_k^2}\right)|A(k)| - \frac{w_{k+1}^2}{\sigma_k^4 w_k^2}\left|\begin{array}{ccc|c} & & & 0 \\ & A(k-1) & & \vdots \\ & & & 0 \\ \hline 0 & \cdots & 0 & -\frac{w_{k+1}}{\sigma_k^2 w_k} \end{array}\right| \\
&= \left(\frac{1}{\sigma_{k+1}^2} + \frac{w_{k+1}^2}{\sigma_k^2 w_k^2}\right)|A(k)| - \frac{w_{k+1}^2}{\sigma_k^4 w_k^2}|A(k-1)| \\
&= \left(\frac{1}{\sigma_{k+1}^2} + \frac{w_{k+1}^2}{\sigma_k^2 w_k^2}\right) \cdot \frac{\sum_{i=1}^{k} \sigma_i^2 w_i^2}{w_1^2 \prod_{i=1}^{k} \sigma_i^2} - \frac{w_{k+1}^2}{\sigma_k^4 w_k^2} \cdot \frac{\sum_{i=1}^{k-1} \sigma_i^2 w_i^2}{w_1^2 \prod_{i=1}^{k-1} \sigma_i^2} \\
&= \frac{\sum_{i=1}^{k} \sigma_i^2 w_i^2}{w_1^2 \prod_{i=1}^{k+1} \sigma_i^2} + \frac{w_{k+1}^2}{\sigma_k^2 w_k^2}\left(\frac{w_k^2 \sigma_k^2}{w_1^2 \prod_{i=1}^{k} \sigma_i^2}\right) \\
&= \frac{\sum_{i=1}^{k} \sigma_i^2 w_i^2}{w_1^2 \prod_{i=1}^{k+1} \sigma_i^2} + \frac{w_{k+1}^2 \sigma_{k+1}^2}{w_1^2 \prod_{i=1}^{k+1} \sigma_i^2} \\
&= \frac{\sum_{i=1}^{k+1} \sigma_i^2 w_i^2}{w_1^2 \prod_{i=1}^{k+1} \sigma_i^2} \qquad \text{(D.1)}
\end{aligned}
$$

2. Assume $w_k = 0$.

   Then,

$$
\begin{aligned}
&|A(k+1)| \\
&= \begin{vmatrix}
\frac{w_2^2}{\sigma_1^2 w_1^2} + \frac{1}{\sigma_2^2} & \frac{w_2 w_3}{\sigma_1^2 w_1^2} & \cdots & \frac{w_2 w_k}{\sigma_1^2 w_1^2} & \frac{w_2 w_{k+1}}{\sigma_1^2 w_1^2} \\
\frac{w_3 w_2}{\sigma_1^2 w_1^2} & \frac{w_3^2}{\sigma_1^2 w_1^2} + \frac{1}{\sigma_3^2} & \cdots & \frac{w_3 w_k}{\sigma_1^2 w_1^2} & \frac{w_3 w_{k+1}}{\sigma_1^2 w_1^2} \\
\vdots & \vdots & \ddots & \vdots & \vdots \\
\frac{w_k w_2}{\sigma_1^2 w_1^2} & \frac{w_k w_3}{\sigma_1^2 w_1^2} & \cdots & \frac{w_k^2}{\sigma_1^2 w_1^2} + \frac{1}{\sigma_k^2} & \frac{w_k w_{k+1}}{\sigma_1^2 w_1^2} \\
\frac{w_{k+1} w_2}{\sigma_1^2 w_1^2} & \frac{w_{k+1} w_3}{\sigma_1^2 w_1^2} & \cdots & \frac{w_{k+1} w_k}{\sigma_1^2 w_1^2} & \frac{w_{k+1}^2}{\sigma_1^2 w_1^2} + \frac{1}{\sigma_{k+1}^2}
\end{vmatrix}
\end{aligned}
$$

$$
\begin{aligned}
&= \begin{vmatrix}
\frac{w_2^2}{\sigma_1^2 w_1^2} + \frac{1}{\sigma_2^2} & \frac{w_2 w_3}{\sigma_1^2 w_1^2} & \cdots & \frac{w_2 w_{k-1}}{\sigma_1^2 w_1^2} & 0 & \frac{w_2 w_{k+1}}{\sigma_1^2 w_1^2} \\
\frac{w_3 w_2}{\sigma_1^2 w_1^2} & \frac{w_3^2}{\sigma_1^2 w_1^2} + \frac{1}{\sigma_3^2} & \cdots & \frac{w_3 w_{k-1}}{\sigma_1^2 w_1^2} & \vdots & \frac{w_3 w_{k+1}}{\sigma_1^2 w_1^2} \\
\vdots & \vdots & \ddots & \vdots & \vdots & \\
\frac{w_{k-1} w_2}{\sigma_1^2 w_1^2} & \frac{w_{k-1} w_3}{\sigma_1^2 w_1^2} & \cdots & \frac{w_{k-1}^2}{\sigma_1^2 w_1^2} + \frac{1}{\sigma_k^2} & 0 & \frac{w_{k-1} w_{k+1}}{\sigma_1^2 w_1^2} \\
0 & \cdots & \cdots & 0 & \frac{1}{\sigma_k^2} & 0 \\
\frac{w_{k+1} w_2}{\sigma_1^2 w_1^2} & \frac{w_{k+1} w_3}{\sigma_1^2 w_1^2} & \cdots & \frac{w_{k+1} w_{k-1}}{\sigma_1^2 w_1^2} & 0 & \frac{w_{k+1}^2}{\sigma_1^2 w_1^2} + \frac{1}{\sigma_{k+1}^2}
\end{vmatrix} \\
&= \frac{1}{\sigma_k^2} \cdot \begin{vmatrix}
\frac{w_2^2}{\sigma_1^2 w_1^2} + \frac{1}{\sigma_2^2} & \frac{w_2 w_3}{\sigma_1^2 w_1^2} & \cdots & \frac{w_2 w_{k-1}}{\sigma_1^2 w_1^2} & \frac{w_2 w_{k+1}}{\sigma_1^2 w_1^2} \\
\frac{w_3 w_2}{\sigma_1^2 w_1^2} & \frac{w_3^2}{\sigma_1^2 w_1^2} + \frac{1}{\sigma_3^2} & \cdots & \frac{w_3 w_{k-1}}{\sigma_1^2 w_1^2} & \frac{w_3 w_{k+1}}{\sigma_1^2 w_1^2} \\
\vdots & \vdots & \ddots & \vdots & \vdots \\
\frac{w_{k-1} w_2}{\sigma_1^2 w_1^2} & \frac{w_{k-1} w_3}{\sigma_1^2 w_1^2} & \cdots & \frac{w_{k-1}^2}{\sigma_1^2 w_1^2} + \frac{1}{\sigma_k^2} & \frac{w_{k-1} w_{k+1}}{\sigma_1^2 w_1^2} \\
\frac{w_{k+1} w_2}{\sigma_1^2 w_1^2} & \frac{w_{k+1} w_3}{\sigma_1^2 w_1^2} & \cdots & \frac{w_{k+1} w_{k-1}}{\sigma_1^2 w_1^2} & \frac{w_{k+1}^2}{\sigma_1^2 w_1^2} + \frac{1}{\sigma_{k+1}^2}
\end{vmatrix} \\
&= \frac{1}{\sigma_k^2} \cdot \frac{\sigma_1^2 w_1^2 + \sigma_2^2 w_2^2 + \cdots + \sigma_{k-1}^2 w_{k-1}^2 + \sigma_{k+1}^2 w_{k+1}^2}{w_1^2 \sigma_1^2 \sigma_2^2 \cdots \sigma_{k-1}^2 \sigma_{k+1}^2} \\
&= \frac{\sum_{i=1}^{k+1} \sigma_i^2 w_i^2}{w_1^2 \prod_{i=1}^{k+1} \sigma_i^2}
\end{aligned} \tag{D.2}
$$

The second last equation is because of the induction assumption, and the last equation is true considering $w_k = 0$.

Therefore the Lemma is proved for both cases. □

Bibliography

[1] http://path.berkeley.edu/∼raja/CCWVers4.mpeg.

[2] Dedicated Short Range Communications (DSRC) home. http://www.leearmstrong.com/dsrc/dsrchomeset.htm.

[3] Freeway performance measurement system (PeMS). http://pems.eecs.berkeley.edu.

[4] Monarch project. http://www.monarch.cs.cmu.edu/cmu-ns.html.

[5] The netowrk simulator: NS-2. http://www.isi.edu/nsnam/ns.

[6] Wireless LAN Medium Access Control (MAC) and Physical Layer (PHY) specifications. *IEEE Standard 802.11a-1999*, 1999.

[7] *IEEE Control Systems Magazine*, 21(1), February 2001.

[8] *IEEE Transactions on Automatic Control*, 49(9), September 2004.

[9] National Automated Highway System Consortium C3 Interim Report. Technical Report Phase 1, October 1996-March 1998.

[10] N. Abramson. The throughput of packet broadcasting channels. *IEEE Trans. Comm.*, COM-25:117–128, January 1977.

[11] K. Ahmed. *Modeling Driver's Acceleration and Lane Change Behavior*. PhD thesis, MIT, 1999.

[12] G. Anastasi, L. Lanzini, and E. Mingozzi. HIPERLAN/1 MAC protocol: stability and performance analysis. *IEEE Journal on Selected Areas in Communications*, 18(9):1787–1798, September 2000.

[13] S. Arimoto. An algorithm for calculating the capacity of an arbitrary discrete memoryless channel. *IEEE Trans. Inform Theory*, IT-18:14–20, 1972.

[14] V. Bharghavan, A. Demers, S. Shanker, and L. Zhang. MACAW: A media access protocol for wireless LANs. *ACM SIGCOMM'94*, pages 212–225, August 1994.

[15] G. Bianchi. Performance analysis of the IEEE 802.11 distributed coordination function. *IEEE Journal on Selected Areas in Communications*, 18(3):535–547, March 2000.

[16] R. Blahut. Computation of channel capacity and rate-distortion function. *IEEE Trans. Information Theory*, IT-18:460–473, 1972.

[17] A. Bose and P. Ioannou. Analysis of traffic flow with mixed manual and semi-

automated vehicles. Technical Report UCS-ITS-PRR-99-14, California PATH, 1999.

[18] T. Chang and I. Lai. Analysis of characteristics of mixed traffic flow of autopilot vehicles and manual vehicles. *Transportation Research Part C: Emerging Technologies*, 5C(6):333–348, December 1997.

[19] Federal Communications Commission. FCC 99-305. FCC Report and Order, October 1999.

[20] Federal Communications Commission. FCC 03-024. FCC Report and Order, Feburary 2004.

[21] M. Cremer, C. Demir, S. Donikian, S. Espie, and M. McDonald. Investigating the impact of AICC concepts on the traffic flow quality. *Fifth World Congress on Intelligent Transportation Systems*, 1998.

[22] T. Şimşek. *Anytime channel coding with feedback*. PhD thesis, University of California at Berkeley, 2004.

[23] T. Şimşek and P. Varaiya. Noisy data-rate limited estimation: Renewal codes. *IEEE Conference on Decision and Control*, December 2003.

[24] S. Darbha and K.R. Rajagopal. Intelligent cruise control systems and traffic flow stability. *Transportation Research Part C: Emerging Technologies*, 7C(6):329–352, December 1999.

[25] M. Ergen, D. Lee, , R. Sengupta, and P. Varaiya. Wireless token ring protocol. *IEEE transactions on Vehicular Technology*, 53(6):1863–1881, November 2004.

[26] N. Farvardin and V. Vaishampayan. Optimal quantizer design for noisy channels: An approach to combined source-channel coding. *IEEE Trans. Information Theory*, 33(6):827–838, November 1987.

[27] N. Farvardin and V. Vaishampayan. On the performance and complexity of channel-optimized vector quantizers. *IEEE Trans. Information Theory*, 37(1):155–160, January 1991.

[28] W. Feller. *An introduction to Probability Theory and its Applications*, volume 1. John Wiley and Sons, 1968.

[29] E. Frew, T. McGee, Z. Kim, X. Xiao, S. Jackson, M. Morimoto, R. Rathinam, M. Zennaro, J. Padial, and R. Sengupta. Vision based road-following using a small autonomous aircraft. *IEEE Aerospace Conference*, March 2004.

[30] S. Friedberg, A. Insel, and L. Spence. *Linear Algebra*. Prentice Hall, 4th edition, 2002.

[31] J. Garcia-Luna-Aceves and C. Fullmer. Floor aquisition multiple access (FAMA) in single channel wireless networks. *ACM Mobile networks and applications*, 4:157–174, 1999.

[32] P. Gupta and P. Kumar. The capacity of wireless networks. *IEEE Transactions on Information Theory*, IT-46(2):388–404, March 2000.

[33] F. Hall, V. Hurdle, and H. James. Synthesis of recent work on the nature of speed-flow and flow-occupancy (or density) relationships on freeways. *Transportation Research Record*, 28(1365):12–18, 1992.

[34] J.K. Hedrick, D. Godbole, R. Rajamani, and P. Seiler. Stop and go cruise control final report. http://vehicle.me.berkeley.edu/Publications/AVC/pqixu_vtc02.ps.

[35] K. Hedrick, Q. Xu, and M. Uchanski. Enhanced AHS safety through the integration of vehicle control and communication. Technical Report UCS-ITS-PRR-2001-28, California PATH, 2001.

[36] E. Hoffman and R. Mortimer. Scaling of relative velocity between vehicles. *Accid. Anal. And Prev.*, 28(4):415–421, 1996.

[37] E. Hoffmann and R. Mortimer. Scaling of relative velocity between vehicles. *Accident Analysis and Prevention*, 28(4):415–421, 1996.

[38] T. Iijima, A. Higashimata, S. Tange, and et. al. Development of an adaptive cruise control system with brake actuation. *Intelligent Vehicle Systems*, (SAE SP-1538):173–178, 2000.

[39] R. Kalman. A new approach to liner filtering and prediction problems. *Transactions of the ASME, Journal of Basic Engineering*, 82D:34–45, March 1960.

[40] R. Kalman and R. Bucy. New results in linear filtering and prediction theory. *Transactions of the ASME, Journal of Basic Engineering*, 83D(1):95–108, March 1961.

[41] P. Karn. MACA-a new channel access method for packet radio. *ARRL/CRRL Amateur Radio 9th Computer Networking Conference*, pages 134–140, 1990.

[42] A. Kato, K. Sato, and M. Fujise. Wave propagation characteristics of inter-vehicle communication on an expressway. *Eighth World Congress on Intelligent Transportation Systems*, 2001.

[43] A. Kurtenbach and P. Wintz. Quantizing for noisy channels. *IEEE Trans. Communication Technology*, COM-17(2):291–302, April 1969.

[44] W. C. Y. Lee. *Mobile Communications Design Fundamentals*. John Wiley & Sons, 2 edition, 1993.

[45] S. Lloyd. Least squares quantization in PCM. *IEEE Transactions on Information Theory*, IT-28(2):129–137, March 1982.

[46] A. Mahajan, J. Ko, and R. Sengupta. Distributed probabilistic map service. *Proc. of the 41st IEEE Conference on Decision and Control*, December 2002.

[47] Bill McFraland. Private Communication.

[48] M. Minderhoud and P. Bovy. Impact of intelligent cruise control in motorway capacity. *Transportation Research Record*, (1679):1–9, 1999.

[49] R. Murray, K. Astrom, S. Boyd, R. Brockett, and G. Stein. Future directions in control in an information-rich world. *IEEE Control Systems Magazine*, 23(2):20–33, April 2003.

[50] G. Nair. *State Estimation Under Communication Constraints*. PhD thesis, University of Melbourne, 1999.

[51] G. Nair and R. Evens. State estimation via a capacity-limited communication channel. *Proc. IEEE 36th Conference on Decision and Control*, 1997.

[52] G. Nair and R. Evens. State estimation under bit-rate constraints. *Proc. IEEE 37th Conference on Decision and Control*, 1998.

[53] G. Nair and R. Evens. Structural results for finite bit-rate state estimation. *Proc. 1999 Information, Decision, and Control, Adelaide, Australia*, 1999.

[54] D. Neuhoff and R. Gilbert. Causal source codes. *IEEE Trans. on Information Theory*, IT-28(5):701–713, September 1982.

[55] California PATH. SHIFT: The hybrid system simulation programming language. http://www.path.berkeley.edu/shift/.

[56] W. Pattra-Atikom, P. Krishnamurthy, and S. Banerjee. Distributed mechanisms for quality of serivce in wireless LAN. *IEEE Wireless Communications*, pages 26–34, June 2003.

[57] J. Proakis. *Digital Communications*. WCB/McGraw Hill, third edition, 1995.

[58] B.S.Y. Rao and P. Varaiya. Flow benefits of autonomous intelligent cruise control in mixed manual and automated traffic. *Transportation Research Record*, (1408):36–43, 1993.

[59] L. Roberts. Aloha packet system with and without slots and capture. *Computer Communication Review*, 5(2):28–42, 1975.

[60] A. Sahai. Evaluating channels for control: Capacity reconsidered. *American Control Conference*, June 2000.

[61] A. Sahai. *Anytime Information Theory*. PhD thesis, Massachusetts Institute of Technology, 2001.

[62] A. Sahai and Q. Xu. The anytime capacity of AWGN+erasure channel with feedback. *Submitted to the Allerton Conference*, 2004.

[63] A. Sahai and Q. Xu. The anytime reliability of constrained packet erasure channels with feedback. *Submitted to the Allerton Conference*, 2004.

[64] P. Seiler and R. Sengupta. Analysis of communication losses in vehicle control problems. *American Control Conference*, June 2001.

[65] J. Sobrinho and A. Krishnakumar. Quality-of-service in ad hoc carrier sense multiple access wireless networks. *IEEE Journal on Selected Areas in Communications*, 17(8):1353–1368, August 1999.

[66] B. Song and D. Delorme. Human driver model for smartAHS based on cognitive and control approaches. *Tenth Annual Meeting of the Intelligent Transportation Society of America*, May 2000.

[67] S. Tatikonda. *Control Under Communication Constraints*. PhD thesis, Massachusetts Institute of Technology, 2000.

[68] D. Teneketzis. On the optimal structure of real-time encoders and decoders in noisy communication. Technical Report Report No. CGR-04-03, Control Group, Department of Electrical Engineering and Computer Science,University of Michigan, Ann Arbor, March 2004.

[69] F. Tobagi and L. Kleinrock. Packet switching in radio channels: Part I- carrier sense multiple-access modes and their throughput/delay characteristics. *IEEE Trans. Comm.*, COM-23:1400–1416, December 1975.

[70] B. van Arem, J. Hogema, M. Vanderschuren, and C. Verheul. An assessment of the impact of autonomous intelligent cruise control. *TNO Report INRO-VVG, Netherlands*, March 1996.

[71] J. VanderWerf, N. Kourjanskaia, S. Shladover, H. Krishnan, and M. Miller. Modeling the effects of driver control assistance systems on traffic. *National Research Council Transportation Research Board 80th Annual Meeting*, January 2001.

[72] J. Walrand and P. Varaiya. Optiaml causal coding-decoding problems. *IEEE Trans. Inform. Theory*, IT-29(6):814–820, November 1983.

[73] H. Weatherspoon and J. Kubiatowicz. Erasure coding vs. replication: A quantitative comparison. *The First International Workshop on Peer-to-Peer Systems*, March 2002.

[74] H. S. Witsenhausen. On the structure of real-time source coders. *The Bell System Technical Journal*, 58(6):1437–1451, July-August 1978.

[75] W. Wong and R. Brockett. Systems with finite communication bandwidth constraints I: State estimation problems. *IEEE Trans. on Automatic Control*, 42(9):1294–1299, September 1997.

[76] Y. Xiao. Enhanced DCF of IEEE 802.11e to support Qos. *Proceedings of IEEE WCNC*, pages 1291–1296, 2003.

[77] Q. Xu. The anytime capacity of AWGN+erasure channel with feedback. Master's thesis, University of California at Berkeley, August 2004.

[78] Q. Xu, K. Hedrick, R. Sengupta, and J. VanderWerf. Effects of vehicle-vehicle/roadside-vehicle communication on adaptive cruise controlled highway systems. *IEEE Vehicular Technology Conference*, October 2002.

[79] Q. Xu, D. Jiang, and R. Sengupta. Design and analysis of highway safety com-

munication protocol in 5.9 ghz dedicated short range communication spectrum. *IEEE Vehicular Technology Conference*, April 2003.

[80] Q. Xu, T. Mak, J. Ko, and R. Sengupta. Vehicle-vehicle safety messaging in dsrc. *Proc. of the 1st ACM Workshop on Vehicular Ad-hoc Networks*, October 2004.

[81] Q. Xu and R. Sengupta. Simulation, analysis, and comparison of ACC/CACC in highway merging control. *IEEE Intelligent Vehicles Symposium*, June 2003.

[82] Y. Xu and J. Hespanha. Optimal commuication logics in networked control systems. *The 43rd IEEE Conference on Decision and Control*, December 2004.

[83] Y. Yamamura, M. Tabe, M. Kanehira, and T. Murakami. Development of an adaptive cruise control system with stop-and-go capability. *Intelligent Vehicle Initiative: Technology and Navigation Systems*, (SAE SP-1593):37–44, 2001.

[84] T. Yokota, M. Kuwahara, and H. Ozaki. A study of ahs effects on traffic flow at bottlenecks. *Fifth World Congress on Intelligent Transport Systems*, October 1998.

[85] S. Yuksel and T. Başar. Minimum rate coding for state estiamtion over noiseless channels. *The 43rd IEEE Conference on Decision and Control*, December 2004.

[86] M. Zennaro and J. Misener. A state-map architecture for safe intelligent intersection. *ITSA, Minneapolis*, 2003.

[87] J. Zhu and S. Roy. MAC for Dedicated Short Range Communications in Intelligent Transporation System. *IEEE Communications Magazine*, pages 60–67, December 2003.

[88] P. Zwaneveld and B. van Arem. Traffic efffects of automated vehicle guidance systems. *Fifth World Congress on Intelligent Transportation Systems*, October 1998.